THE UNIVERSITY OF CALGARY

Design of Circular Concrete Tanks for Thermal Effects

by

Michel Sabri Samaan

A THESIS

SUBMITTED TO THE FACULTY OF GRADUATE STUDIES

IN PARTIAL FULFILLMENT OF THE REQUIREMENTS FOR THE

DEGREE OF MASTER OF SCIENCE

DEPARTMENT OF CIVIL ENGINEERING

CALGARY, ALBERTA

AUGUST, 1993

ISBN 0-315-88615-3

Name Michel Samaan

Dissertation Abstracts International is arranged by broad, general subject categories. Please select the one subject which most nearly describes the content of your dissertation. Enter the corresponding four-digit code in the spaces provided.

Civil Engineering — SUBJECT TERM

0543 — SUBJECT CODE

U·M·I

Subject Categories

THE HUMANITIES AND SOCIAL SCIENCES

COMMUNICATIONS AND THE ARTS
Architecture 0729
Art History 0377
Cinema 0900
Dance 0378
Fine Arts 0357
Information Science 0723
Journalism 0391
Library Science 0399
Mass Communications 0708
Music 0413
Speech Communication 0459
Theater 0465

EDUCATION
General 0515
Administration 0514
Adult and Continuing 0516
Agricultural 0517
Art 0273
Bilingual and Multicultural 0282
Business 0688
Community College 0275
Curriculum and Instruction 0727
Early Childhood 0518
Elementary 0524
Finance 0277
Guidance and Counseling 0519
Health 0680
Higher 0745
History of 0520
Home Economics 0278
Industrial 0521
Language and Literature 0279
Mathematics 0280
Music 0522
Philosophy of 0998
Physical 0523
Psychology 0525
Reading 0535
Religious 0527
Sciences 0714
Secondary 0533
Social Sciences 0534
Sociology of 0340
Special 0529
Teacher Training 0530
Technology 0710
Tests and Measurements 0288
Vocational 0747

LANGUAGE, LITERATURE AND LINGUISTICS
Language
- General 0679
- Ancient 0289
- Linguistics 0290
- Modern 0291

Literature
- General 0401
- Classical 0294
- Comparative 0295
- Medieval 0297
- Modern 0298
- African 0316
- American 0591
- Asian 0305
- Canadian (English) 0352
- Canadian (French) 0355
- English 0593
- Germanic 0311
- Latin American 0312
- Middle Eastern 0315
- Romance 0313
- Slavic and East European 0314

PHILOSOPHY, RELIGION AND THEOLOGY
Philosophy 0422
Religion
- General 0318
- Biblical Studies 0321
- Clergy 0319
- History of 0320
- Philosophy of 0322

Theology 0469

SOCIAL SCIENCES
American Studies 0323
Anthropology
- Archaeology 0324
- Cultural 0326
- Physical 0327

Business Administration
- General 0310
- Accounting 0272
- Banking 0770
- Management 0454
- Marketing 0338

Canadian Studies 0385
Economics
- General 0501
- Agricultural 0503
- Commerce-Business 0505
- Finance 0508
- History 0509
- Labor 0510
- Theory 0511

Folklore 0358
Geography 0366
Gerontology 0351
History
- General 0578
- Ancient 0579
- Medieval 0581
- Modern 0582
- Black 0328
- African 0331
- Asia, Australia and Oceania 0332
- Canadian 0334
- European 0335
- Latin American 0336
- Middle Eastern 0333
- United States 0337

History of Science 0585
Law 0398
Political Science
- General 0615
- International Law and Relations 0616
- Public Administration 0617

Recreation 0814
Social Work 0452
Sociology
- General 0626
- Criminology and Penology 0627
- Demography 0938
- Ethnic and Racial Studies 0631
- Individual and Family Studies 0628
- Industrial and Labor Relations 0629
- Public and Social Welfare 0630
- Social Structure and Development 0700
- Theory and Methods 0344

Transportation 0709
Urban and Regional Planning 0999
Women's Studies 0453

THE SCIENCES AND ENGINEERING

BIOLOGICAL SCIENCES
Agriculture
- General 0473
- Agronomy 0285
- Animal Culture and Nutrition 0475
- Animal Pathology 0476
- Food Science and Technology 0359
- Forestry and Wildlife 0478
- Plant Culture 0479
- Plant Pathology 0480
- Plant Physiology 0817
- Range Management 0777
- Wood Technology 0746

Biology
- General 0306
- Anatomy 0287
- Biostatistics 0308
- Botany 0309
- Cell 0379
- Ecology 0329
- Entomology 0353
- Genetics 0369
- Limnology 0793
- Microbiology 0410
- Molecular 0307
- Neuroscience 0317
- Oceanography 0416
- Physiology 0433
- Radiation 0821
- Veterinary Science 0778
- Zoology 0472

Biophysics
- General 0786
- Medical 0760

EARTH SCIENCES
Biogeochemistry 0425
Geochemistry 0996
Geodesy 0370
Geology 0372
Geophysics 0373
Hydrology 0388
Mineralogy 0411
Paleobotany 0345
Paleoecology 0426
Paleontology 0418
Paleozoology 0985
Palynology 0427
Physical Geography 0368
Physical Oceanography 0415

HEALTH AND ENVIRONMENTAL SCIENCES
Environmental Sciences 0768
Health Sciences
- General 0566
- Audiology 0300
- Chemotherapy 0992
- Dentistry 0567
- Education 0350
- Hospital Management 0769
- Human Development 0758
- Immunology 0982
- Medicine and Surgery 0564
- Mental Health 0347
- Nursing 0569
- Nutrition 0570
- Obstetrics and Gynecology 0380
- Occupational Health and Therapy 0354
- Ophthalmology 0381
- Pathology 0571
- Pharmacology 0419
- Pharmacy 0572
- Physical Therapy 0382
- Public Health 0573
- Radiology 0574
- Recreation 0575
- Speech Pathology 0460
- Toxicology 0383

Home Economics 0386

PHYSICAL SCIENCES
Pure Sciences

Chemistry
- General 0485
- Agricultural 0749
- Analytical 0486
- Biochemistry 0487
- Inorganic 0488
- Nuclear 0738
- Organic 0490
- Pharmaceutical 0491
- Physical 0494
- Polymer 0495
- Radiation 0754

Mathematics 0405
Physics
- General 0605
- Acoustics 0986
- Astronomy and Astrophysics 0606
- Atmospheric Science 0608
- Atomic 0748
- Electronics and Electricity 0607
- Elementary Particles and High Energy 0798
- Fluid and Plasma 0759
- Molecular 0609
- Nuclear 0610
- Optics 0752
- Radiation 0756
- Solid State 0611

Statistics 0463

Applied Sciences

Applied Mechanics 0346
Computer Science 0984
Engineering
- General 0537
- Aerospace 0538
- Agricultural 0539
- Automotive 0540
- Biomedical 0541
- Chemical 0542
- Civil 0543
- Electronics and Electrical 0544
- Heat and Thermodynamics 0348
- Hydraulic 0545
- Industrial 0546
- Marine 0547
- Materials Science 0794
- Mechanical 0548
- Metallurgy 0743
- Mining 0551
- Nuclear 0552
- Packaging 0549
- Petroleum 0765
- Sanitary and Municipal 0554
- System Science 0790

Geotechnology 0428
Operations Research 0796
Plastics Technology 0795
Textile Technology 0994

PSYCHOLOGY
General 0621
Behavioral 0384
Clinical 0622
Developmental 0620
Experimental 0623
Industrial 0624
Personality 0625
Physiological 0989
Psychobiology 0349
Psychometrics 0632
Social 0451

Nom ______________________________

Dissertation Abstracts International est organisé en catégories de sujets. Veuillez s.v.p. choisir le sujet qui décrit le mieux votre thèse et inscrivez le code numérique approprié dans l'espace réservé ci-dessous.

______________________________ ☐☐☐☐ U·M·I

SUJET — CODE DE SUJET

Catégories par sujets

HUMANITÉS ET SCIENCES SOCIALES

COMMUNICATIONS ET LES ARTS
- Architecture 0729
- Beaux-arts 0357
- Bibliothéconomie 0399
- Cinéma 0900
- Communication verbale 0459
- Communications 0708
- Danse 0378
- Histoire de l'art 0377
- Journalisme 0391
- Musique 0413
- Sciences de l'information 0723
- Théâtre 0465

ÉDUCATION
- Généralités 515
- Administration 0514
- Art 0273
- Collèges communautaires 0275
- Commerce 0688
- Économie domestique 0278
- Éducation permanente 0516
- Éducation préscolaire 0518
- Éducation sanitaire 0680
- Enseignement agricole 0517
- Enseignement bilingue et multiculturel 0282
- Enseignement industriel 0521
- Enseignement primaire. 0524
- Enseignement professionnel 0747
- Enseignement religieux 0527
- Enseignement secondaire 0533
- Enseignement spécial 0529
- Enseignement supérieur 0745
- Évaluation 0288
- Finances 0277
- Formation des enseignants 0530
- Histoire de l'éducation 0520
- Langues et littérature 0279
- Lecture 0535
- Mathématiques 0280
- Musique 0522
- Orientation et consultation 0519
- Philosophie de l'éducation 0998
- Physique 0523
- Programmes d'études et enseignement 0727
- Psychologie 0525
- Sciences 0714
- Sciences sociales 0534
- Sociologie de l'éducation 0340
- Technologie 0710

LANGUE, LITTÉRATURE ET LINGUISTIQUE
- Langues
  - Généralités 0679
  - Anciennes 0289
  - Linguistique 0290
  - Modernes 0291
- Littérature
  - Généralités 0401
  - Anciennes 0294
  - Comparée 0295
  - Mediévale 0297
  - Moderne 0298
  - Africaine 0316
  - Américaine 0591
  - Anglaise 0593
  - Asiatique 0305
  - Canadienne (Anglaise) 0352
  - Canadienne (Française) 0355
  - Germanique 0311
  - Latino-américaine 0312
  - Moyen-orientale 0315
  - Romane 0313
  - Slave et est-européenne 0314

PHILOSOPHIE, RELIGION ET THÉOLOGIE
- Philosophie 0422
- Religion
  - Généralités 0318
  - Clergé 0319
  - Études bibliques 0321
  - Histoire des religions 0320
  - Philosophie de la religion 0322
- Théologie 0469

SCIENCES SOCIALES
- Anthropologie
  - Archéologie 0324
  - Culturelle 0326
  - Physique 0327
- Droit 0398
- Économie
  - Généralités 0501
  - Commerce-Affaires 0505
  - Économie agricole 0503
  - Économie du travail 0510
  - Finances 0508
  - Histoire 0509
  - Théorie 0511
- Études américaines 0323
- Études canadiennes 0385
- Études féministes 0453
- Folklore 0358
- Géographie 0366
- Gérontologie 0351
- Gestion des affaires
  - Généralités 0310
  - Administration 0454
  - Banques 0770
  - Comptabilité 0272
  - Marketing 0338
- Histoire
  - Histoire générale 0578
  - Ancienne 0579
  - Médiévale 0581
  - Moderne 0582
  - Histoire des noirs 0328
  - Africaine 0331
  - Canadienne 0334
  - États-Unis 0337
  - Européenne 0335
  - Moyen-orientale 0333
  - Latino-américaine 0336
  - Asie, Australie et Océanie 0332
- Histoire des sciences 0585
- Loisirs 0814
- Planification urbaine et régionale 0999
- Science politique
  - Généralités 0615
  - Administration publique 0617
  - Droit et relations internationales 0616
- Sociologie
  - Généralités 0626
  - Aide et bien-àtre social 0630
  - Criminologie et établissements pénitentiaires 0627
  - Démographie 0938
  - Études de l' individu et de la famille 0628
  - Études des relations interethniques et des relations raciales 0631
  - Structure et développement social 0700
  - Théorie et méthodes. 0344
  - Travail et relations industrielles 0629
- Transports 0709
- Travail social 0452

SCIENCES ET INGÉNIERIE

SCIENCES BIOLOGIQUES
- Agriculture
  - Généralités 0473
  - Agronomie. 0285
  - Alimentation et technologie alimentaire 0359
  - Culture 0479
  - Élevage et alimentation 0475
  - Exploitation des péturages 0777
  - Pathologie animale 0476
  - Pathologie végétale 0480
  - Physiologie végétale 0817
  - Sylviculture et faune 0478
  - Technologie du bois 0746
- Biologie
  - Généralités 0306
  - Anatomie 0287
  - Biologie (Statistiques) 0308
  - Biologie moléculaire 0307
  - Botanique 0309
  - Cellule 0379
  - Écologie 0329
  - Entomologie 0353
  - Génétique 0369
  - Limnologie 0793
  - Microbiologie 0410
  - Neurologie 0317
  - Océanographie 0416
  - Physiologie 0433
  - Radiation 0821
  - Science vétérinaire 0778
  - Zoologie 0472
- Biophysique
  - Généralités 0786
  - Medicale 0760

SCIENCES DE LA TERRE
- Biogéochimie 0425
- Géochimie 0996
- Géodésie 0370
- Géographie physique 0368
- Géologie 0372
- Géophysique 0373
- Hydrologie 0388
- Minéralogie 0411
- Océanographie physique 0415
- Paléobotanique 0345
- Paléoécologie 0426
- Paléontologie 0418
- Paléozoologie 0985
- Palynologie 0427

SCIENCES DE LA SANTÉ ET DE L'ENVIRONNEMENT
- Économie domestique 0386
- Sciences de l'environnement 0768
- Sciences de la santé
  - Généralités 0566
  - Administration des hipitaux 0769
  - Alimentation et nutrition 0570
  - Audiologie 0300
  - Chimiothérapie 0992
  - Dentisterie 0567
  - Développement humain 0758
  - Enseignement 0350
  - Immunologie 0982
  - Loisirs 0575
  - Médecine du travail et thérapie 0354
  - Médecine et chirurgie 0564
  - Obstétrique et gynécologie 0380
  - Ophtalmologie 0381
  - Orthophonie 0460
  - Pathologie 0571
  - Pharmacie 0572
  - Pharmacologie 0419
  - Physiothérapie 0382
  - Radiologie 0574
  - Santé mentale 0347
  - Santé publique 0573
  - Soins infirmiers 0569
  - Toxicologie 0383

SCIENCES PHYSIQUES

Sciences Pures
- Chimie
  - Genéralités 0485
  - Biochimie 487
  - Chimie agricole 0749
  - Chimie analytique 0486
  - Chimie minérale 0488
  - Chimie nucléaire 0738
  - Chimie organique 0490
  - Chimie pharmaceutique 0491
  - Physique 0494
  - PolymÇres 0495
  - Radiation 0754
- Mathématiques 0405
- Physique
  - Genéralités 0605
  - Acoustique 0986
  - Astronomie et astrophysique 0606
  - Electronique et électricité 0607
  - Fluides et plasma 0759
  - Météorologie 0608
  - Optique 0752
  - Particules (Physique nucléaire) 0798
  - Physique atomique 0748
  - Physique de l'état solide 0611
  - Physique moléculaire 0609
  - Physique nucléaire 0610
  - Radiation 0756
- Statistiques 0463

Sciences Appliqués Et Technologie
- Informatique 0984
- Ingénierie
  - Généralités 0537
  - Agricole 0539
  - Automobile 0540
  - Biomédicale 0541
  - Chaleur et ther modynamique 0348
  - Conditionnement (Emballage) 0549
  - Génie aérospatial 0538
  - Génie chimique 0542
  - Génie civil 0543
  - Génie électronique et électrique 0544
  - Génie industriel 0546
  - Génie mécanique 0548
  - Génie nucléaire 0552
  - Ingénierie des systâmes 0790
  - Mécanique navale 0547
  - Métallurgie 0743
  - Science des matériaux 0794
  - Technique du pétrole 0765
  - Technique minière 0551
  - Techniques sanitaires et municipales 0554
  - Technologie hydraulique 0545
- Mécanique appliquée 0346
- Géotechnologie 0428
- Matières plastiques (Technologie) 0795
- Recherche opérationnelle 0796
- Textiles et tissus (Technologie) 0794

PSYCHOLOGIE
- Généralités 0621
- Personnalité 0625
- Psychobiologie 0349
- Psychologie clinique 0622
- Psychologie du comportement 0384
- Psychologie du développement 0620
- Psychologie expérimentale 0623
- Psychologie industrielle 0624
- Psychologie physiologique 0989
- Psychologie sociale 0451
- Psychométrie 0632

THE UNIVERSITY OF CALGARY

FACULTY OF GRADUATE STUDIES

The undersigned certify that they have read, and recommend to the Faculty of Graduate Studies for acceptance, a thesis entitled " Design of Circular Concrete Tanks for Thermal Effects " submitted by Michel Sabri Samaan in partial fulfillment of the requirements for the degree of Master of Science.

A. Ghali

Supervisor, Dr. A. Ghali
Department of Civil Engineering

Dr. W. H. Dilger
Department of Civil Engineering

A. Torvi

Prof. A. A. Torvi
Department of Mechanical Engineering

August 24, 1993

Date

ABSTRACT

An elastic linear analysis is performed for two tanks with restrained base joints; a reinforced non-prestressed tank and a prestressed tank. The applied loads are mainly liquid and thermal loads. The analysis results are used to carry out a structural design according to ACI 350-89, ACI 344-88 and BS 8007(87). However, the design leads to impractically large cross-sections for the walls of these tanks. A nonlinear analysis for the same cases is conducted based on a nonlinear finite element analysis. A substantial reduction in induced internal forces due to temperature takes place due to the cracking of the concrete.

The control of cracking of concrete is also investigated according to CEB FIP-MC90, ACI 224 and BS 8110 for variable vertical steel ratios and variable vertical prestressing.

It is concluded that the design of cylindrical concrete tanks should allow for cracking of concrete to relieve the induced thermal stresses, however the width of the developed cracks is controlled by the non-prestressed steel at the wall surface.

ACKNOWLEDGEMENTS

I would like to express my gratitude to my supervisor Dr. Amin Ghali under whose supervision this research was carried out. I am indebted for his guidance, support and great encouragement in difficult times.

My appreciation is also extended to the members of my examining committee, Dr. W.H. Dilger and Professor A.A. Torvi.

The financial support from the Natural Science and Engineering Research Council of Canada and the Department of Civil Engineering at The University of Calgary is thankfully acknowledged.

I am grateful to all my dear friends, who provided encouragement and help in due times. Special thanks to Mrs. Samah Rizkalla for her cheerful and judicious typing of the entire manuscript, and to Nader Rizkalla, Emad Khalil, Sami Megally, Alaa Sherif and Ezz Said Ahmed.

I would also like to thank my dear family back home for their care, love and support in all times.

Finally, thanks to Dr. N. Shrive and Mrs. Pat Sherman, all the secretary staff in the Civil Engineering Department and all the colleagues for their nice feelings during my sick leave.

TO MY DEAR FATHER, MOTHER AND SISTER

TABLE OF CONTENTS

APPROVAL PAGE ii

ABSTRACT iii

ACKNOWLEDGEMENTS iv

DEDICATION v

TABLE OF CONTENTS vi

LIST OF TABLES x

LIST OF FIGURES xi

LIST OF SYMBOLS xviii

1 INTRODUCTION 1

1.1 GENERAL OVERVIEW 1

1.2 OBJECTIVES OF THE THESIS 4

1.3 OUTLINE OF THE THESIS 5

2 ELASTIC ANALYSIS OF CIRCULAR CYLINDRICAL TANKS . . 6

2.1 INTRODUCTION 6

2.2 BEAM-ON-ELASTIC-FOUNDATION ANALOGY 6

2.3 ANALYSIS DUE TO TEMPERATURE LOADING 9

2.3.1 Introduction 9

2.3.2 Thermal Loads 10

2.3.3 Analysis due to Temperature Loads 12

2.4 COMPUTER ANALYSIS 13

2.5 LINEAR STRUCTURAL ANALYSIS OF CYLINDRICAL TANKS 16

2.5.1 Analysis Results 21

2.6 DESIGN OF TANKS 38

2.6.1 The Design According to ACI 350-89 and ACI 344-86 38

2.6.2 The Design According to BS 8007 42

2.7 SUMMARY 47

3 NONLINEAR FINITE ELEMENT ANALYSIS 48

3.1 INTRODUCTION 48

3.2 LAYERED FINITE ELEMENTS 48

3.3 FINITE ELEMENTS 49

3.4 MODELLING OF REINFORCEMENT 52

3.5 CONSTITUTIVE MATERIAL RELATIONS 52

3.5.1 Steel Model 52

3.5.2 Concrete Model 52

3.6 TENSION STIFFENING 56

3.7 PROCEDURE OF ANALYSIS 57

3.8 SUMMARY 60

4 NONLINEAR ANALYSIS AND RESULTS 61
4.1 INTRODUCTION 61
4.2 FINITE ELEMENT MODELLING 61
4.3 THE LOADS ACTING ON THE F.E. MODEL 67
4.4 VERIFICATION OF THE AXI-SYMMETRICAL MODEL 70
4.5 PROBLEM DESCRIPTION 70
4.6 RESULTS AND DISCUSSION 77
4.7 CONCLUDING REMARKS 91

5 NONLINEAR BEHAVIOR OF NON-PRESTRESSED TANKS UNDER THERMAL LOADS ONLY 92
5.1 GENERAL 92
5.2 ANALYSIS OF LOADING CASE A 96
5.3 THE ANALYSIS OF LOADING CASE B 102
5.4 CONCLUSIONS 108

6 CRACK CONTROL IN CIRCULAR CONCRETE TANKS 110
6.1 GENERAL 110
6.2 CRACK WIDTH CALCULATION IN DIFFERENT CODES . . 111
6.2.1 CEB-FIP Code 1990 112
6.2.2 ACI Committee 224 117
6.2.3 The British Standards BS 8110 (1989) 119

6.3 CRACK CONTROL IN CIRCULAR TANKS 122

6.3.1 The Crack Control of Reinforced Concrete Tanks 123

6.3.1.1 Circumferential Cracks 124

6.3.2 Crack Control of Prestressed Tanks 130

6.3.2.1 The Effect of Vertical Prestress 131

6.3.2.2 The Effect of Non-Prestressed Steel 132

6.4 DISCUSSION OF RESULTS 139

7 CONCLUSIONS AND RECOMMENDATIONS 141

7.1 CONCLUSIONS 141

7.2 RECOMMENDATIONS FOR DESIGN 142

7.3 RECOMMENDATIONS FOR FURTHER RESEARCH 142

REFERENCES 144

APPENDIX A : DERIVATION OF THE NODAL FORCES FOR A PLATE BENDING ELEMENT SUBJECTED TO A TRAPEZOIDAL LOAD DISTRIBUTION 148

APPENDIX B : CROSS - SECTIONAL AREAS OF STANDARD PRESTRESSED AND NON-PRESTRESSED REINFORCEMENT 152

LIST OF TABLES

Table 2.1: Dimensions and material properties of Tanks 1 and 2 17

Table 2.2: The circumferential prestressing of Tank 2 22

Table 2.3: Internal Forces For Tank 1 28

Table 2.4: Maximum internal forces for Tank 2 32

Table 2.5: Absolute maximum internal forces for Tank 2 38

Table 4.1: Concrete properties 67

Table 4.2: Steel properties 67

Table 6.1: Values for β_a and τ_{bk} 116

Table 6.2: Details of non-prestressed reinforcement 125

Table 6.3: Analysis results of Tank 1, loading case A
t = 300 mm, variable ρ_{iv} 127

Table 6.4: Analysis results of Tank 1, loading case B 127
t = 300 mm, , variable ρ_{ov}

Table 6.5: Analysis results of Tank 2, loading case A 133
t= 300 mm, ρ_{iv} = 0.60 %, ρ_{ov} = 0.25 %, variable σ_{vp}

Table 6.6: Analysis results of Tank 2, loading case B 133
t = 300 mm, $\rho_{ov} = \rho_{iv}$ = 0.75%, variable σ_{vp}

Table 6.7: Analysis results of Tank 2, loading case A 136
t = 300 mm, σ_{vp} = 2.0 MPa, variable ρ_{iv}

Table 6.8: Analysis results of Tank 2, loading case B 136
t = 300 mm, σ_{vp} = 2.0 MPa, variable ρ_{ov}

LIST OF FIGURES

Figure 1.1: Wall-base joint types for circular concrete tanks. 3

Figure 2.1: Positive directions of load and deflections in a cylindrical tank. 8

Figure 2.2: Section normal to the cylinder axis showing the radial resultant of the hoop forces. 8

Figure 2.3: Horizontal wall cross-section at base of Tank 1 18

Figure 2.4: Horizontal wall cross-section at base of Tank 2 18

Figure 2.5: Full height vertical wall cross-section of Tank 1 19

Figure 2.6: Full height vertical wall cross-section of Tank 2 20

Figure 2.7: Conventional circumferential prestressing. 23

Figure 2.8: Internal Forces Due to Liquid Load for Tank 1 25

Figure 2.9: Internal forces due to uniform temperature rise for Tank 1 ($T_o = T_i = 30°C$). 26

Figure 2.10: Deformed shapes of a cylindrical tank fixed at base due to temperature variations. 27

Figure 2.11: Internal forces due to temperature gradient for Tank 1 ($t_o = 15°C$, $T_i = -15°C$) 29

Figure 2.12: Internal forces due to liquid load + linear temperature rise for Tank 1 ($T_o = 45°C$, $T_i = 15°C$). 30

Figure 2.13: Internal forces due to linear temperature drop for Tank 1 ($T_o = -20°C$, $T_i = 5°C$). 31

Figure 2.14: Internal forces due to circumferential prestressing for Tank 2 (residual compression = 1 MPa). 33
Figure 2.15: Radial effect of the vertical prestressing force on the circular tank 34
Figure 2.16: Internal forces due to vertical prestressing for Tank 2 (prestress = 2 MPa) 35
Figure 2.17: Internal forces due to prestressing + liquid load + temperature rise for Tank 2 (T_o = 45°C, T_i = 15°C). 36
figure 2.18: Internal forces due to prestressing + temperature drop for Tank 2 (T_o = -20°C, T_i = 5°C). 37
Figure 2.19: Wall cross-section at bottom for Tank 1. Design according to ACI 350. The distribution is for the effect of liquid load plus temperature rise (T_o=45°C, T_i=15°C). 40
Figure 2.20: Wall cross-section at bottom for Tank 2. Design according to ACI 344. The distribution is for the effect of temperature drop (T_o=-20°C, T_i=5°C) combined with the effect of circm. and vertical prestressing. 43
Figure 2.21: Wall cross-section at bottom for Tank 1. Design according to BS 8007. The distribution is for the effect of liquid load plus temperature rise (T_o=45°C, T_i=15°C). 45
Figure 2.22: Wall cross-section at bottom for Tank 2. Design according to BS 8007. The distribution is for the effect of temperature

drop (T_o=-20°C, T_i=5°C) combined with the effect of circm. and vertical prestressing. 46
Figure 3.1: Layered element 50
Figure 3.2: Quadrilateral plane element 50
Figure 3.3: Quadrilateral plate bending element 51
Figure 3.4: Quadrilateral shell element 51
Figure 3.5: Bilinear stress-strain curve for steel 55
Figure 3.6: Equivalent stress-strain curve for concrete 55
Figure 3.7: Tension stiffening model 58
Figure 3.8: Incremental-iterative method 58
Figure 4.1: Finite element mesh for Tanks 1 and 2 62
Figure 4.2: The layered concrete section 63
Figure 4.3a: Axi-symmetrical boundary conditions for a typical plane shell element. 64
Figure 4.3b: Directions of the boundary elements at the nodes of the shell element to satisfy the axi-symmetrical conditions. . . . 65
Figure 4.4: The input of the temperature variation through the thickness. 69
Figure 4.5: Element nodal forces in the Z-direction, representing the effect of a circumferential prestressing tendon. 69
Figure 4.6: Comparison of M_x due to liquid load according to PCT and FELARC using linear analysis. 71

Figure 4.7: Comparison of N_ϕ due to liquid load according to PCT and FELARC using linear analysis. 72
Figure 4.8: Comparison of M_ϕ due to liquid load according to PCT and FELARC using linear analysis. 73
Figure 4.9: Comparison of M_x due to temperature rise according to PCT and FELARC using linear analysis. 74
Figure 4.10: Comparison of N_ϕ due to temperature rise according to PCT and FELARC using linear analysis (T_o = 45°C, T_i = 15°C). 75
Figure 4.11: Comparison of M_ϕ due to temperature rise according to PCT and FELARC using linear analysis (T_o = 45°C, T_i = 15°C). 76
Figure 4.12: Effect of ρ_{iv} ration on the nonlinear vertical moment at base for load case A 79
Figure 4.13: M_x-diagram for Tank 1 according to the linear and nonlinear analyses. Case of liquid load + temperature rise (T_o = 45°C, T_i = 15°C). 80
Figure 4.14: N_ϕ-diagram for Tank 1 according to the linear and nonlinear analyses. Case of liquid load + temperature rise (T_o = 45°C, T_i = 15°C). 81
Figure 4.15: M_ϕ-diagram for Tank 1 according to the linear and nonlinear analyses. Case of liquid load + temperature rise

(T_o = 45°C, T_i = 15°C). 82

Figure 4.16: M_x-diagram for Tank 1 according to the linear and nonlinear analyses. Case of temperature drop (T_o = -20°C, T_i = 5°C). 83

Figure 4.17: N_ϕ-diagram for Tank 1 according to the linear and nonlinear analyses. Case of temperature drop (T_o = -20°C, T_i = 5°C). 84

Figure 4.18: M_ϕ-diagram for Tank 1 according to the linear and nonlinear analyses. Case of temperature drop (T_o = -20°C, T_i = 5°C). 85

Figure 4.19: M_x-diagram for Tank 2 according to the linear and nonlinear analyses. Case of liquid load + prestressing + temperature rise (T_o = 45°C, T_i =15°C). 86

Figure 4.20: N_ϕ-diagram for Tank 2 according to the linear and nonlinear analyses. Case of liquid load + prestressing + temperature rise (T_o = 45°C, T_i =15°C). 87

Figure 4.21: M_ϕ-diagram for Tank 2 according to the linear and nonlinear analyses. Case of liquid load + prestressing + temperature rise (T_o = 45°C, T_i =15°C). 88

Figure 4.22: M_x-diagram for Tank 2 according to the linear and nonlinear analyses. Case of prestressing + temperature drop (T_o = -20°C, T_i = 5°C). 89

Figure 4.23: M_ϕ-diagram for Tank 2 according to the linear and nonlinear analyses. Case of prestressing + temperature drop (T_o = -20°C, T_i = 5°C). 90

Figure 5.1: The thermal response of a continuous concrete beam. 93

Figure 5.2: The internal forces produced due to a temperature rise (T_o = 10.0°C, T_i =0.0°C). 97

Figure 5.3: The variation of M_x and f_{siv} with T_o for Loading Case A at base. 98

Figure 5.4: The variation of M_ϕ and N_ϕ with T_o for Loading Case A at base. 99

Figure 5.5: The variation of N_ϕ , M_ϕ and M_x with T_o for Loading Case A at x = 4.2 m. 100

Figure 5.6: The variation of M_ϕ , f_{sih} with T_o for Loading Case A at x = 4.2 m. 101

Figure 5.7: The internal forces produced due to a temperature drop (T_o = -10.0°C, T_i =0.0°C). 103

Figure 5.8: The variation of N_ϕ , M_x and M_ϕ with T_o for Loading Case B at base. 105

Figure 5.9: The variation of M_x and f_{sov} with T_o for Loading Case B at base. 106

Figure 5.10: The variation of N_ϕ and M_ϕ with T_o for Loading Case B at top. 107

Figure 6.1: Bond stress - slip relationship (according to CEB-FIP 90). . 113

Figure 6.2: The distribution of steel and concrete strains within $l_{s,max}$. . 113

Figure 6.3: The effective tension area. 116

Figure 6.4: The distance a_{cr} used in Eq. 6.10. 120

Figure 6.5: The variation of the crack width and the Z-factor versus ρ_{iv} for Tank 1 subjected to loading case A. (t = 300 mm). 128

Figure 6.6: The variation of the crack width and the Z-factor versus ρ_{ov} for Tank 1 subjected to loading case B. (t = 300 mm). 129

Figure 6.7: The variation of the crack width and the Z-factor versus ρ_{ov} for Tank 1 subjected to loading case B. (t = 300 mm, ρ_{iv} = 0.60 %, ρ_{ov} = 0.25 %). 134

Figure 6.8: The variation of the crack width and the Z-factor versus σ_{vp} for Tank 2 subjected to loading case B. (t = 300 mm, ρ_{ov}= ρ_{iv} = 0.75 %). 135

Figure 6.9: The variation of the crack width and the Z-factor versus ρ_{vp} for Tank 2 subjected to loading case A. (t = 300 mm, σ_{vp} = 2.0 MPa). 137

Figure 6.10: The variation of the crack width and the Z-factor versus ρ_{vp} for Tank 2 subjected to loading case B. (t = 300 mm, σ_{vp} = 2.0 MPa). 138

Figure A.1: Rectangular plate bending element. 149

LIST OF SYMBOLS

a,b	side lengths of the plate bending element.
A	area of concrete symmetric with reinforcing steel divided by numbers of bars (ACI 224).
[A]	matrix of coefficients.
a'	distance from the compression face to the point at which the crack width is being calculated.
$A_{c,ef}$	effective area of concrete in tension.
a_{cr}	distance from the point, at which crack width is calculated to the surface of the nearest longitudinal bar (BS 8110).
A_{ps}	cross-sectional area of the prestressed steel per unit length.
A_s	area of non-prestressed steel in tension.
A_{sih}	cross-sectional area of the horizontal non-prestressed steel at the inner face of the tank wall per unit length.
A_{siv}	cross-sectional area of the vertical non-prestressed steel at the inner face of the tank wall per unit length.
A_{soh}	cross-sectional area of the horizontal non-prestressed steel at the outer face of the tank wall per unit length.
A_{sov}	cross-sectional area of the vertical non-prestressed steel at the outer face of the tank wall per unit length.
[B]	strain-displacement matrix.

b_t width of the section at the centroid of the tension steel.

c clear concrete cover.

C $= \dfrac{k\lambda^4}{E\ I_r}$

d effective depth.

d_c thickness of cover from tension fiber to center of bar closest thereto (ACI 224).

[D] orthotropic constitutive matrix.

E elastic modulus.

E_c elastic modulus of concrete ($=5000\sqrt{f'_c}$).

E_{co} initial tangent modulus of elasticity of concrete.

E_{cs} secant modulus of concrete at peak stress.

E_{ps} elastic modulus of prestressed steel.

E^*_{ps} strain-hardening modulus of prestressed steel.

E_s elastic modulus of non-prestressed steel.

E^*_s strain-hardening modulus of non-prestressed steel.

E_1,E_2 uniaxial tangent moduli in the principal directions.

{F} equivalent nodal force vector.

$\{\bar{F}\}$ equivalent unbalanced nodal force vector.

f_c maximum compressive stress in the concrete section.

f_c' maximum compressive strength of concrete.

f_{ctm} mean value of the tensile strength of the concrete at the time when the crack appears (CEB FIP).

f_{py} specified yield strength of prestressed steel.

f_p stress in prestressing strand.

f_s stress in non-prestressed steel.

F_s force in non-prestressed steel.

f_{sih} stress in non-prestressed horizontal steel at the inside face of the tank wall.

f_{siv} stress in non-prestressed vertical steel at the inside face of the tank wall.

f_{soh} stress in non-prestressed horizontal steel at the outer face of the tank wall.

f_{sov} stress in non-prestressed vertical steel at the outside face of the tank wall.

f_t' tensile strength of concrete.

f_y yielding strength of non-prestressed steel.

G' elastic shear modulus.

H height of the tank.

h_1 is the distance from the neutral axis to the reinforcing steel.

I moment of inertia of a tank strip of unit width ($= \dfrac{t^3}{12\,(1-\nu^2)}$).

I_r reference moment of inertia (Eq. 2.19).

$l_{s,max}$ length over which slip between steel and concrete occurs.

J $= \dfrac{I}{I_r}$

k modulus of foundation ($= \dfrac{E\ t}{r^2}$).

[K] structure stiffness matrix.

M_{cr} cracking moment.

M_x vertical moment per unit length.

M_ϕ circumferential moment per unit length.

[N] matrix of the shape functions for a plate bending element.

N_ϕ hoop force per unit length.

$N_{\phi r}$ radial force per unit length.

P prestressing force.

q axi-symmetrical radial distributed load.

Q equivalent concentrated radial load.

r radius of the tank.

s slip of steel relative to the concrete.

t wall thickness.

t_b bottom cover to center of bar.

T_i temperature at the inner face of the tank wall.

T_o temperature at the outer face of the tank wall.

t_s side cover to center of bar.

V shearing force per unit length.

V^e volume of a finite element.

v^* displacement along the local y-axis.

w radial deflection of cylindrical tank.

w_{ACI} crack width according to ACI 224.

w_b most probable maximum crack width at bottom of the beam.

w_{BS} crack width according to BS 8110.

w_{CEB} crack width according to CEB-FIP MC90.

w_s most probable maximum crack width at level of reinforcement.

x vertical distance measured from the tank base.

$\bar{x}$ vertical distance measured from the top of the tank (= H-x).

x_n depth of the neutral axis.

x_1 effective depth of concrete in tension (CEB-FIP).

Z $= f_s \sqrt[3]{d_c A}$

Z_1 $= e^{-\beta x} (\cos \beta x + \sin \beta x)$

$\bar{Z}_1$ $= e^{-\beta \bar{x}} (\cos \beta \bar{x} + \sin \beta \bar{x})$

Z_3 $= e^{-\beta x} (\cos \beta x - \sin \beta x)$

$\bar{Z}_3$ $= e^{-\beta \bar{x}} (\cos \beta \bar{x} - \sin \beta \bar{x})$

α coefficient of thermal expansion.

α_c coefficient of thermal expansion of concrete.

α_e is the ratio E_s/E_c,

α_s coefficient of thermal expansion of steel.

β $= \dfrac{[3\ (1-\nu^2)]^{\frac{1}{4}}}{\sqrt{rt}}$

β_a empirical averaging factor (CEB-FIP MC90).

β_g constant to account for the drop of shear stiffness due to cracking.

β_s ratio of distance between neutral axis and tension face to distance between neutral axis and centroid of reinforcing steel (ACI 224).

γ_w specific weight of water.

ΔT difference in temperature.

$\Delta\varepsilon_{sr}$ difference of ε_{sr2} and ε_{sr1} (Fig. 6.2).

$\{\delta\}$ nodal displacement vector.

$\{\Delta\sigma\}$ vector of the stress increment.

$\{\Delta\varepsilon\}$ vector of the strain increment.

ε_{cm} average concrete strain within $l_{s,max}$.

ε_{cs} strain of concrete due to shrinkage.

ε_{cu} strain at the maximum compressive strength of concrete.

ε_m average strain in steel at the level where the cracking is being considered.

ε_{pu} ultimate strain of prestressed steel.

ε_{sm} average steel strain within $l_{s,max}$.

ε_{sr1} steel strain at the point of zero slip under cracking forces reaching f_{ctm}.

ε_{sr2} steel strain at the crack due to forces causing f_{ctm} within $A_{c,ef}$.

ε_{su} ultimate strain of non-prestressed steel.

ε_{s1} steel strain in uncracked concrete.

ε_{s2} steel strain at the crack.

ε_{tu} ultimate tensile strain of concrete.

ε_{u} ultimate compressive strain of concrete.

ε_{1} strain in steel calculated on the basis of a totally cracked section.

θ_x rotation around the global x-axis.

θ_x^* rotation around the local x-axis

θ_y rotation around the global y-axis.

θ_y^* rotation around the local y-axis

θ_z rotation around the global z-axis.

θ_z^* rotation around the local z-axis.

λ spacing between the nodes of the finite difference analysis.

ν Poisson's ratio.

ν_1,ν_2 Poisson's ratios in the principal directions.

ξ,η natural coordinates.

ρ_{ih} horizontal non-prestressed steel ratio at the inner face of the tank wall.

ρ_{iv} vertical non-prestressed steel ratio at the inner face of the tank wall.

ρ_{min} $= 0.24 \dfrac{f_t'}{f_y}$

ρ_{oh} horizontal non-prestressed steel ratio at the outer face of the tank wall.

ρ_{ov} vertical non-prestressed steel ratio at the outer face of the tank wall.

$\rho_{s,ef}$ effective reinforcement ratio ($=A_s/A_{c,ef}$).

σ stress.

$\{\bar{\sigma}_i\}$ unbalanced stress vector.

σ_{sE} steel stress at the point of zero slip.

σ_{s2} steel stress at the crack.

σ_{vp} vertical prestress at the centre of the cross-section.

σ_1,σ_2 principal stresses.

ΣO summation of the perimeters of the rebars.

τ_{bk} lower fractile value of the average bond stress.

τ_{max} maximum bond strength of concrete.

ϕ_s reinforcement bar diameter.

bar size designation; example #10, #20, ... For cross-section area of bars, see Appendix B.

CHAPTER 1

INTRODUCTION

1.1 GENERAL OVERVIEW

Concrete liquid retaining structures have been widely used in practice for many decades. The earliest concrete vessels consisted of open rectangular tanks with massive concrete walls and floors.

With the introduction of the reinforced concrete by the end of last century, tanks with more slender proportions started to be constructed. In the third decade of the century prestressed concrete started to be used for storage tanks. The first prestressed concrete tank in North America was constructed in 1938 (Shupack 1989).

The design of liquid retaining tanks has been usually based on the nonrealistic assumption of non-cracked structures. In the late seventies the concept of designing concrete liquid retaining structures with the allowance for cracking emerged, as a result of the advances of crack widths assessment at service loads.

The ACI Committee reports 350-89 and 344-88 and the British Standard Code of Practice BS 8007-87 allow for cracking of tanks and specify a certain steel stress as a means of control.

The present study focuses on axi-symmetrical circular cylindrical concrete tanks, with and without prestressing, subjected to axi-symmetrical loads. In such tanks, loads produce hoop stresses and vertical stresses. There are three basic types of wall-floor joints:

1) <u>Free Sliding Joint:</u> which allows rotation and radial movement. Usually, it consists of elastomeric pad supporting the base of the wall on the footing (Fig. 1.1 a).

2) <u>Pinned Joint:</u> which allows for rotation only (Fig. 1.1 b).

3) <u>Fixed Joint:</u> which provides total restraint (Fig. 1.1 c).

However, a combination of two types of joints is also applicable as to construct a partially fixed joint or semi sliding-fixed joint (Fig 1.1 d).

The simplest type, which does not require additional precautions for watertightness is the fixed wall-floor joint (Fig 1.1 c). The aim of the present study is to explore the effect of thermal stresses on prestressed and non-prestressed cylindrical concrete tanks with fixed wall-floor joints.

Some research was carried out to determine the thermal loads acting on cylindrical concrete tanks (Priestley 1976, Wood and Adams 1977 and Jofriet et al 1991). However, little research was done in order to determine analytically the stresses produced in cylindrical tanks due to the thermal loads. It has been proved by Ghali and Elliott (1992) and confirmed by the present research that these stresses are of significant magnitudes exceeding the magnitudes of the stresses produced by the liquid loads.

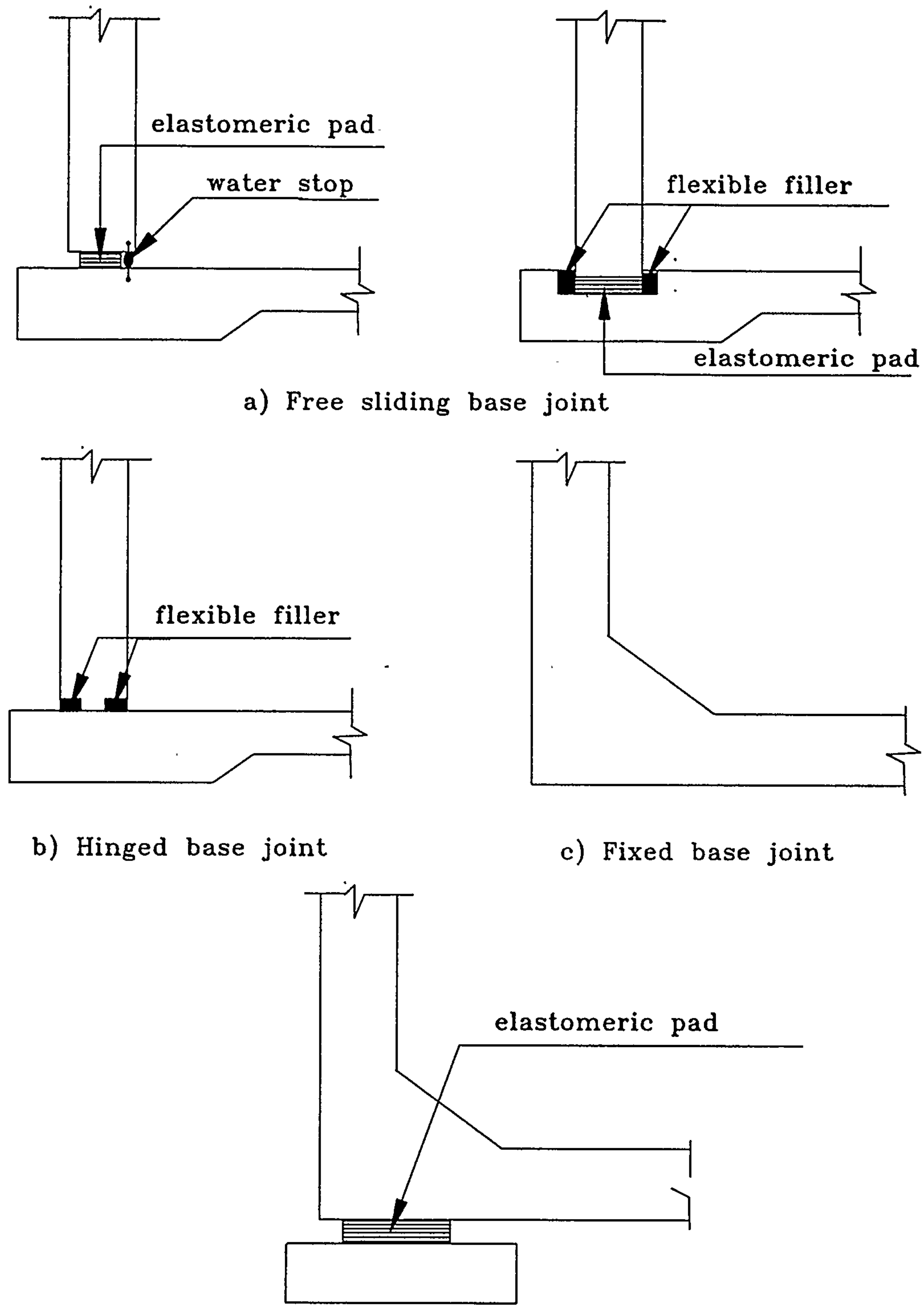

Figure 1.1 Wall-base joint types for circular concrete tanks

This also confirms the findings of Slater (1985), who investigated the performance of 53 reinforced and prestressed concrete tanks in Ontario and attributed the deterioration of some of the tanks to thermal effects.

Two thirds of the surveyed tanks were defective. The reason, he concluded, for the defects were the unexpected stresses produced by internal ice formation, thermal gradients and shrinkage.

Thermal stresses in concrete structures are greatly alleviated by cracking. The reduction in stiffness due to cracking causes the stresses to be much smaller than the stresses determined by elastic analysis. Nonlinear analysis is essential to determine the actual thermal stresses.

A nonlinear finite element analysis is performed for two tanks:

1) a reinforced (non-prestressed) circular tank (Tank 1),

2) a circumferentially and vertically prestressed tank (Tank 2).

The aim of this analysis is to investigate the actual thermal effects on concrete circular tanks. A study of the widths of the associated cracks is carried out along with a parametric study of the controlling factors.

1.2 OBJECTIVES OF THE THESIS

The objectives of this research are:

1) To study the nonlinear behavior of circular concrete tanks under variable temperature differences.

2) To study the parameters that effect crack width.

1.3 OUTLINE OF THE THESIS

The second chapter deals with elastic linear analysis and behavior of circular tanks subjected to liquid and/or thermal loads. A structural design of a reinforced and a prestressed circular tank is performed based on the ACI 350-89, ACI 344-88 and BS 8007 (1987).

In the third chapter, the procedure of the nonlinear finite element analysis is discussed based on the computer program used.

The finite element model used for the analysis is presented in Chapter 4. The results of the nonlinear analysis are discussed in the same chapter.

A detailed study of the effects of increasing thermal loads on a reinforced concrete circular tank, without prestressing, is discussed in Chapter 5.

The crack width calculation according to the CEB FIP (1990), ACI 224-86 and BS 8110 (1987) are discussed in Chapter 6. A parametric study is performed on crack width control in the same chapter.

At the end, the conclusions of the study and some recommendations for practical tank design and for further research are presented in Chapter 7.

CHAPTER 2

ELASTIC ANALYSIS OF CIRCULAR CYLINDRICAL TANKS

2.1 INTRODUCTION

This chapter presents a review of some aspects concerning the elastic analysis of circular cylindrical tanks. A common analogy with beams on elastic foundation and its derivation is reviewed. A set of equations for the elastic analysis for thermal loads are presented. The internal forces resulted from some critical load combinations are investigated.

2.2 BEAM-ON-ELASTIC-FOUNDATION ANALOGY

The cylindrical tank is an axi-symmetrical structure and it is sufficient to consider the forces and deformations of an elemental strip parallel to the cylinder axis for its structural analysis. The radial deflection of that strip is accompanied by hoop forces make the strip behave as a beam on elastic foundation. The transverse reaction at each point is proportional to the radial deflection (Ghali 1979).

Consider an axi-symmetrical outward radial loading of intensity q per unit area acting on a cylindrical shell of thickness t, radius r and an elastic modulus E (Fig. 2.1). This loading will cause a radial deflection w accompanied by a circumferential strain of magnitude w/r and a hoop force per unit length N_ϕ (Fig. 2.2) where:

$$N_\phi = \frac{w}{r} E\ t \tag{2.1}$$

A radial force $N_{\phi r}$ per unit circumferential width is created where,

$$N_{\phi r} = -\frac{N_\phi}{r} = -w\ E\ \frac{t}{r^2} \tag{2.2}$$

$N_{\phi r}$ is acting in the inward direction. The strip is thus behaving as a beam on elastic foundation subjected to external applied load of intensity q and receiving an elastic reaction of intensity $N_{\phi r}$, such that $N_{\phi r}$ = -kw. Thus the modulus of the foundation is given by:

$$k = \frac{E\ t}{r^2} \tag{2.3}$$

The flexural rigidity of the strip of unit width is equal to:

$$EI = \frac{E\ t^3}{12\ (\ 1 - \nu^2\ )} \tag{2.4}$$

where ν is the Poisson's ratio. The increase in the flexural rigidity, compared to that of strip of unit width and thickness t is caused by the circumferential moment M_ϕ where:

$$M_\phi = \nu\ M_x \tag{2.5}$$

and M_x is the vertical bending moment caused by the external load on the strip. Summing up the forces in the radial direction (Fig. 2.2) we get:

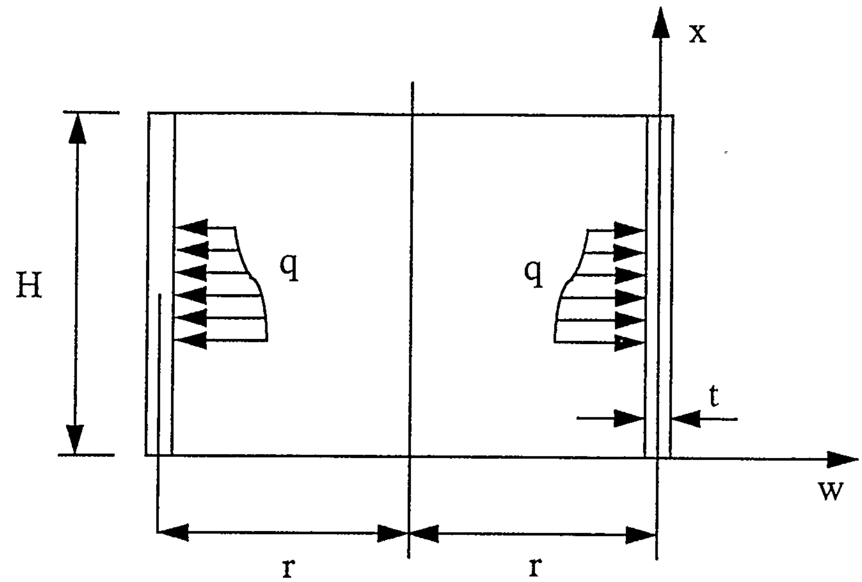

Figure 2.1 Positive directions of load and deflections in a cylindrical tank

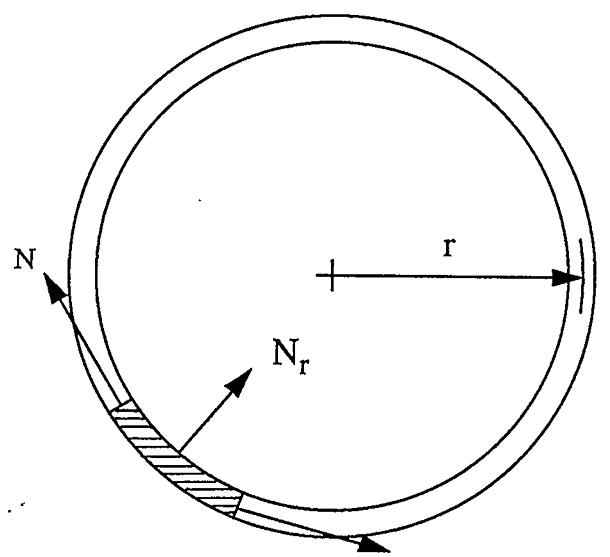

Figure 2.2 Section normal to the cylinder axis showing the radial resultant of the hoop forces

$$p = q - k\,w \tag{2.6}$$

where p is the resultant transverse load at any position. The basic differential relations for a beam applies :

$$p = -\frac{dV}{dx} = -\frac{d^2M_x}{dx^2} \tag{2.7}$$

but

$$M_x = -EI\frac{d^2w}{dx^2} \tag{2.8}$$

Hence,

$$\frac{d^2}{dx^2}\left(EI\frac{d^2w}{dx^2}\right) + kw = q \tag{2.9}$$

which is the general differential equation for a beam supported on elastic foundation with modulus k and subjected to external load of intensity q.

2.3 ANALYSIS DUE TO TEMPERATURE LOADING

2.3.1 Introduction

One of the main load cases for the design of circular tanks is the temperature loading. Slater (1985) reported on cases of deteriorated prestressed concrete tanks in Ontario and he concluded that one of the important causes of failure was the temperature differential effects. Ghali and Elliott (1992) and Priestley (1985) showed that tensile stresses produced by thermal loads were sufficient to cause cracking of prestressed tanks. The next sections deal with the elastic analysis due to temperature loadings. The inelastic analysis is presented later in Chapters 4 and 5.

2.3.2 Thermal Loads

Priestley (1976) investigated the problem of thermal stresses induced in prestressed concrete cylindrical water reservoirs by diurnal fluctuations of ambient conditions using actual meteorological records, of Christchurch, New Zealand. He used a dynamic heat-flow analysis to investigate the likely magnitude of temperature gradients induced in tank walls. He concluded that prestressed concrete water reservoirs should be designed for the effects of thermal gradients through the wall. A temperature difference of 30°C with the outside hotter than the inside and a difference of 20°C outside colder than the inside could be considered for climates similar to the climate of Christchurch.

However, for different local meteorological data, different thermal gradient could be adopted. Jofriet and Jiang (1991) used meteorological records of southern Ontario to determine the temperature gradients in walls of cylindrical tanks. They carried out a number of transient heat transfer finite element analyses and recommended the following for the circular tank design:

1) A temperature difference of 25°C between the outer and inner faces of the tank wall for a summer day, with the temperature at the inner face equal to the water temperature of 10°C.

2) A temperature difference of 25°C for a winter day, with the temperature at the inner face equal to the water temperature of 5°C.

In the present study a temperature difference of 30°C is considered for the case representing a summer day, with the inside colder than the outside; water temperature = 15°C. In addition, the case of a winter day is examined, assuming a temperature difference of 25°C, with the tank empty and a temperature of 5°C is assumed for the warmer inside face.

Usually, thermal loads are not axi-symmetrical, however, the maximum stresses are obtained by assuming axi-symmetrical temperature gradients (Priestley 1985, Ghali and Elliott 1992).

It is here assumed that the temperature distribution over the wall thickness is the same at all levels (over the whole height of the wall). However, in many practical cases the exterior surface of the wall is covered with earth over the lower part of the height. This has a favourable effect, particularly when the wall is rigidly connected to the base as considered in this thesis.

But, one must consider the conditions during construction and testing of the tank; in such case the full height of the wall is commonly not covered by filling at this stage. For this reason, and for the sake of simplicity, the full height of the wall is considered subjected to the same temperature distributions in the analysis presented below.

2.3.3 Analysis due to Temperature Loads

In order to analyze the circular tank due to the previously mentioned thermal loads, the beam-on-elastic-foundation analogy is to be recalled. A set of equations were proposed by Ghali and Elliott (1992) for the thermal analysis of a semi-infinitely long strip resting on elastic foundation, which represented the case of a deep tank. The tank is assumed "deep" when its height H satisfies the following condition (Ghali 1979):

$$H \geq \frac{\pi}{\beta} \qquad (2.10)$$

where:

$$\beta = \frac{[\,3\,(\,1-\nu^2\,)\,]^{\frac{1}{4}}}{\sqrt{rt}} \qquad (2.11)$$

where t is the wall thickness and ν is Poisson's ratio. Substituting ν=0.15 we get:

$$\frac{H^2}{r\,t} \geq 5.76 \qquad (2.12)$$

Many tanks in practice satisfy this inequality.

In addition, the temperature distribution along the wall thickness is assumed linear and axi-symmetrical, where T_i is the temperature at the inner face and T_o the temperature at the outer face of the tank wall.

The present study is interested mainly in fixed base tanks. The equations for the thermal elastic analysis for this case are as follows:

$$N_\phi = -E\alpha\left[\frac{t}{2}(T_o+T_i)Z_1 + \frac{(1+\nu)}{2r\beta^2}(T_o-T_i)\bar{Z}_3\right] \tag{2.13}$$

$$M_\phi = -E\alpha\left[\frac{\nu r\beta^2 t^3}{12(1-\nu^2)}(T_o+T_i)Z_3 + \frac{t^2}{12(1-\nu)}(T_o-T_i)(1-\nu\bar{Z}_1)\right] \tag{2.14}$$

$$M_x = -E\alpha\left[\frac{r\beta^2 t^3}{12(1-\nu^2)}(T_o+T_i)Z_3 + \frac{t^2}{12(1-\nu)}(T_o-T_i)(1-\bar{Z}_1)\right] \tag{2.15}$$

where,

$$Z_1 = e^{-\beta x}(\cos\beta x + \sin\beta x)$$
$$\bar{Z}_1 = e^{-\beta\bar{x}}(\cos\beta\bar{x} + \sin\beta\bar{x}) \tag{2.16}$$

$$Z_3 = e^{-\beta x}(\cos\beta x - \sin\beta x)$$
$$\bar{Z}_3 = e^{-\beta\bar{x}}(\cos\beta\bar{x} - \sin\beta\bar{x}) \tag{2.17}$$

where $\bar{x} = H - x$ (Fig. 2.1).

2.4 COMPUTER ANALYSIS

The elastic analyses of circular prestressed tanks subjected to liquid load and/or temperature loads are performed using the computer program PCT (Prestressed Concrete Tanks) developed by Ghali (1990). The Program performs analysis to circular cylindrical walls of variable thickness subjected to axi-symmetrical external applied loads or to temperature variations.

The Program can analyze for the following load types:

1) Concentrated line load: to account for circumferential prestressing tendons.

2) Trapezoidal surface load: to account for the case of liquid load or distributed circumferential prestressing.

3) Thermal load: to account for the case of temperature rise or drop varying linearly between the outer and inner faces of the wall.

4) Prescribed radial and/or rotation at bottom or top edge: to account for the case of vertical prestressing.

5) Distributed load defined by a shape function: to help in derivation of the optimum circumferential prestress distribution (Ghali and Elliott 1991).

The Program uses the finite difference method to solve the following equation, which is the governing differential equation of a beam on elastic foundation (Eq. 2.9) using central differences :

$$\frac{d^2}{dx^2} \left(EI \frac{d^2 w}{dx^2} \right) + kw = q \tag{2.18}$$

At a general node i away from the edges, the finite-difference form of Eq. 2.18 is (Ghali 1979):

$$\frac{EI_r}{\lambda^3}\left[J_{i-1} \quad -2(J_{i-1}+J_i) \quad J_{i-1}+4J_i+J_{i+1}+C_i \quad -2(J_i+J_{i+1}) \quad J_{i+1}\right] \times \begin{Bmatrix} w_{i-2} \\ w_{i-1} \\ w_i \\ w_{i+1} \\ w_{i+2} \end{Bmatrix} = Q_i \tag{2.19}$$

where,

E is the elastic modulus of the construction material.

I_r is the reference moment of inertia at an arbitrary chosen node, usually at base.

λ is the spacing between the nodes.

$J_i = \frac{I_i}{I_r}$, where $I_i = \frac{t_i^3}{12\,(1-\nu^2)}$, t_i is the thickness at node i and ν is Poisson's ratio.

$C_i = \frac{k_i \lambda^4}{E\ I_r}$, where k_i is the modulus of elastic modulus at node i.

$k_i = \frac{Et_i}{r^2}$, where r is the radius of the cylinder.

w_i is the radial deflection at node i.

Q_i is an equivalent concentrated load at node i.

At top and bottom edges the coefficients of w in the finite-difference equation are adjusted according to the boundary condition. Fictitious nodes are assumed outside the wall; their deflections are eliminated by expressing their values in terms of the deflections at other nodes.

A set of simultaneous equations are generated by applying the finite-difference equation at n nodes in order to determine the unknown deflections {w}. The equations are in the following form:

$$[A]_{nxn}\{w\}_{nx1} = \{Q\}_{nx1} \tag{2.20}$$

where the matrix [A] includes the coefficients of {w}. The determined deflections w are then used to calculate the hoop forces N_ϕ and the vertical moments M_x at each node according to the following equations:

$$N_{\phi i} = \left(\frac{Eh_i}{r}\right) w_i \tag{2.21}$$

$$M_{xi} = \left(\frac{EI_r}{\lambda^2}\right) J_i \left(-w_{i-1}+2w_i-w_{i+1}\right) \tag{2.22}$$

2.5 LINEAR STRUCTURAL ANALYSIS OF CYLINDRICAL TANKS

In the present study the behavior of two circular tanks subjected to liquid and/or temperature loads is investigated. Tank 1 is a cylindrical reinforced concrete tank, while Tank 2 is a cylindrical prestressed tank. Both tanks are fixed at the base and free at the top. Figures 2.3 and 2.4 show the details of the reinforcement* (prestressed and non-prestressed) in a horizontal cross-section at the base of the walls of Tanks 1 and 2, respectively. Vertical cross-sections are also provided in Figs. 2.5 and 2.6 for both tanks. The arrangement of the reinforcement is basically the same for all the applications in the other chapters. However, the steel ratios, ρ_{iv} and ρ_{ov}, and the vertical prestress, σ_{vp} are variable according to the different applications; ρ_{iv} and ρ_{ov} are the vertical steel ratios at the inner and the outer faces of the tank walls, respectively. Table 2.1 summarizes the dimensions and material properties of Tanks 1 and 2.

Table 2.1 Dimensions and material properties of Tanks 1 and 2

	H (m)	r (m)	t (m)	E_c (MPa)	ν	α (°C^{-1})
Tank 1	7.0	12.5	0.3	31.6E6	0.167	1E-5
Tank 2	12.0	25.0	0.3	31.6E6	0.167	1E-5

* At a late stage it was noted that the circumferential steel in Tank 1 is not sufficient to resist the hoop force due to hydrostatic pressure. Repetition of the nonlinear analysis, increasing the hoop reinforcement from 600 mm^2 to 2100 mm^2 (Fig. 2.3) give negligible change in the moment M_x at the base. Thus, this has no influence on the conclusions of this thesis.

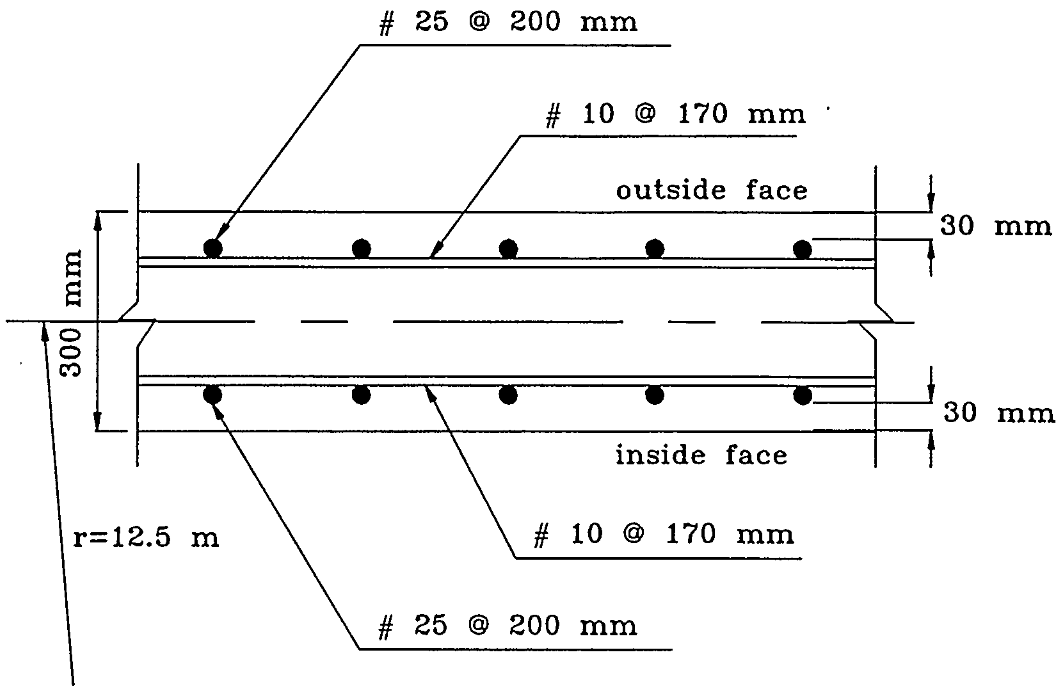

Figure 2.3 Horizontal wall cross-section at base of Tank 1

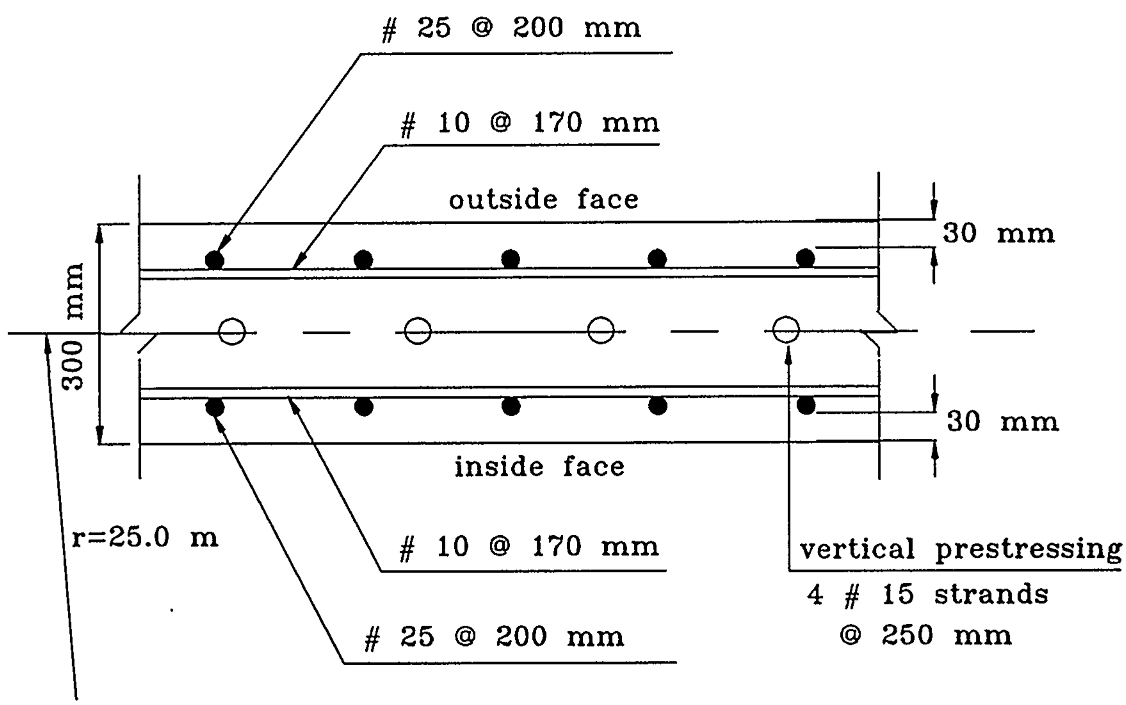

Figure 2.4 Horizontal wall cross-section at base of Tank 2

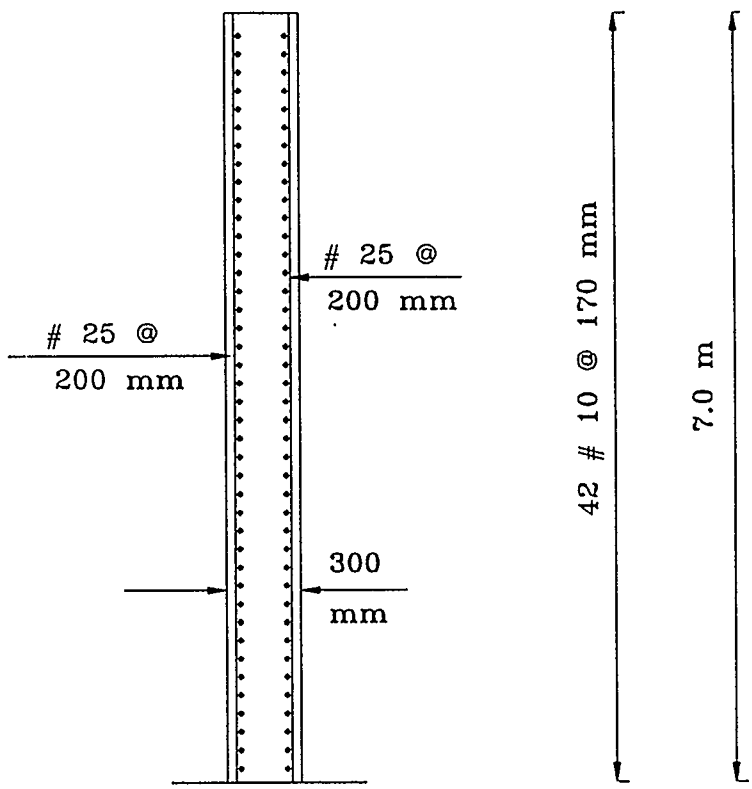

Figure 2.5 Full height vertical wall cross-section of Tank 1

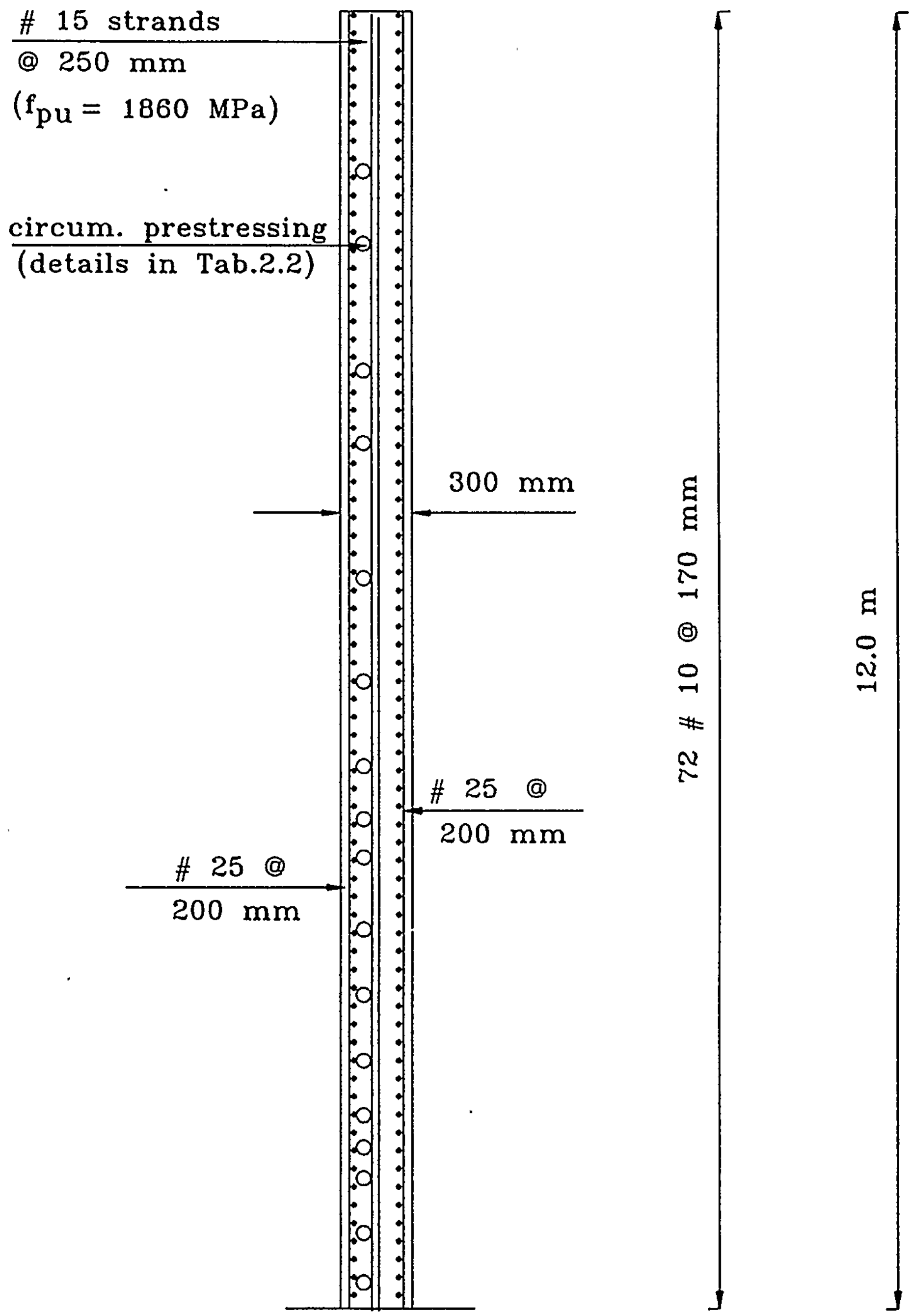

Figure 2.6 Full height vertical wall cross-section of Tank 2

The loads considered are mainly:

1) The Liquid Load (ll):

This study is interested mainly in water tanks. The water level is taken at the top edge of the tank for a full tank (γ_w = 9.81 kN/m^3).

2) The Prestressing Load :

Tank 2 is prestressed in the circumferential and vertical directions. For the preliminary linear analysis, a vertical prestress of 2.0 MPa is estimated. The conventional distribution of circumferential prestress is applied, in order to balance the effect of the liquid load, providing a residual compression of 1.0 MPa (Fig. 2.7). Table 2.2 shows the circumferential prestressed reinforcements and their locations, where:

x is a vertical distance measured from base,

P is the applied prestressing force,

f_p is the prestress per strand.

3) The Temperature Load:

a) Nonuniform temperature rise (tr): T_o = 45°C and T_i = 15°C.

b) Nonuniform temperature drop (td): T_o = -20°C and T_i = 5°C.

2.5.1 Analysis Results

The computer program PCT is used to perform the elastic analysis. The following sign conventions are adopted:

- the hoop force is positive when tensile;

Table 2.2 The circumferential prestressing of Tank 2

x (m)	Reinforcement	P (MN)	f_p (MPa)
0.23	7 x 7 wire strand # 15*	1.358	1.386
0.71	7 x 7 wire strand # 15	1.358	1.386
1.22	7 x 7 wire strand # 15	1.358	1.386
1.50	7 x 7 wire strand # 13**	0.900	1.300
1.74	7 x 7 wire strand # 15	1.358	1.386
2.30	7 x 7 wire strand # 15	1.358	1.386
2.89	7 x 7 wire strand # 15	1.358	1.386
3.50	7 x 7 wire strand # 15	1.358	1.386
4.20	7 x 7 wire strand # 15	1.358	1.386
4.50	7 x 7 wire strand # 13	0.900	1.300
5.00	7 x 7 wire strand # 15	1.358	1.386
5.78	7 x 7 wire strand # 15	1.358	1.386
6.75	7 x 7 wire strand # 15	1.358	1.386
7.50	7 x 7 wire strand # 13	0.900	1.300
8.00	7 x 7 wire strand # 15	1.358	1.386
9.78	7 x 7 wire strand # 15	1.358	1.386
10.50	7 x 7 wire strand # 13	0.900	1.300

* one 7-wire strand #15 has cross-section area = 140 mm^2
** one 7-wire strand #13 has cross-section area = 99 mm^2

- the bending moment (vertical and circumferential) is positive when producing tension at the outer face of the wall;
- an outward radial pressure is considered positive.

Tank 1

1) Liquid load: The water level is taken at the top edge of the tank. The resulting internal forces are plotted in Fig. 2.8.

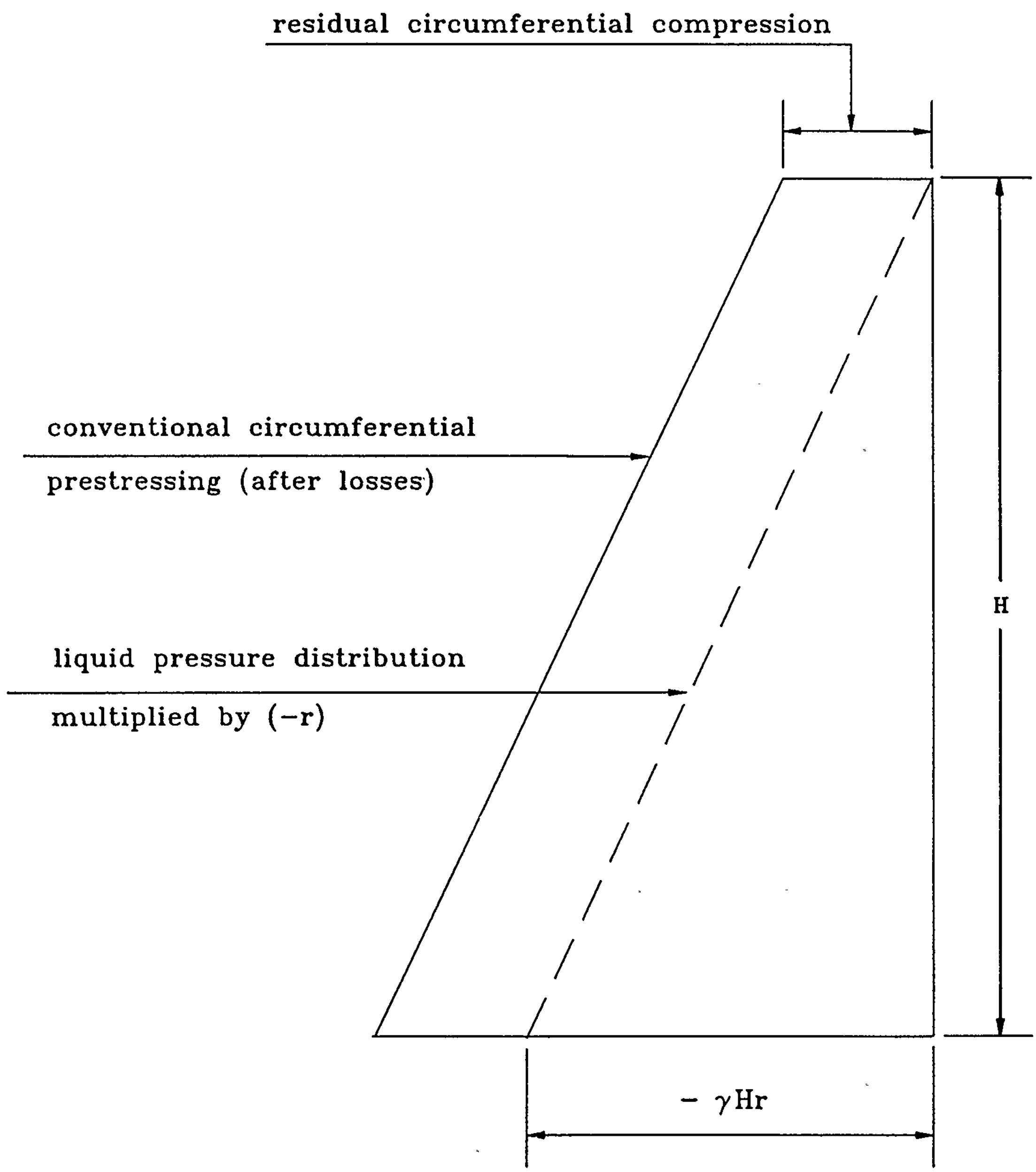

Figure 2.7 Conventional circumferential prestressing.

As could be seen, the maximum vertical negative moment M_x occurs at base. The values of the circumferential moments M_ϕ are the same as those of M_x multiplied by ν.

The hoop force distribution is proportional to the distribution of the radial deflections.

2) Uniform temperature rise: A uniform temperature rise of 30°C is applied to Tank 1. The internal force diagrams are shown in Fig. 2.9. Due to the rise of temperature, the tank expands in the both the radial and the vertical directions. However, the expansion is prevented at base due to the fixation. As a result, vertical tensile stresses are created at the inside face of the tank wall at base. This explains the negative values of M_x and M_ϕ at base, where M_ϕ is equal to νM_x. On the other hand, N_ϕ has a negative value at bottom (compression) as reaction to the restraining of the outward radial deflection.

3) Temperature gradient: T_o = 15°C and T_i = -15°C with a linear variation through the thickness. Due to the temperature differential the tank tends to curl in the vertical and the circumferential directions (Fig. 2.10b). However, the vertical rotation is restrained due to the axi-symmetry and the circumferential rotation is restrained at base due to the fixation. Consequentially, this restraint produces circumferential and vertical moments. M_ϕ is almost constant along the height of the tank, while M_x has a maximum value at base and a zero-value at the free top edge.

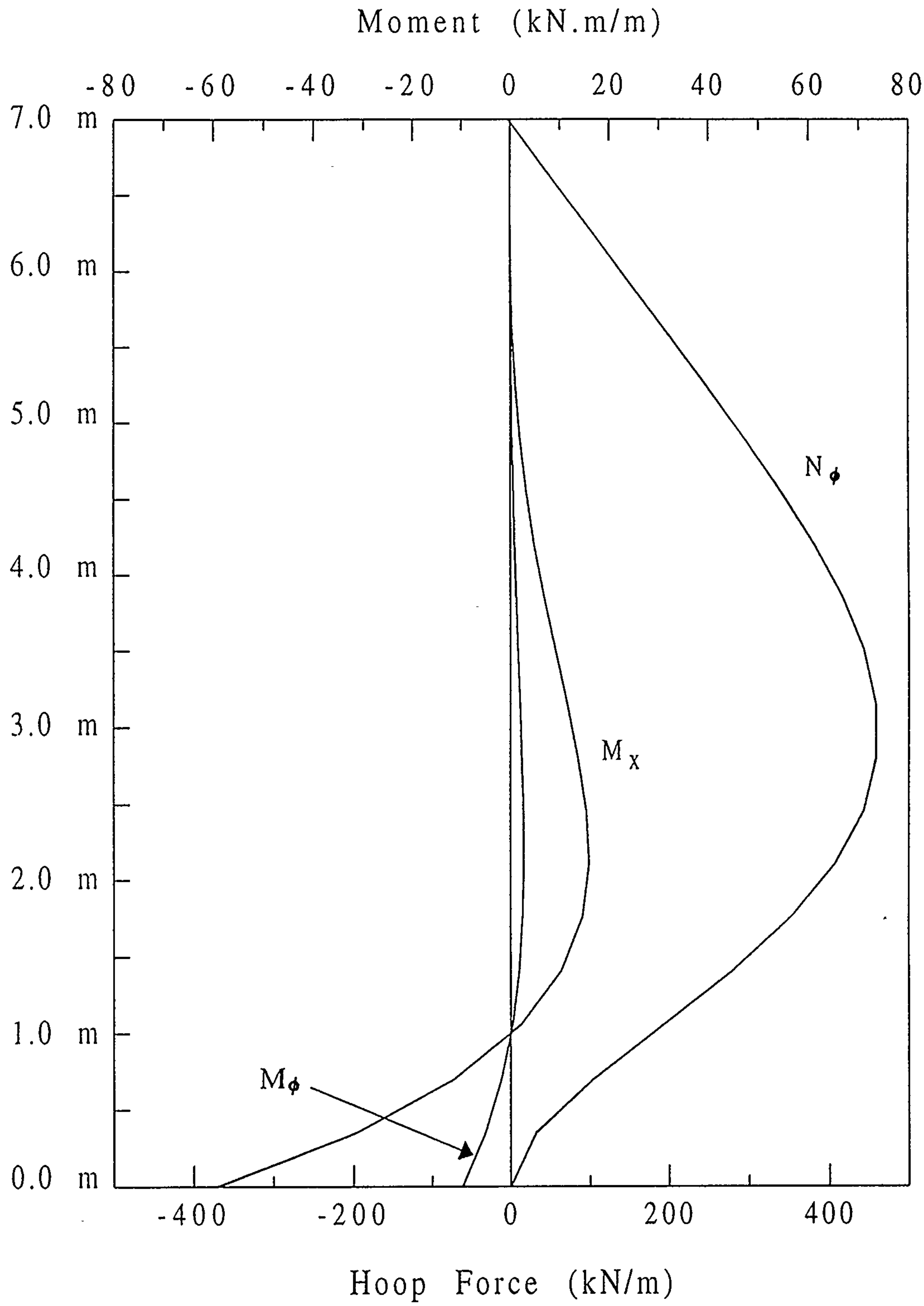

Figure 2.8 Internal forces due to liquid load for Tank 1

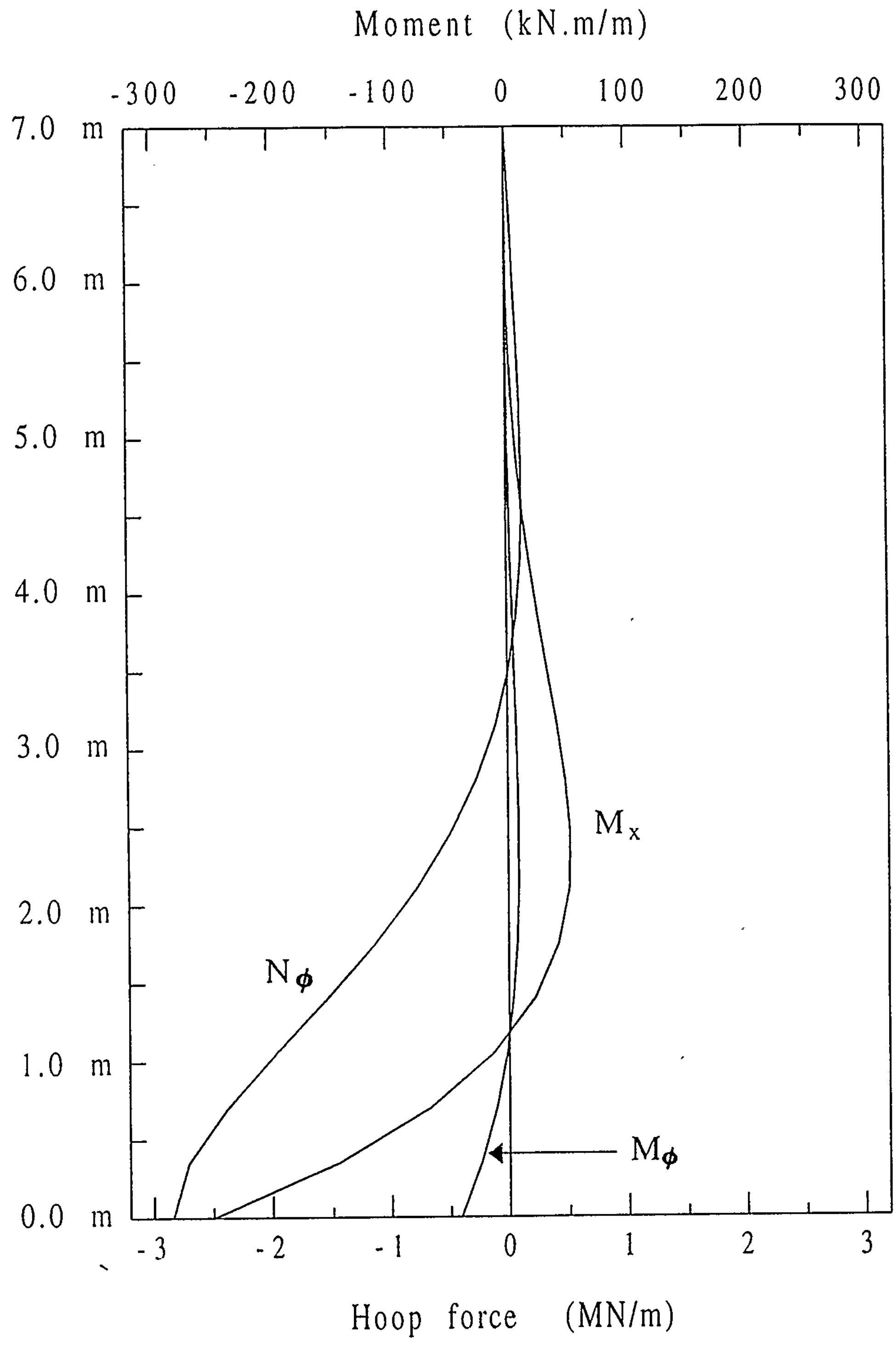

Figure 2.9 Internal forces due to uniform temperature rise for Tank 1 ($T_o = T_i = 30°C$)

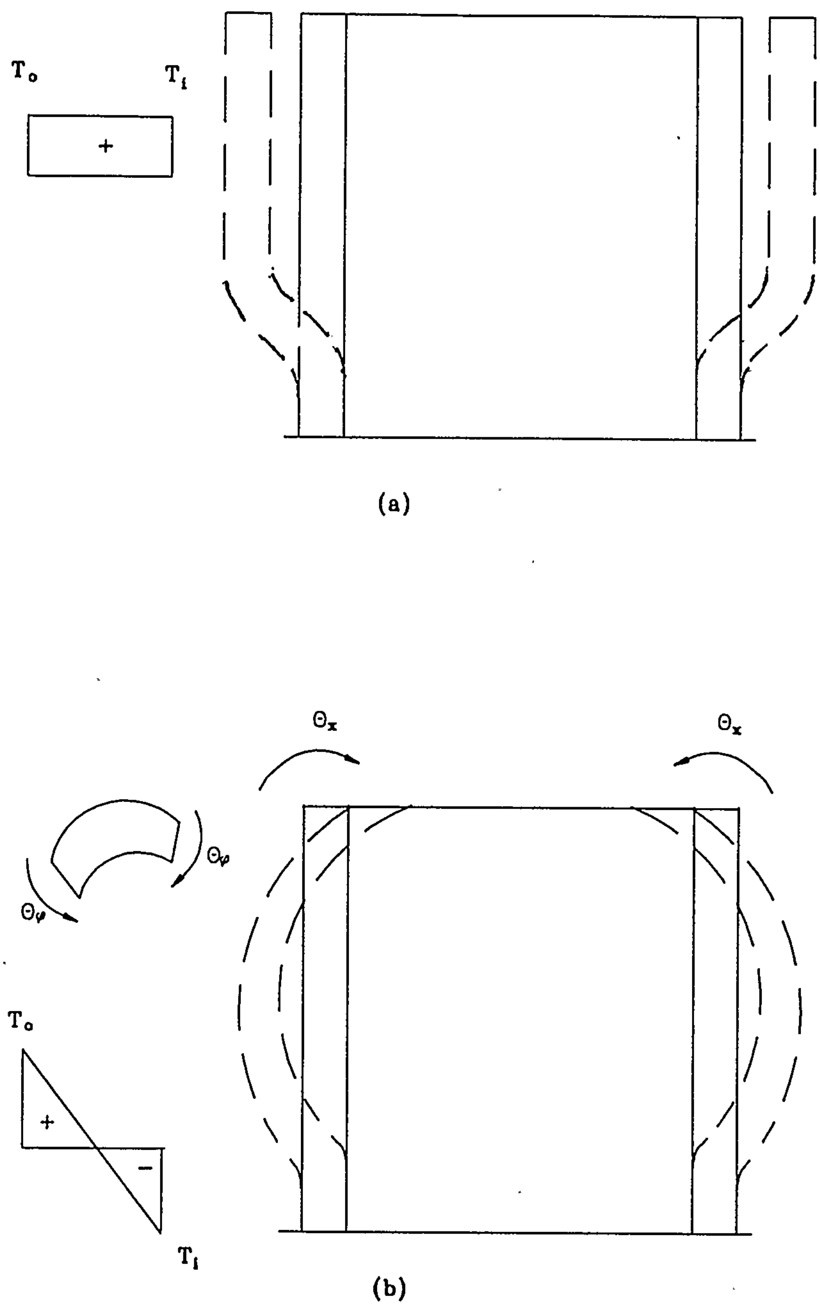

Figure 2.10 Deformed shapes of a cylindrical tank fixed at base due to temperature variations

a) uniform rise ($T_o = T_i$)

b) temperature gradient ($T_o > T_i$)

However, the N_ϕ-distribution has the same shape as the distribution of the radial deflections (Fig. 2.11).

The internal-force diagrams in Fig. 2.12 are a result of the superposition of the internal forces of the load cases 2 and 3. On the other hand, the diagrams of Fig. 2.13 have the same shape as those of Fig. 2.12 with a reversed sign.

The maximum values of the internal forces are shown in Table 2.3.

Table 2.3 Internal Forces For Tank 1

Case of loading	M_x (max) (kN.m/m)	x (m)	N_ϕ (max +ve) (kN/m)	x (m)	M_ϕ (max) (kN.m/m)	x (m)
ll	-60.0	0.0	+460.0	2.80	-10.0	4.20
tr	-335.0	0.0	+323.0	4.55	-81.0	4.55
td	+133.0	0.0	+711.0 +809.0	0.00 7.00	+81.5 +60.0	0.00 7.00
ll + tr	-394.0	0.0	+679.0	4.20	-80.0	4.20

Tank 2

1) Circumferential prestressing (cp): The prestressing forces are considered as concentrated line loads at the position of the prestressing tendons. The distribution of these forces is shown in Fig. 2.7. The internal forces have the same distribution as of the liquid load, but with a reversed sign (Fig. 2.14).

2) Vertical prestressing (vp): The vertical prestressing is presented by a prescribed radial inward translation at the bottom edge.

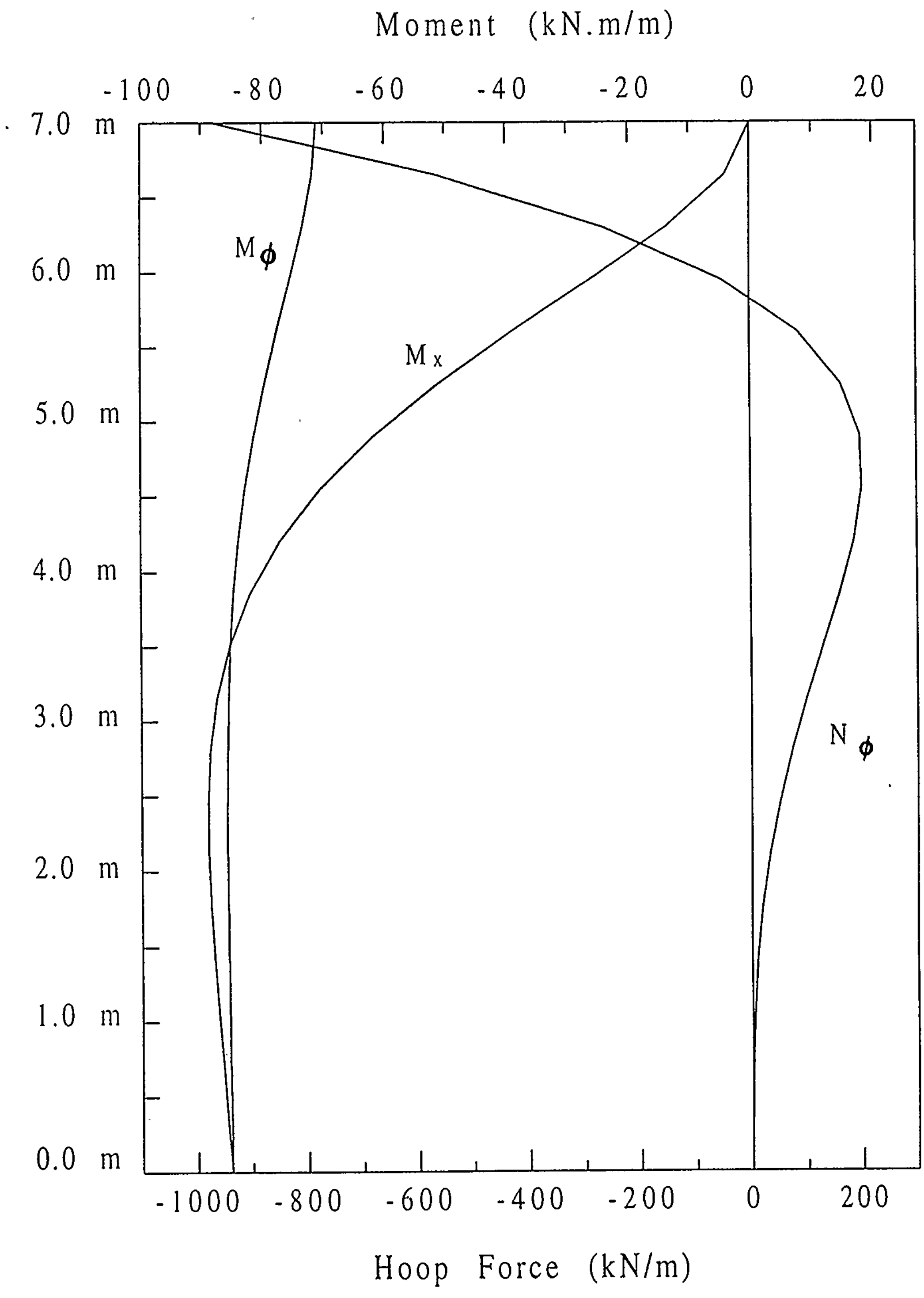

Figure 2.11 Internal forces due to temperature gradient for Tank 1 (T_o = 15°C, T_i = -15°C)

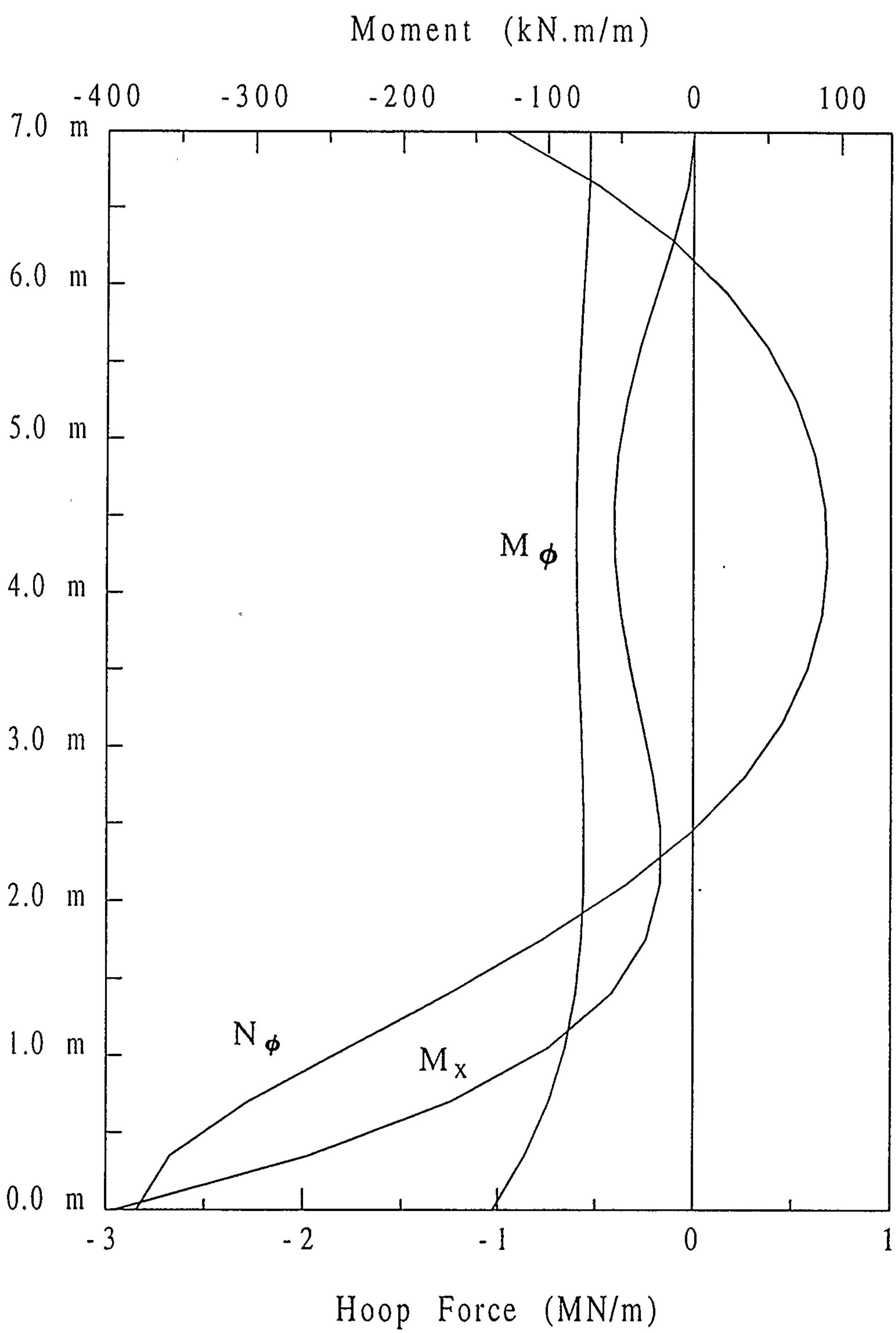

Figure 2.12 Internal forces due to liquid load + linear temperature rise for Tank 1 (T_o = 45°C, T_i = 15°C).

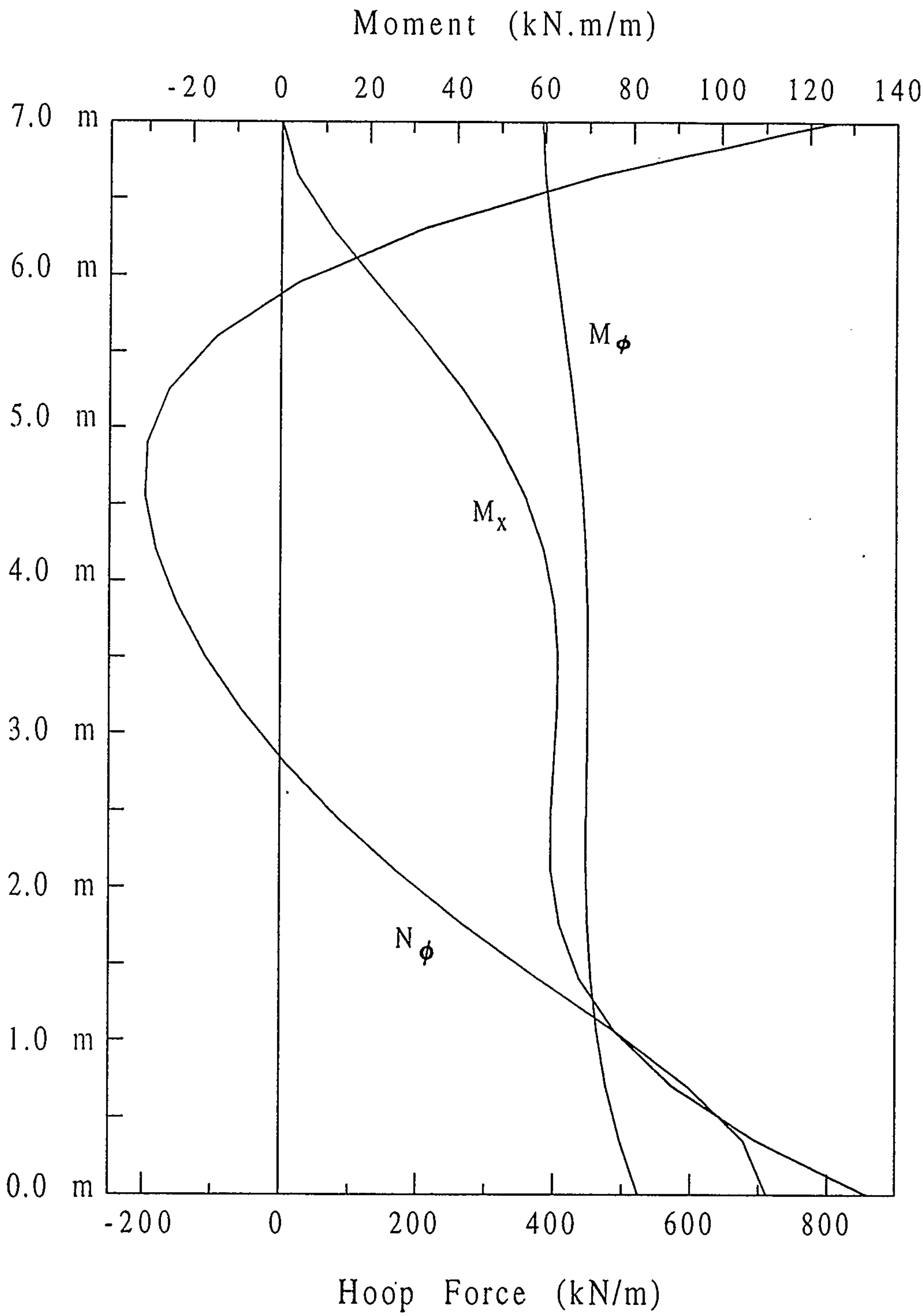

Figure 2.13 Internal forces due to linear temperature drop for Tank 1 (To = -20°C, Ti = 5°C)

For the prestressing force P the associated inward prescribed radial translation w (Fig. 2.15) is taken as:

$$w = \nu \frac{Pr}{Et} \tag{2.23}$$

The distribution of the internal forces is similar to the case of the uniform temperature rise previously discussed (Fig. 2.16).

The two critical loading cases mentioned for Tank 1 apply for Tank 2 after adding the vertical and circumferential prestressing. The distributions of the internal forces are plotted in Figs. 2.17 and 2.18.

The maximum and the absolute maximum values of the internal forces for each of the above mentioned loadings are shown in Tables 2.4 and 2.5, respectively.

Table 2.4 Maximum internal forces for Tank 2

Case of loading	M_x (at bottom) (kN.m/m)	N_ϕ (kN/m)	x (m)	M_ϕ (kN.m/m)	x (m)
cp	+244.0	0.0 -1290.0 -150.0	0.00 8.40 12.00	+41.0 +0.5 0.0	0.00 8.40 12.00
vp	-9.0	+100.0 +3.0 -1.0	0.00 8.40 12.00	0.0 -1.5 0.0	0.00 8.40 12.00
ll	-213.0	+954.0	8.40	-0.1	8.40
tr	-334.0	+273.0	8.40	-83.2	8.40
td	+133.0	+711.0 +816.0	0.00 12.00	+81.0 +59.0	0.00 12.00

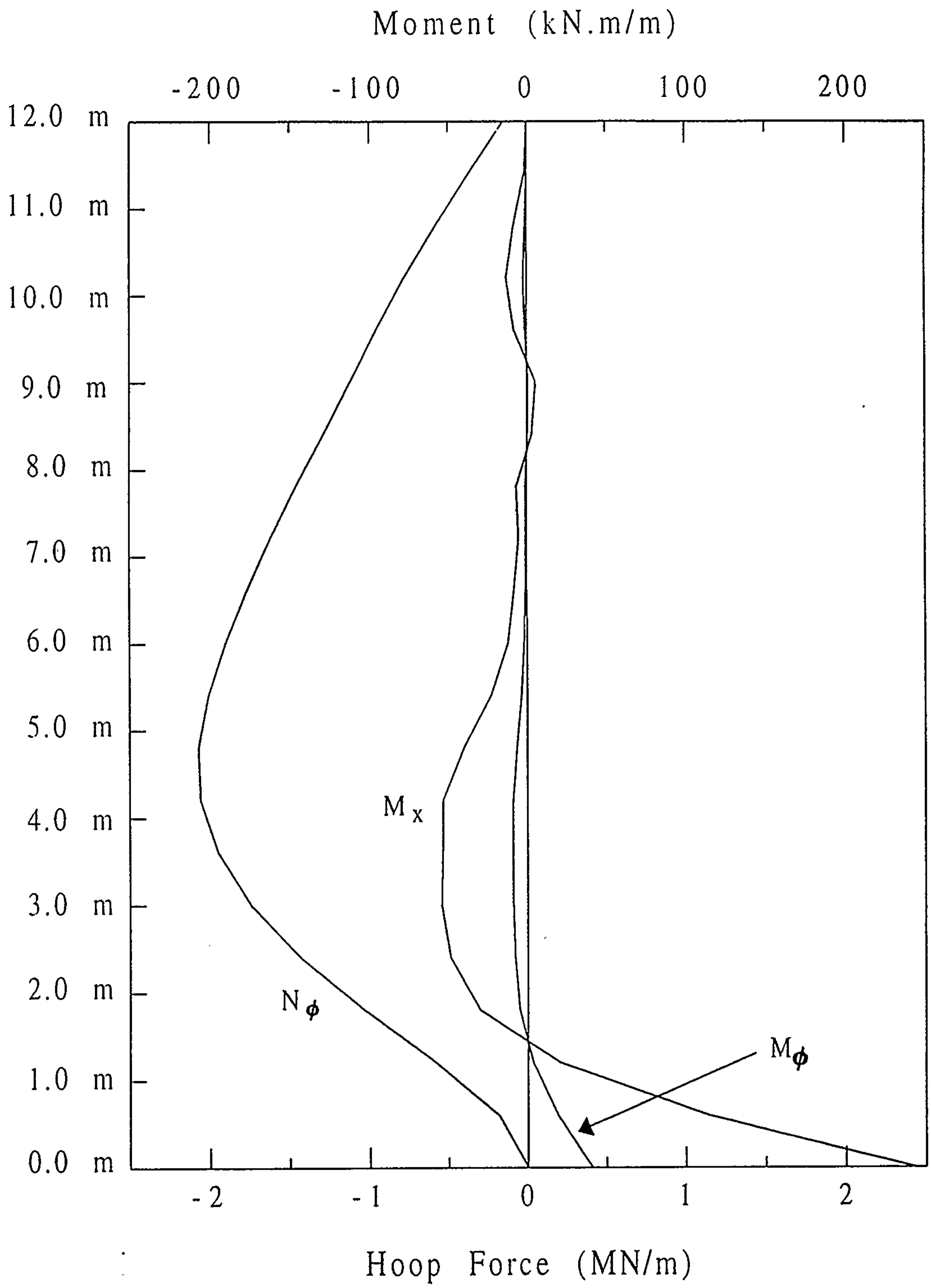

Figure 2.14 Internal forces due to circumferential prestressing for Tank 2 (residual compression = 1 MPa)

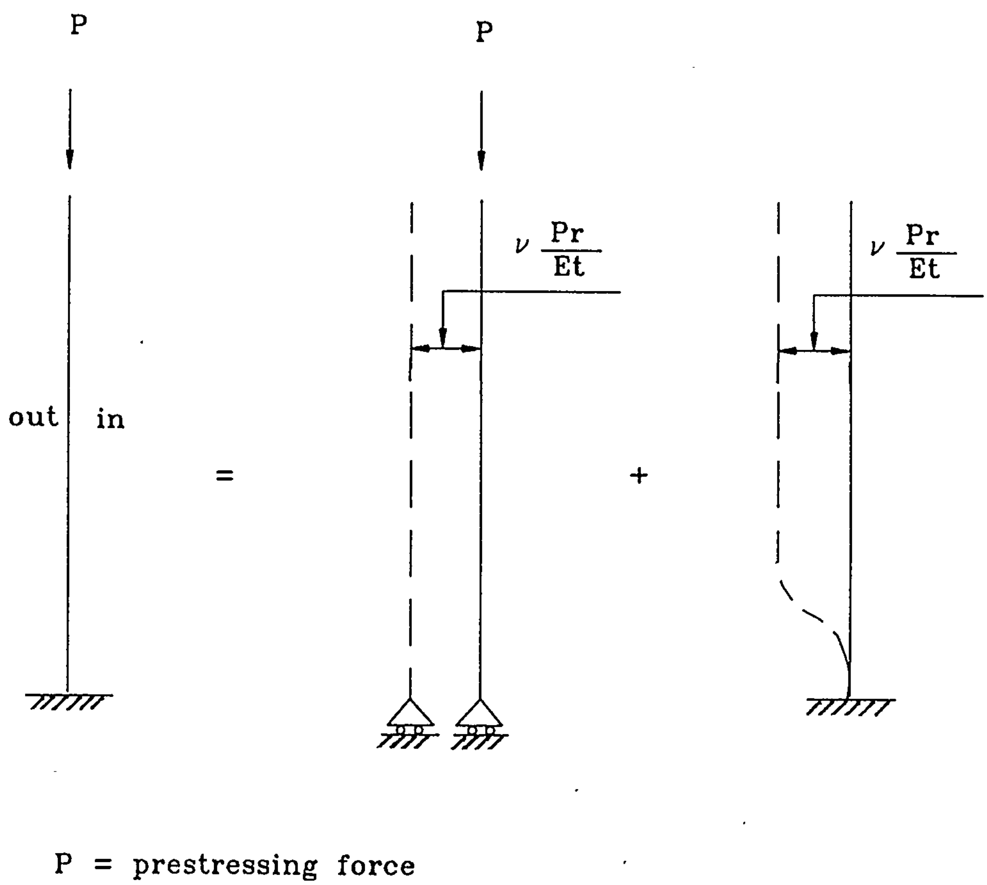

Figure 2.15 Radial effect of the vertical prestressing force on the circular tank

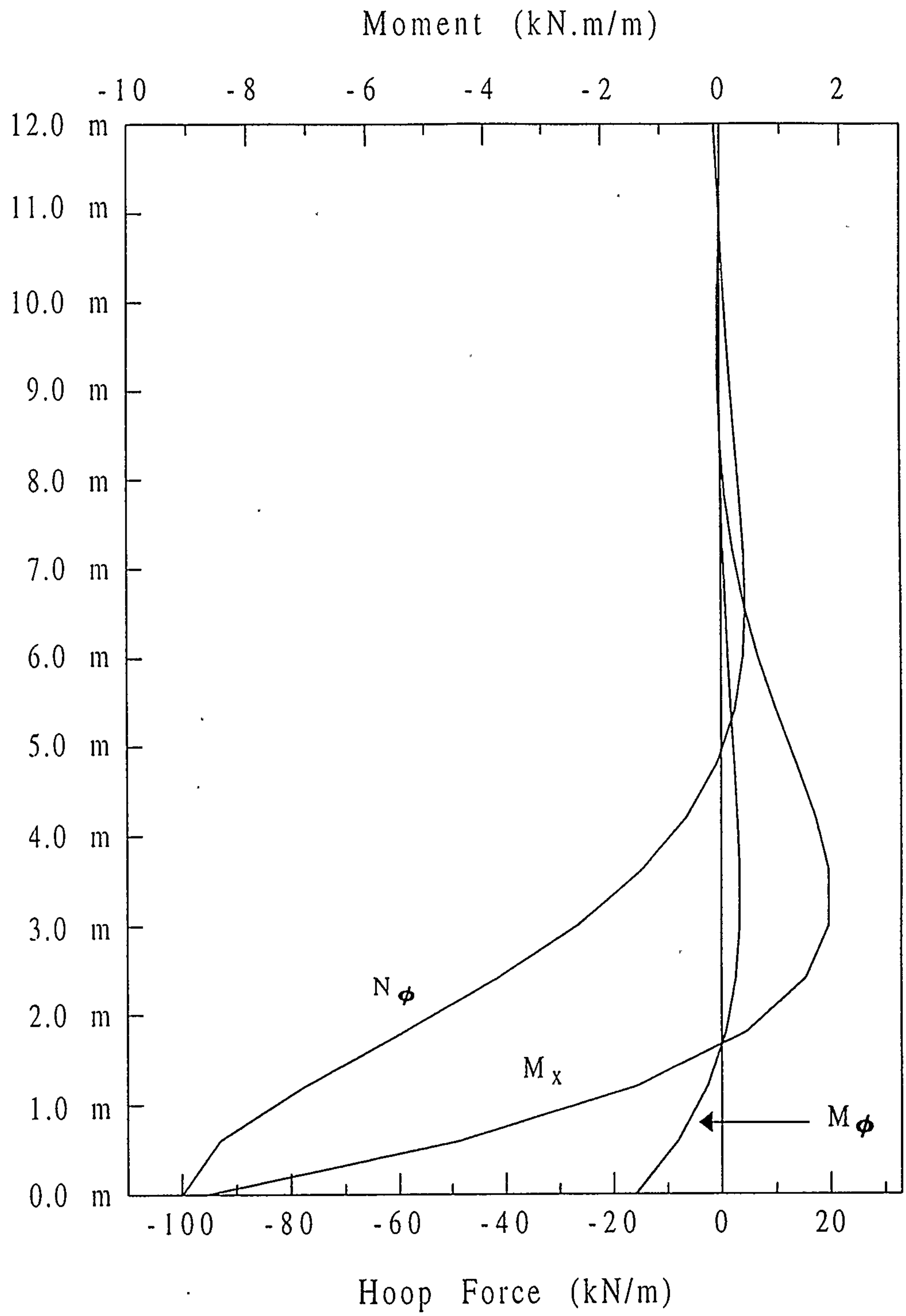

Figure 2.16 Internal forces due to vertical prestressing for Tank 2 (prestress = 2 MPa)

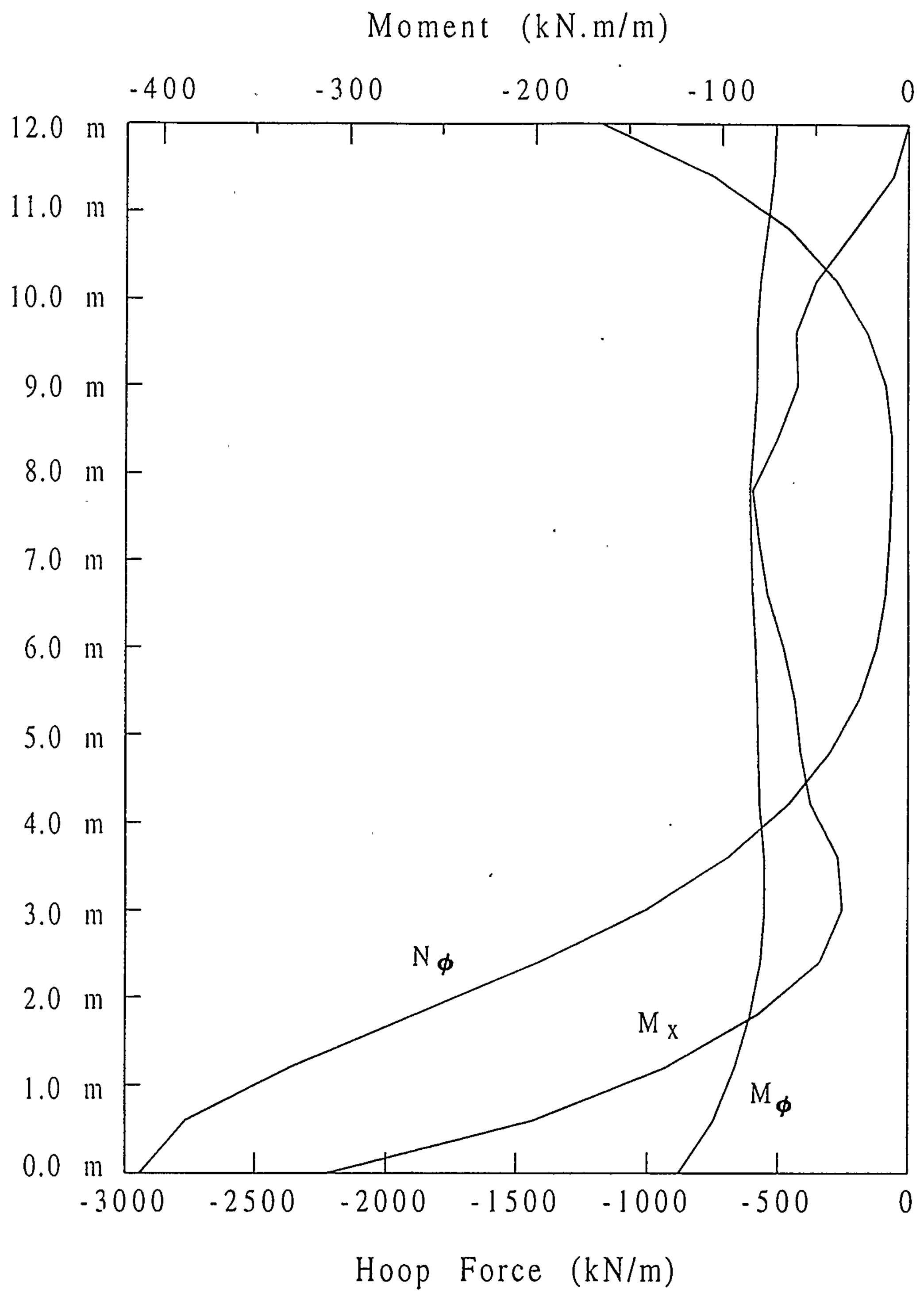

Figure 2.17 Internal forces due to prestressing + liquid load + temperature rise for Tank 2 (T_o= 45 °C, T_i = 15 °C).

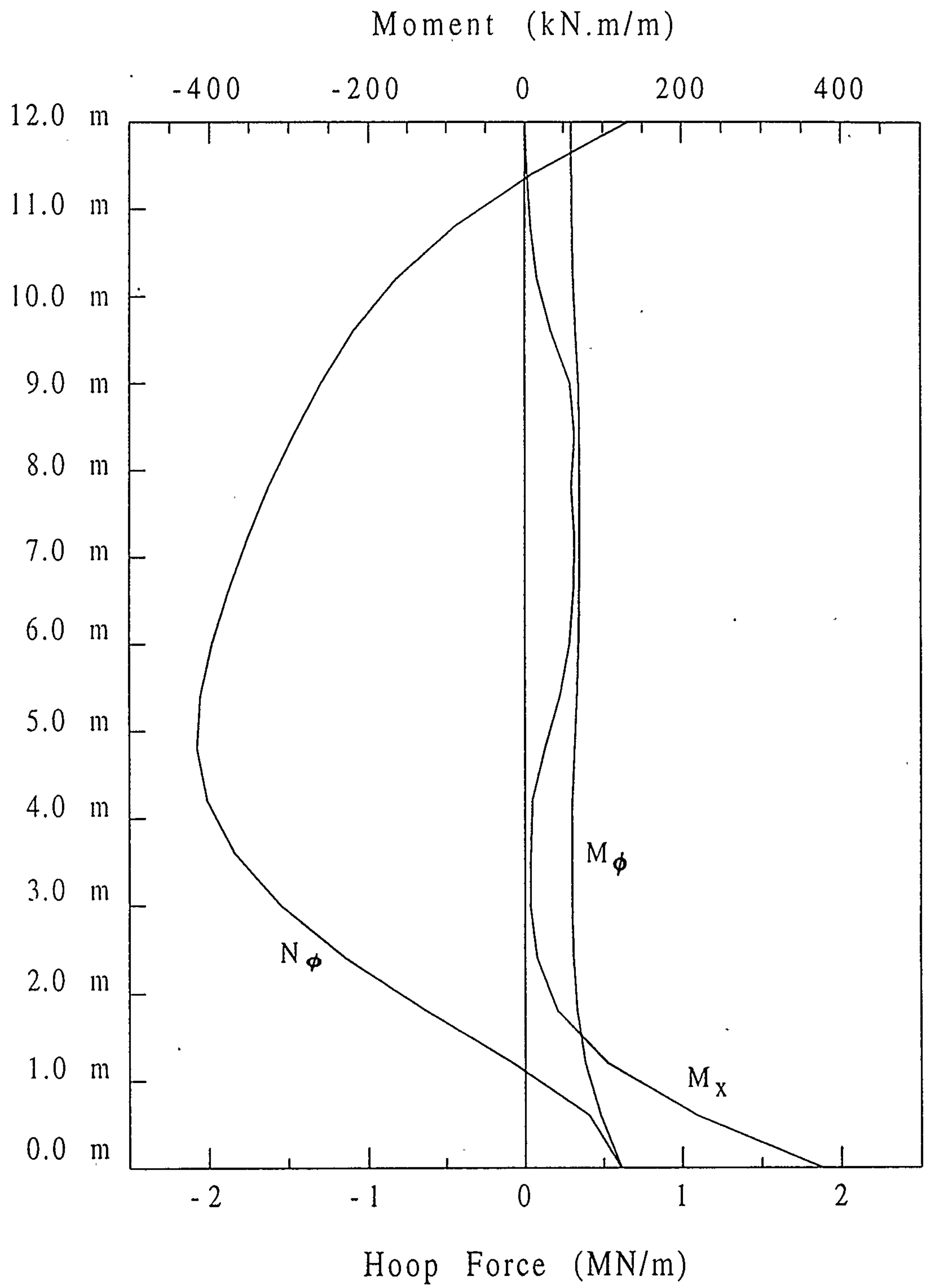

Figure 2.18 Internal Forces due to prestressing + temperature drop for Tank 2 (T_o = -20°C, T_i = 5°C).

Table 2.5 Absolute maximum internal forces for Tank 2

Load combination	M_x (max) (kN.m/m)	x (m)	N_ϕ (max +ve) (kN/m)	x (m)	M_ϕ (max) (kN.m/m)	x (m)
ll + tr + cp + vp	-312.0	0.00	-60.0 -63.0	8.40 7.80	-83.0 -85.0	8.40 7.80
td + cp + vp	+367.0	0.00	611.0 665.0	0.00 12.00	+120.5 +59.0	0.00 12.00

2.6 DESIGN OF TANKS

In this section the structural design of Tanks 1 and 2 is presented in accordance to the American and the British Design Codes. However, the reinforcement bars and the prestressing strands are chosen according to the specifications of the Canadian Standards CSA (G279-M82, CSA-G30.12-M77)

The stresses in concrete and steel are determined using the computer program CRACK (Ghali and Elbadry 1985) for all cross-sections.

2.6.1 The Design According to ACI 350-89 and ACI 344-88

ACI Committee 350 provides recommendations for the structural design of concrete tanks and reservoirs; while ACI Committee 344 provides the recommendations for the design and construction of prestressed tanks. The structural design recommendations for both committees are based on elastic cylindrical shell analysis.

Tank 1

The structural design of Tank 1 is based on the recommendations of ACI Committee 350 (89). The minimum cover for the reinforcement of the tank walls is equal to 2 in (51 mm). The strength design and the working stress design are accepted as two alternative methods for the structural design of the reinforced concrete tanks. In the present study the working stress design is employed in accordance to ACI 318-89 Appendix B. The maximum allowable compressive stress in concrete is limited to 0.45 f'_c, while the maximum stress in steel is determined according to the limitation of the quantity Z. The quantity Z is used to control the crack width according to the Gergely-Lutz Equation, as will be explained in Chapter 6. The quantity Z is defined by:

$$Z = f_s \sqrt[3]{d_c \, A} \tag{2.24}$$

where f_s is the stress in steel (ksi), d_c is the thickness of cover from tension fiber to center of closest rebar, and A is the area of concrete symmetric with reinforcing steel divided by numbers of bars (in^2). The value of Z is limited to 115 kips/in (20 kN/mm) for flexural reinforcement located in one layer. The report of ACI 350-89 presents a set of charts relating f_s, Z and the bar spacing s for different grades and sizes of steel bars, based on a concrete cover of 2 in (51 mm) or less.

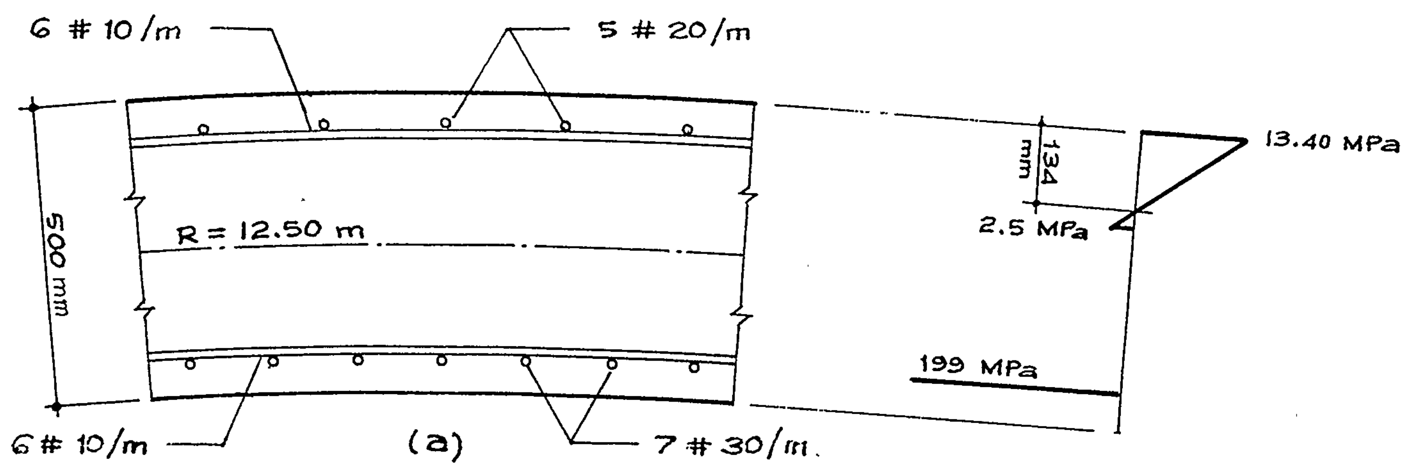

Figure 2.19 Wall cross-section at bottom for Tank 1. Design according to ACI 350. The stress distribution is for the effect of liquid load plus temperature rise (T_o=45°C, T_i=15°C). Cross-section areas of bars # 10, # 20, ... are given in Appendix B.

The maximum values of the internal forces mentioned in Table 2.3 are used for the structural design of the cross-section of the tank wall. The cross-section shown in Fig. 2.19 satisfies the above requirements.

Tank 2

Tank 2 is vertically and circumferentially prestressed due to its large dimensions. The recommended residual compression provided by the circumferential prestressing for open-top tanks is 400 psi (2.76 MPa) at the top, reducing to not less than 200 psi (1.38 MPa) at $0.6\sqrt{rt}$ below the open top, where t is the wall thickness and r the tank radius.

The vertical prestressed reinforcement is proportioned to fulfil the following conditions:

i The maximum allowable compression in concrete should not exceed $0.45 f'_c$ (ACI 318-89 section 18.4.2), where f'_c is the compressive strength of the concrete.

ii The maximum allowable tensile stress in the non-prestressed reinforcement should be limited to 18 ksi (124 MPa).

The values of the internal forces for the two cases mentioned in Table 2.5 are used for the design. The following cross-section satisfies the requirement :

Depth	= 450 mm,
Vertical prestress force after loss	= 1.64 MN,

Vertical prestress reinforcement = strands # 15

(A_{ps} = 10x140 mm^2/m = 1400 mm^2/m),

Vertical non-prestressed reinforcement = 5 # 25 / m

(A_{siv} = A_{sov} = 2500 mm^2/m)

where A_{siv} and A_{sov} are the cross-sectional areas of the non-prestressed vertical steel at the inner and outer wall faces, respectively.

Fig. 2.20 shows the cross-section and the stress distributions in the two cases. A linearly varying thickness is assumed for the tank wall. The proposed depth of the cross-section at top is 300 mm with no vertical prestressing.

The elastic analysis is repeated for Tank 2 using the designed cross-sections and prestressing. A substantial increase in vertical and circumferential stresses is obtained as a result of increasing the stiffness of the tank.

It is concluded that using the recommendation of the ACI 344 committee for the structural design of fixed base cylindrical tanks based on the elastic analysis results in an uneconomic design.

2.6.2 The Design According to BS 8007

The British Standards for the design of aqueous retaining structures BS 8007 (1987) provides a method of design based on the limit state philosophy.

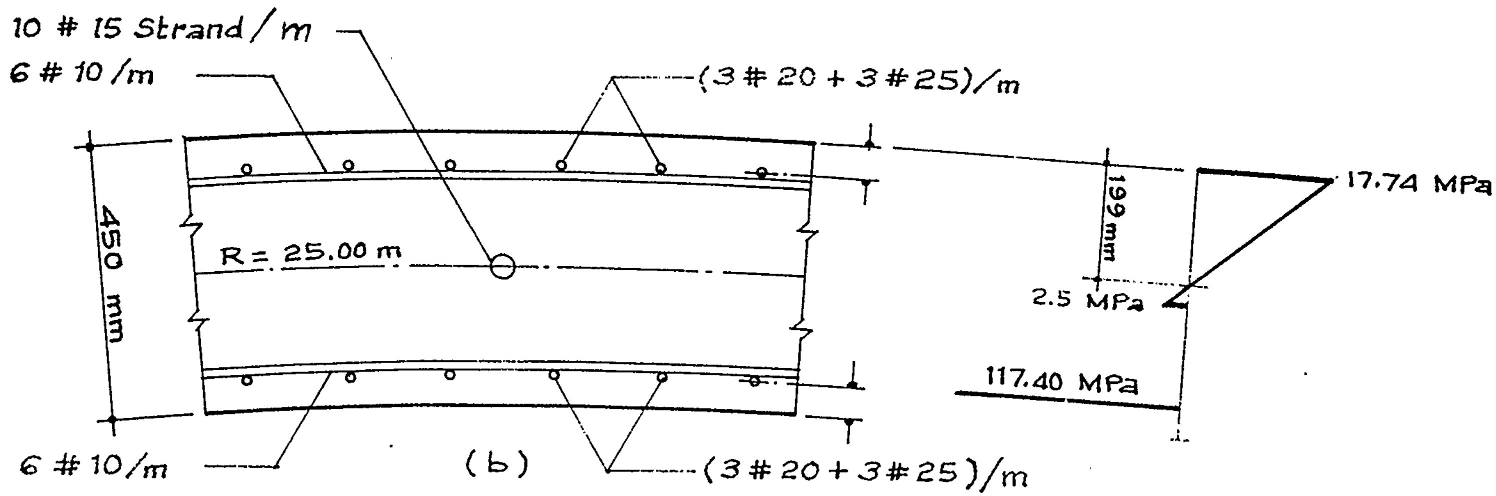

Figure 2.20 Wall cross-section at bottom for Tank 2. Design according to ACI 344. The stress distribution is for the effect of temperature drop (T_o=-20°C, T_i=5°C) combined with the effect of circumferential and vertical prestressing. Cross-section areas of bars # 10, # 20, ... are given in Appendix B.

The serviceability crack width limit state is recommended to be the basis, on which the size of the elements and the amounts of the reinforcement are assessed.

Tank 1

The cross-section at the base is designed to resist the critical load combination mentioned in Table 2.5, and to comply with requirements of BS 8007 including the minimum net concrete cover of 40 mm. The designed section at base is shown in Fig. 2.21. It has the same depth as that designed by ACI 350.

Tank 2

The amount of circumferential prestressing is determined to counteract the resultant tension in the concrete in the circumferential direction after allowance for all losses of prestress. However, the code does not specify a definite amount of residual compression as it is the case in the ACI code (Section 2.6.1).

On the other hand, cracking is allowed with a maximum design surface crack width of 0.2 mm. It is considered satisfactory to limit the steel stress in service conditions to 130 MPa.

The final cross-section at the base is as follows:

Depth = 500 mm,

Vertical prestress force after loss = 2.08 MN,

Vertical prestress reinforcement = Strands # 15

(A_{ps} = 12x140 mm^2/m = 1680 mm^2/m),

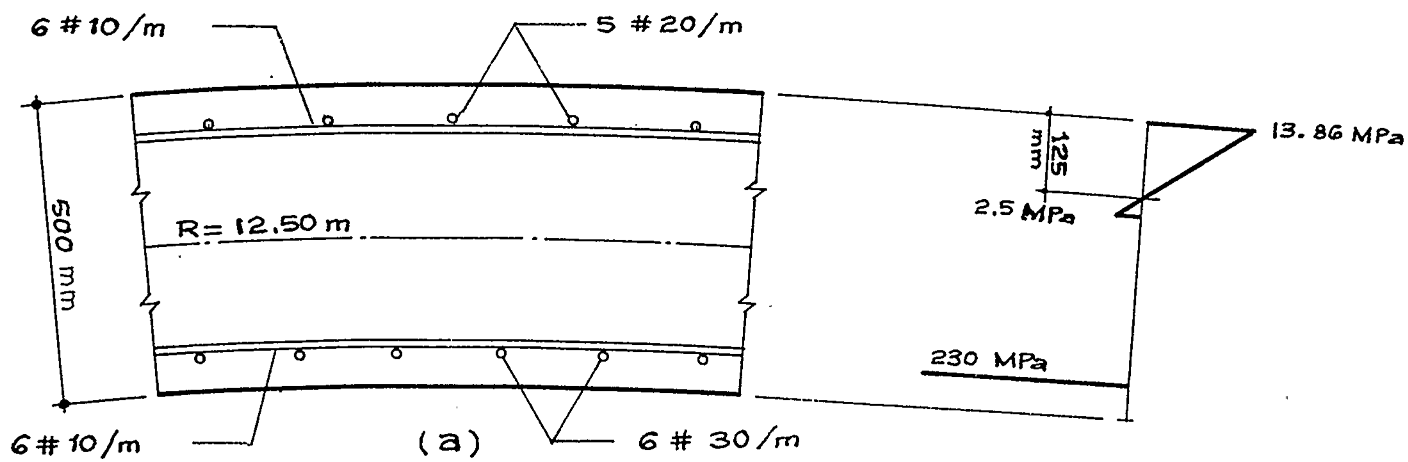

Figure 2.21 Wall cross-section at bottom for Tank 1. Design according to BS 8007. The stress distribution is for the effect of liquid load plus temperature rise (T_o=45°C, T_i=15°C). Cross-section areas of bars # 10, # 20, ... are given in Appendix B.

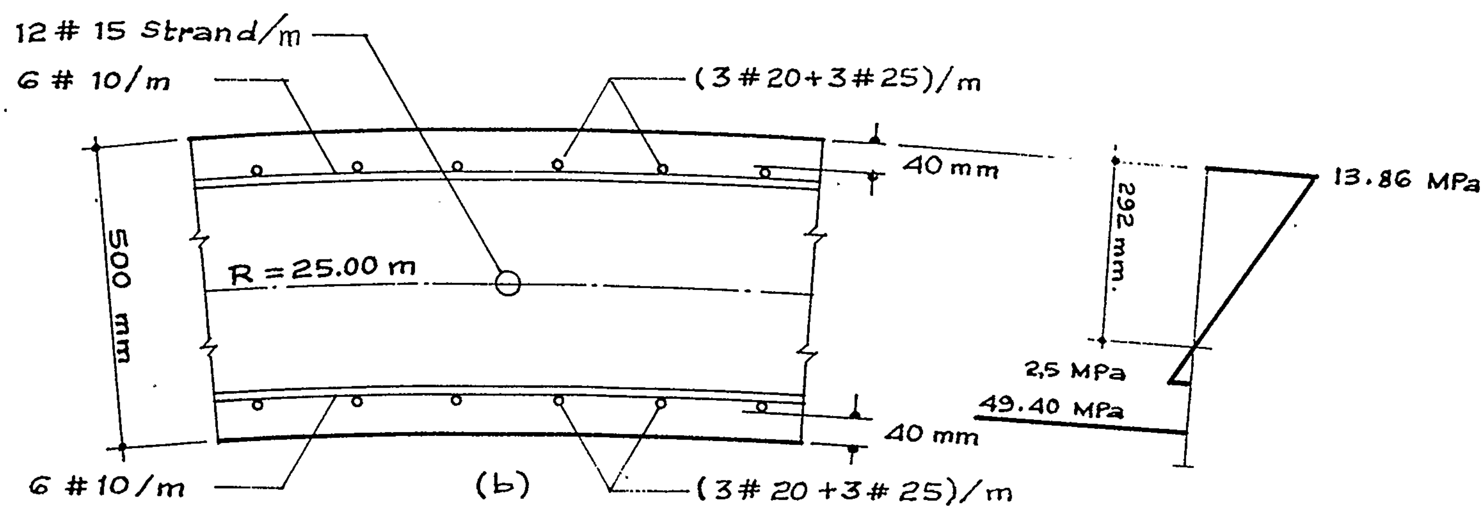

Figure 2.22 Wall cross-section at bottom for Tank 2. Design according to BS 8007. The stress distribution is for the effect of temperature drop (T_o=-20°C, T_i=5°C) combined with the effect of circumferential and vertical prestressing. Cross-section areas of bars # 10, # 20, ... are given in Appendix B.

Vertical non-prestressed reinforcement = 5 # 25 / m

$(A_{siv} = A_{sov} = 2500\ mm^2/m)$

Figure 2.22 shows the designed cross-section. A linearly varying thickness is assumed for the tank wall. The proposed depth of the cross-section at top is 300 mm with no vertical prestressing.

The depth of the cross-section at base is larger than the depth according to ACI 344 and a higher amount of prestressing is required.

2.7 SUMMARY

A brief review of the elastic analysis of circular prestressed tanks is presented in this chapter. The derivation of the differential equation for a tank strip and the thermal loads affecting the circular tanks are briefly discussed. At the end the analyses results of two circular tanks of different sizes are illustrated. The critical cases of loading are used for the structural design of the Tanks according to the American and British codes.

The next chapters deal with the nonlinear analysis of circular tanks.

CHAPTER 3

NONLINEAR FINITE ELEMENT ANALYSIS

3.1 INTRODUCTION

The finite element computer program FELARC (Ghoneim and Ghali 1979) is used for the nonlinear analysis of circular prestressed tanks discussed in Chapter 4. In this chapter the basic assumptions involved in FELARC are reviewed. The procedure of the nonlinear analysis using incremental linear analyses is also discussed.

3.2 LAYERED FINITE ELEMENTS

FELARC stands for Finite Element Layered Analysis of Reinforced Concrete. The analyzed reinforced concrete structure is idealized by an assemblage of constant thickness shell elements; each element is divided into a number of layers (Fig. 3.1). Each finite element layer is treated as an orthotropic material, that can assume any of the following states: elastic, yielded, cracked or crushed depending on the stress level reached. A reference surface is to be selected by the user; all local z-coordinates of the concrete layers are referred to this surface. Integrations in the z-direction are transformed into a summation over the layers.

3.3 FINITE ELEMENTS

Three types of finite elements are employed for the finite element modelling of the circular tank, namely:

1) a quadrilateral in-plane element
2) a quadrilateral plate bending element
3) a boundary element

Quadrilateral In-Plane Element - QLC3

QLC3 is a quadrilateral in-plane element with twelve degrees of freedom, two translations and a rotation at each corner node (Fig. 3.2).

Quadrilateral Plate Bending Element - QBE

QBE is a quadrilateral plate bending element with twelve degrees of freedom, a translation and two rotations at each corner node (Fig. 3.3).

The two stiffnesses of QLC3 and QBE are combined to form a quadrilateral shell element.

Boundary Element

A spring element having an axial and/or torsional stiffness and is used for the following purposes:

1) to provide elastic supports at the nodes,
2) to calculate the reactions at these supports,
3) to prescribe displacements at the nodes,

The reactions or the prescribed displacements can be in any direction.

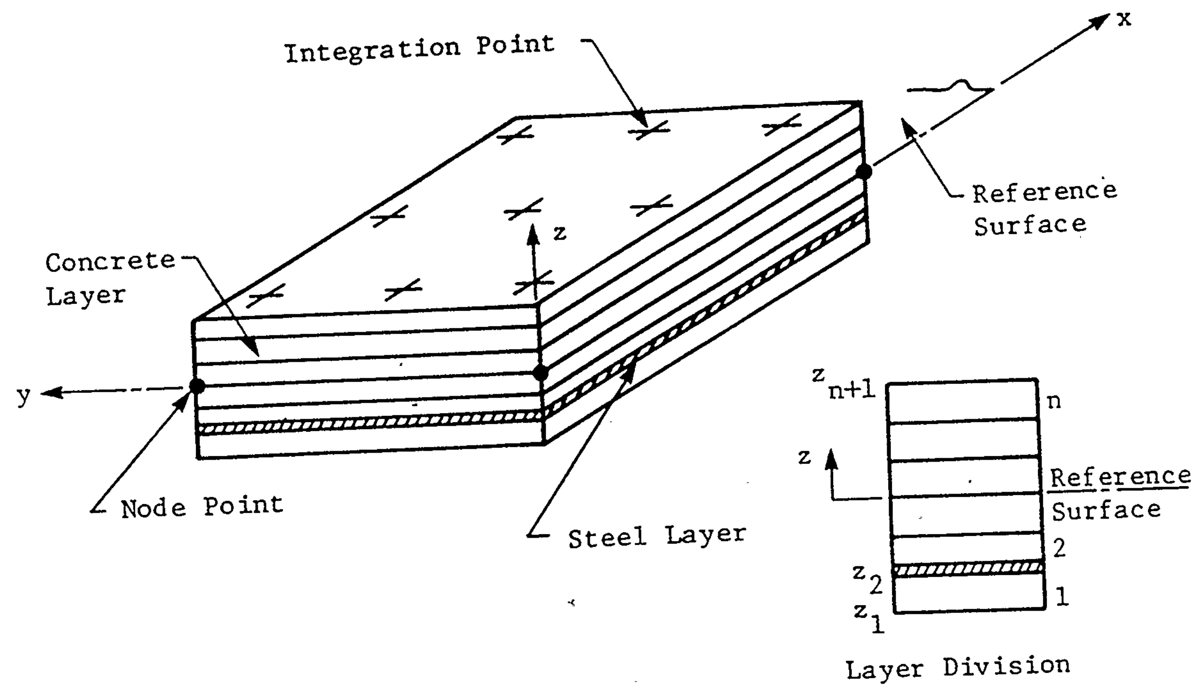

Figure 3.1 Layered element

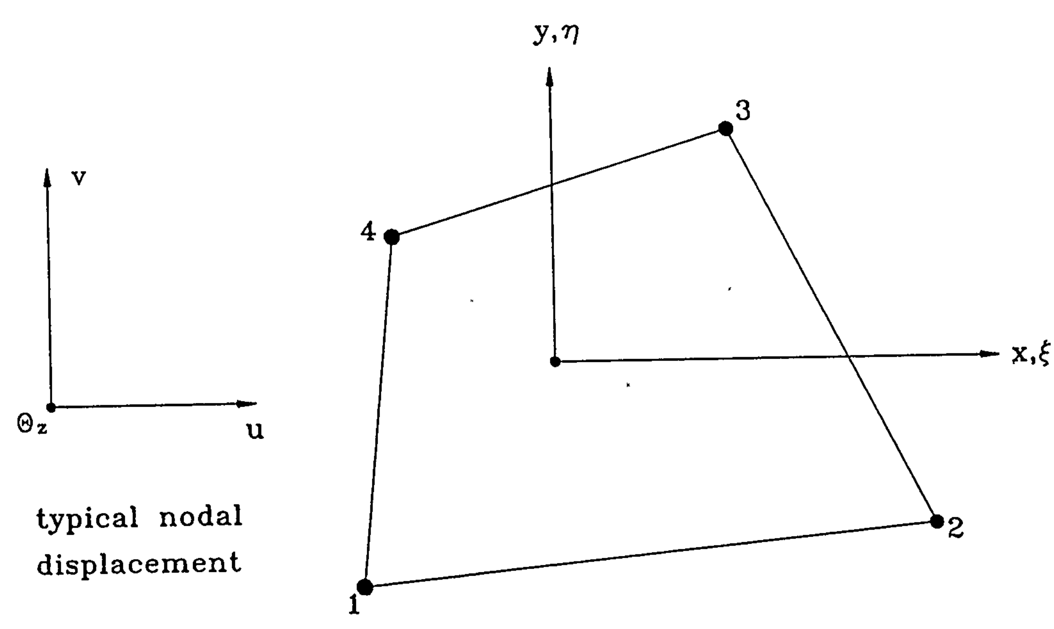

Figure 3.2 Quadrilateral plane element

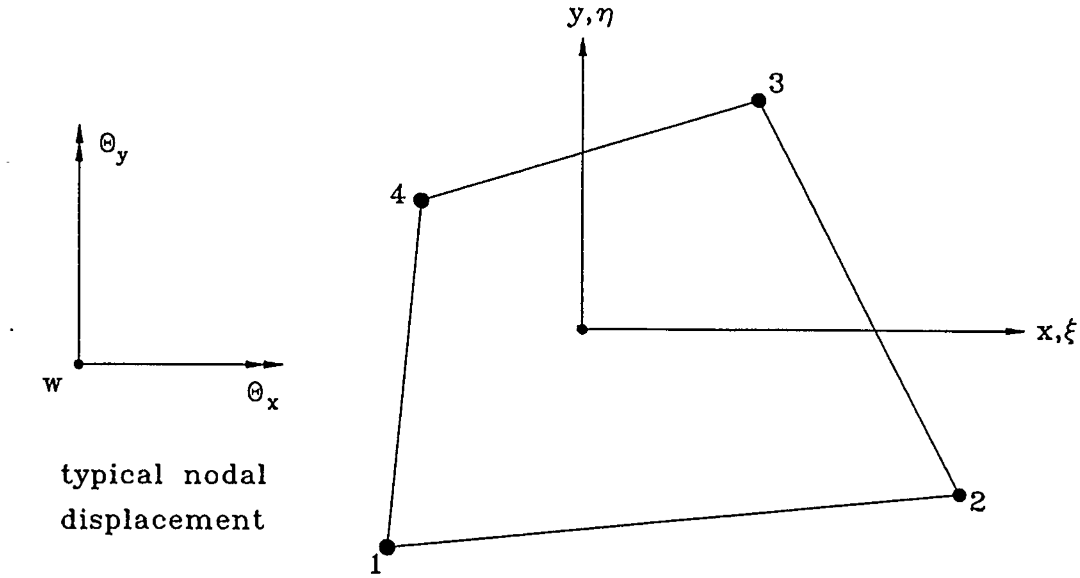

Figure 3.3 Quadrilateral plate bending element

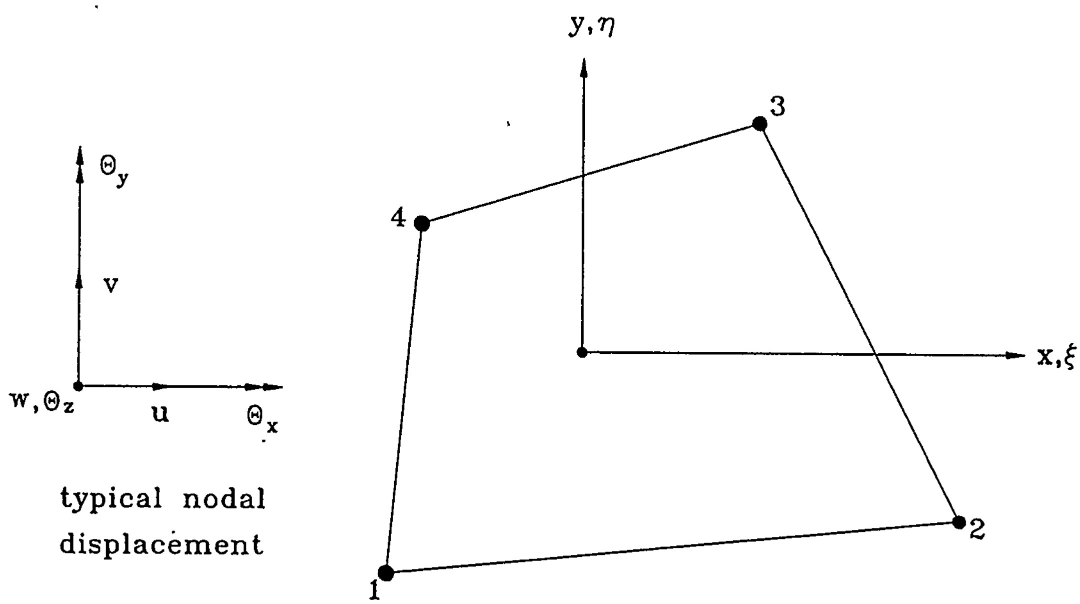

Figure 3.4 Quadrilateral shell element

3.4 MODELLING OF REINFORCEMENT

Equally spaced reinforcement within an element is idealized by a smeared steel layer of equivalent stiffness. For a reinforcement mesh, two perpendicular steel layers are used. However, heavy reinforcement bars and prestressing cables are idealized by an "element bar". An element bar is a straight bar connecting any two points on the reference surface.

Perfect bond between the reinforcing or the prestressing bars and the concrete is assumed. This implies that no bond slip is allowed. The contribution of the "element bar" to the stiffness is accounted for in the stiffness matrix of the shell element.

3.5 CONSTITUTIVE MATERIAL RELATIONS

3.5.1 Steel Model

The behavior of the reinforcing and prestressing steels is modelled by a bilinear constitutive model. This model is defined by four parameters: the yield strength f_y, the elastic modulus E_s, the strain-hardening modulus E_s^* and the ultimate strain ε_{su}, as shown in Fig. 3.5.

3.5.2 Concrete Model

The concrete model adopted in the computer program FELARC is based on an assumption that the concrete under biaxial state of stress behaves as an orthotropic material in the principal stress directions.

Kupfer et al (1969) developed an experimental stress-strain diagram for concrete under biaxial stress maintaining the ratio between the two principal stresses σ_1 and σ_2 constant. They got different values for the slope of the curve (i.e. the tangent modulus) in the two directions at any stress level. The conclusion is that a linear isotropic elastic material subjected to biaxial state of stress, where the ratio of σ_1 and σ_2 is kept constant, is equivalent to a "stress-induced" orthotropical material.

Thus, an equivalent uniaxial stress-strain curve for each principal direction is proposed (Ghoneim 1978). The orthotropic constitutive matrix adopted is as follows:

$$[D] = \frac{1}{1 - \nu^2} \begin{bmatrix} E_1 & \nu\sqrt{E_1 E_2} & 0 \\ \nu\sqrt{E_1 E_2} & E_2 & 0 \\ 0 & 0 & \frac{1}{4}(E_1 + E_2 - 2\nu\sqrt{E_1 E_2}\,) \end{bmatrix} \qquad (3.1)$$

where:

E_1, E_2 are the uniaxial tangent moduli in the principal directions;

ν is the uniaxial Poisson's ratio.

This formulation of [D] is based on the following assumptions:

1) $\nu^2 = \nu_1 \nu_2$

2) $\nu_1 E_2 = \nu_2 E_1 = \nu \sqrt{E_1 E_2}$

3) $G' = \dfrac{1}{4(1-\nu^2)} (E_1 + E_2 - 2\nu \sqrt{E_1 E_2}\,)$

where,

ν_1, ν_2 are the Poisson's ratios in the principal directions.

G' is the shear modulus.

The equivalent uniaxial stress-strain curve is shown in Fig. 3.6. For the compressive loading part, up to the maximum stress, Saenz's formula (1964) is used as follows:

$$\sigma = \frac{E_{co}\,\varepsilon}{1 + [\frac{E_{co}}{E_{cs}} - 2]\frac{\varepsilon}{\varepsilon_{cu}} + [\frac{\varepsilon}{\varepsilon_{cu}}]^2} \tag{3.2}$$

where,

σ and ε are the stress and the corresponding strain;

E_{co} is the initial tangent modulus of elasticity;

ε_{cu} is the strain at the maximum compressive strength f'_c;

E_{cs} is the secant modulus at peak stress $= \frac{f'_c}{\varepsilon_{cu}}$.

For the unloading portion of the curve beyond the compressive strength, Smith and Young's equation (1955) is used. The equation is written as:

$$\sigma = f'_c\,[\frac{\varepsilon}{\varepsilon_{cu}}]\,e^{[1-\frac{\varepsilon}{\varepsilon_{cu}}]} \tag{3.3}$$

However, in tension a linear stress-strain relationship is assumed. The slope of the tensile loading part is the same as the initial tangent modulus. A linear unloading portion is considered beyond cracking, the slope of which is determined according to the ultimate tensile strain ε_{tu} (Fig. 3.6).

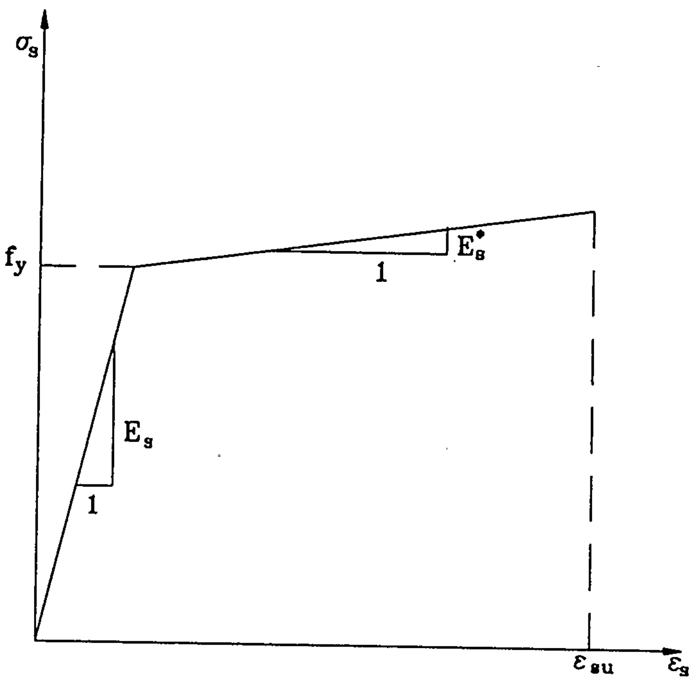

Figure 3.5 Bilinear stress-strain curve for steel

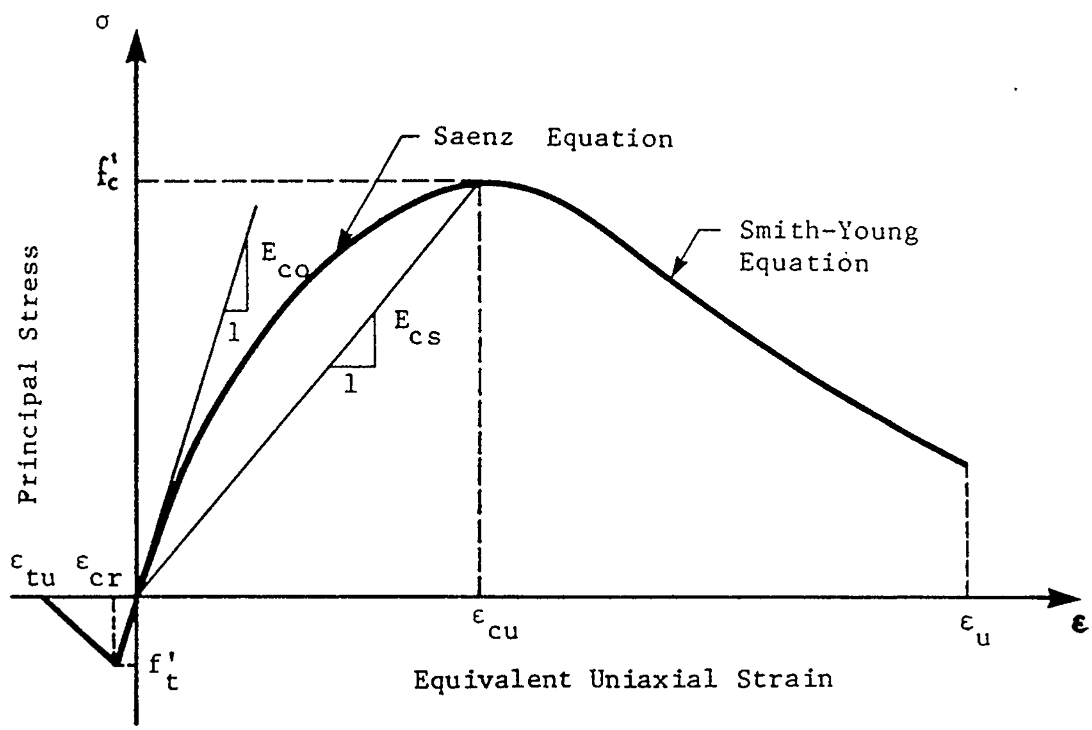

Figure 3.6 Equivalent stress-strain curve for concrete

3.6 TENSION STIFFENING

As the principle tensile stresses reach the uniaxial tensile strength of concrete f'_t, cracks are assumed to form perpendicular to the direction of the principal stress. However, the concrete between cracks is still capable of carrying some tension transferred by bond action between the concrete and the reinforcement. The adopted tension stiffening model assumes a linear unloading curve for concrete in tension (Fig. 3.6).

As σ_1 reaches the uniaxial tensile strength f'_t the constitutive matrix becomes :

$$[D] = \begin{bmatrix} 0 & 0 & 0 \\ 0 & E_2 & 0 \\ 0 & 0 & \beta_g G' \end{bmatrix} \qquad (3.4)$$

where β_g is a constant smaller than unity to account for the drop of shear stiffness due to cracking. It accounts for the shear stiffness due to aggregate interlock and dowel action. However, it has a little effect on the results in the problem treated in this thesis.

Equation 3.4 implies that the elastic modulus is assumed to be zero within a load step or an iteration in the tension stiffening region of the stress-strain curve. Therefore the unloading curve actually followed is a stepped function as shown in Fig. 3.7. Once one crack is formed at an integration point, the principal directions are not allowed to rotate at that point. A second crack is formed when $\sigma_2 \geq f'_t$; hence [D] becomes :

$$[D] = \begin{bmatrix} 0 & 0 & 0 \\ 0 & 0 & 0 \\ 0 & 0 & \beta_g G' \end{bmatrix} \tag{3.5}$$

3.7 PROCEDURE OF ANALYSIS

The equations of equilibrium of the finite element method are :

$$[K]\ \{\delta\} = \{F\} \tag{3.6}$$

where,

[K] is the structure stiffness matrix;

$\{\delta\}$ is the nodal displacement vector;

{F} is the equivalent nodal force vector.

In linear problems the stiffness matrix [K] is constant. However, in nonlinear problems [K] is dependent on the displacement and forces :

$$[K] = [\ K\ (\{\delta\},\{F\})\ ] \tag{3.7}$$

The incremental-iterative tangent stiffness technique is adopted for the nonlinear finite element analysis (Fig. 3.8). The nodal force vector is divided into a number of load increments m such that :

$$\{F\} = \sum_{i=1}^{m} \{\Delta F_i\} \tag{3.8}$$

For each load increment the incremental nodal displacements are calculated using the tangent stiffness matrix evaluated at the end of the preceding load increment. Thus,

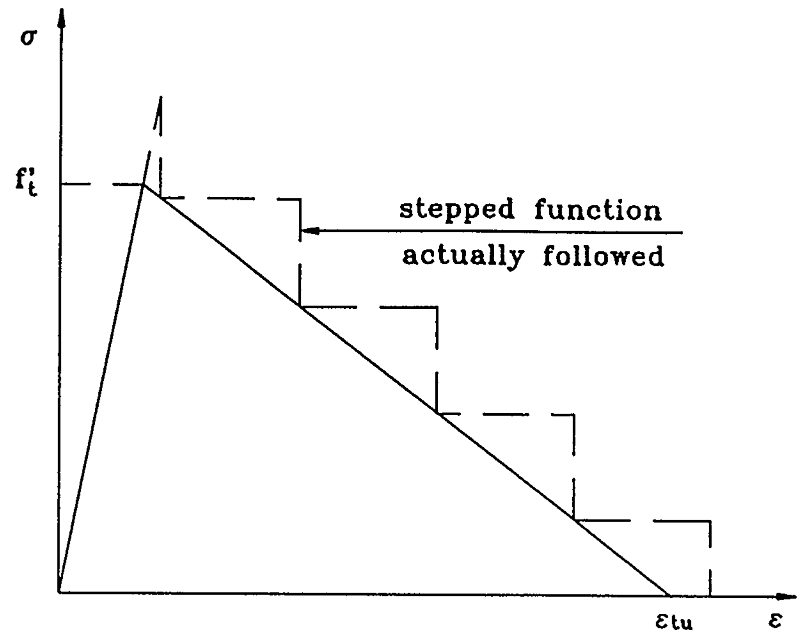

Figure 3.7 Tension stiffening model

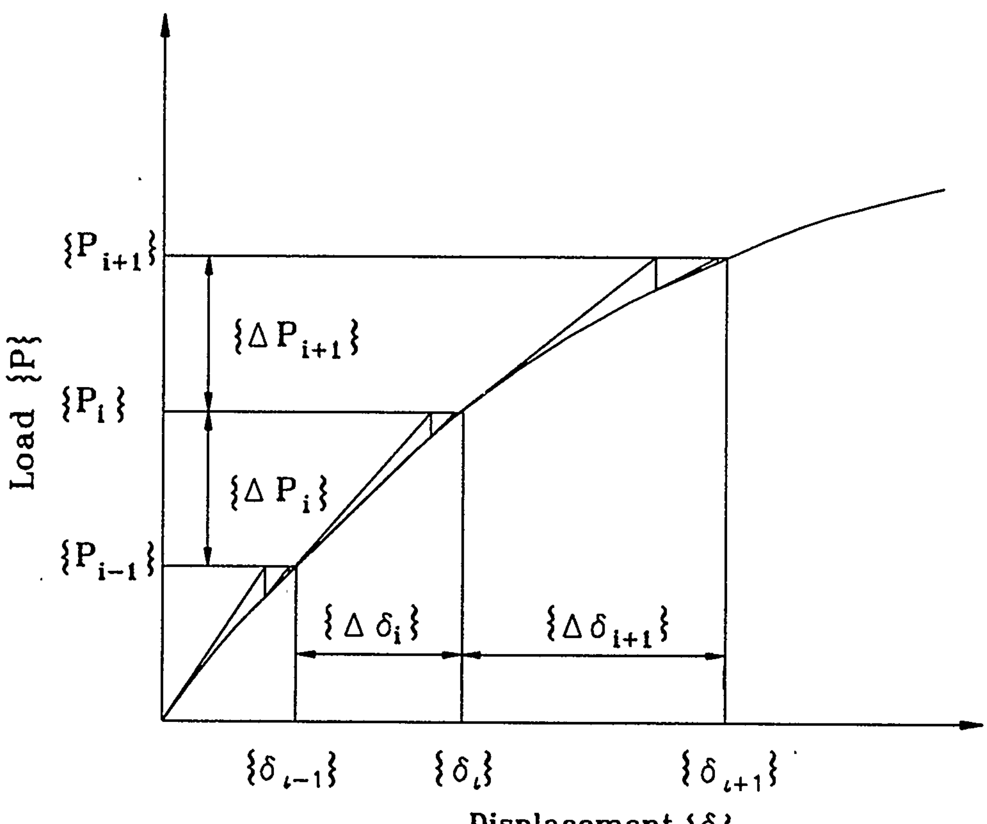

Figure 3.8 Incremental-iterative method

$$[K_{i-1}] \{\Delta\delta_i\} = \{\Delta F_i\} \qquad i = 1, 2, 3, \ldots\ldots m \tag{3.9}$$

where,

$$[K_{i-1}] = [\ K_{i-1} (\{\delta_{i-1}\},\{F_{i-1}\})\ ] \tag{3.10}$$

The strain increment vector is calculated, and hence the unbalanced stress vector is determined according to the following:

$$\{\bar{\sigma}_i\} = \{\Delta\sigma_i\} - [D_{i-1}] \{\Delta\varepsilon_i\} \tag{3.11}$$

where,

$\{\bar{\sigma}_i\}$ is the unbalanced stress vector;

$\{\Delta\sigma_i\}$ is the vector of the true stress increment obtained from the stress-strain relationship;

$[D_{i-1}]$ is the tangent constitutive matrix corresponding to the stress level at the end of the preceding increment;

$\{\Delta\varepsilon_i\}$ is the vector of the strain increment;

The unbalanced stress vector is then used to calculate equivalent unbalanced nodal forces as follows:

$$\{\ \bar{F}_i\ \} = -\sum_e \int_{V^e} [\ B\ ]^T \{\ \bar{\sigma}_i\ \}\ dV^e \tag{3.12}$$

where,

$\{\bar{F}_i\}$ is the equivalent unbalanced nodal force vector calculated at the end of iteration i;

$\sum_e$ is the summation over all elements;

V^e is the volume of an element;

[B] is the strain-displacement matrix.

The unbalanced nodal force vector $\{\bar{F}_i\}$ is applied in the (i+1) iteration and the same procedure described above is repeated. Iterations are continued until convergence or divergence criteria are satisfied or until the maximum number of iterations allowed is reached.

3.8 SUMMARY

In this chapter the computer program FELARC is reviewed. It will be the tool for the nonlinear finite element analysis of the circular concrete tanks investigated in the next chapter.

The theory of the layered finite elements is presented. The simulation of the biaxial state of stress by an equivalent uniaxial state is also discussed. Finally, the incremental iterative technique of nonlinear analysis is presented.

CHAPTER 4

NONLINEAR ANALYSIS AND RESULTS

4.1 INTRODUCTION

In this chapter the results of the nonlinear finite element analysis of Tanks 1 and 2 are illustrated and compared with the results of the linear analysis discussed in Chapter 2. The finite element model is also presented and verified.

4.2 FINITE ELEMENT MODELLING

In this section the finite element modelling of Tanks 1 and 2 is discussed (data for the two tanks are given in section 2.5). The finite elements used for the model are the plane shell element, the boundary spring element and the bar element.

Due to the axi-symmetry, a single shell element is used to represent the total perimeter. The finite element idealizations for Tanks 1 and 2 are shown in Figs. 4.1 to 4.3. Each finite element is divided into layers as shown in Fig. 4.2. The boundary elements are introduced to represent axi-symmetrical displacements. The degrees of freedom v^*, θ_x^*, and θ_z^* are restrained at the nodes on the vertical sides of the model (Fig. 4.3).

In order to model the material behavior of concrete, the following material properties are required:

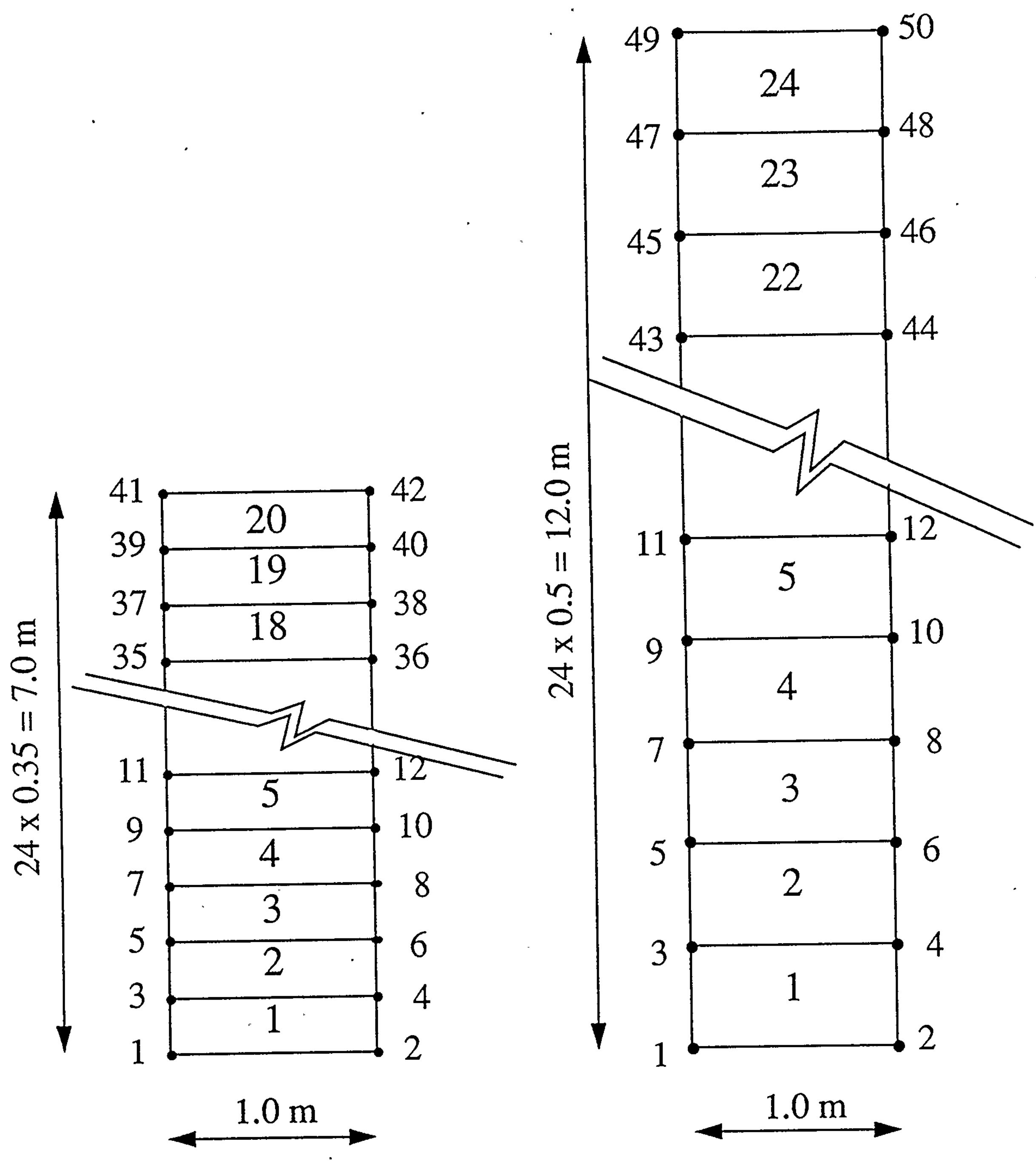

Figure 4.1 Finite element mesh for Tanks 1 and 2

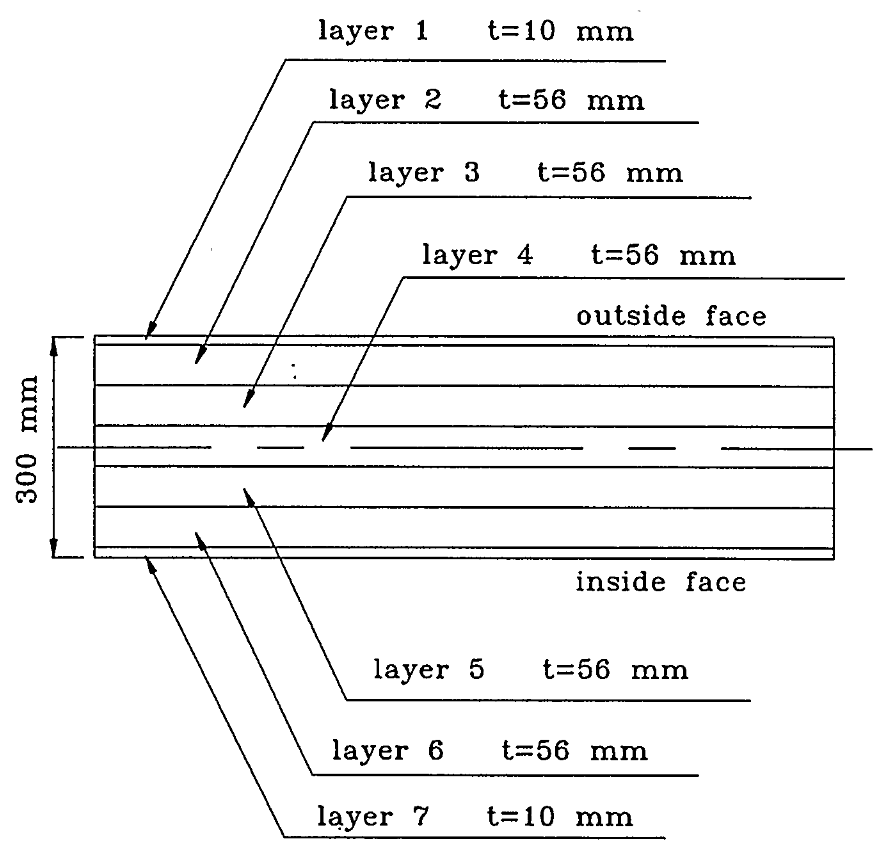

Figure 4.2 The layered concrete section

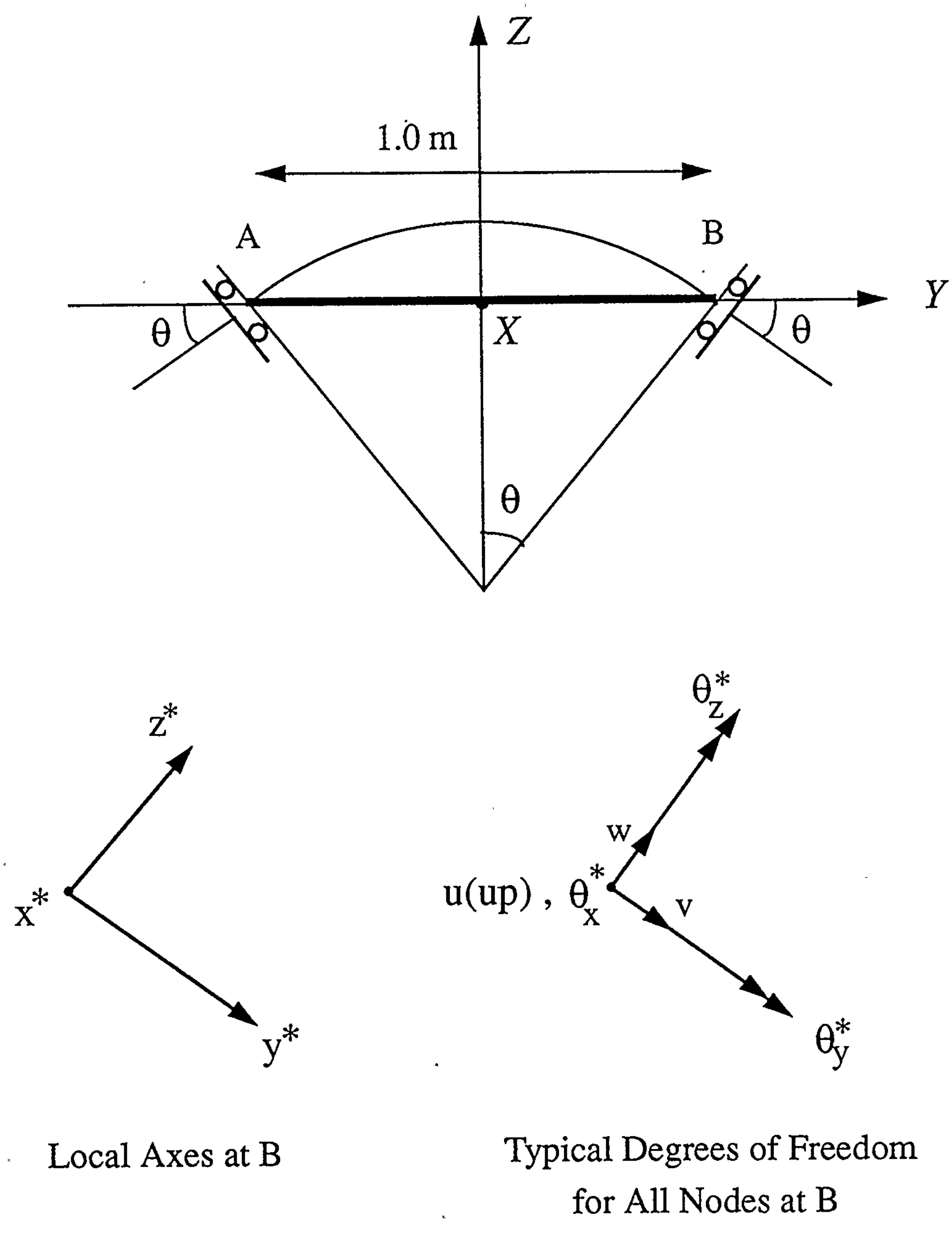

Figure 4.3a Axi-symmetrical boundary conditions for a typical plane shell element

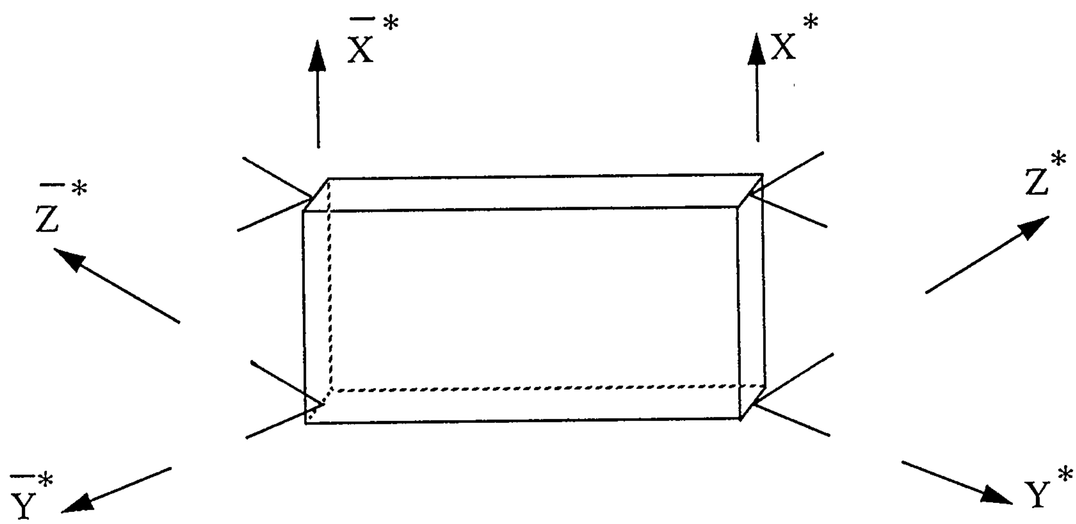

Figure 4.3b Directions of the boundary elements at the nodes of the shell element to satisfy the axi-symmetrical conditions.

1- The uniaxial cylinder strength, f'_c.

2- The strain corresponding to f'_c, ε_{cu}.

3- The ultimate uniaxial strain at failure, ε_u.

4- The tensile strength of concrete in bending, f'_t.

5- The ultimate tensile strain, ε_{tu}.

6- The initial tangent modulus of elasticity, E_{co}.

7- Poisson's ratio, ν.

8- The coefficient of thermal expansion, α_c.

For the reinforcing and prestressing steel, the following material properties are required:

1- The yield strengths, f_y and f_{py}.

2- The tangent moduli of elasticity, E_s and E_{ps}.

3- The strain hardening moduli, E_s^* and E_{ps}^* (Fig. 3.5).

(The values selected for these parameters have no influence on the result of the present study, because this level of stress for the strain hardening to occur is not reached.)

4- The ultimate strains at rupture, ε_{su}, ε_{pu}.

5- The coefficient of thermal expansion, α_s.

The values of the material parameters used for the analysis of Tanks 1 and 2 are presented in Tables 4.1 and 4.2.

Table 4.1 Concrete properties

f'_c MPa	ε_{cu} 10^{-6}	ε_u 10^{-6}	f'_t MPa	ε_{tu} 10^{-6}	E_{co} MPa	ν	α_c 10^{-6} $^\circ C^{-1}$
40	2000	3500	2.5	1200	31600	1/6	10

Table 4.2 Steel properties

Non-prestressed steel				Prestressing steel				
f_y MPa	E_s MPa	E_s^* MPa	ε_{su} 10^{-3}	α_s 10^{-6} $^\circ C^{-1}$	f_{py} MPa	E_{ps} MPa	E_{ps}^* MPa	ε_{pu} 10^{-3}
400	200000	500	120	10	1600	200000	500	350

4.3 THE LOADS ACTING ON THE F.E. MODEL

1) The Liquid Load

For the case of full tank, the total tank height is subjected to the liquid load. Each finite element along the height receives a trapezoidal load. The equivalent nodal forces are given as input and are calculated using the nodal shape functions as follows:

$$\{F\} = \int_0^b \int_0^a [N]\, q\, dx\, dy = a\, b \int_0^1 \int_0^1 [N]\, q\, d\xi\, d\eta \tag{4.1}$$

where:

{F} is the equivalent nodal force vector;

a,b are the side lengths of the element;

[N] is the matrix of the shape functions for a plate bending element;

q the trapezoidal liquid load.

The shape functions, and the equivalent nodal forces are presented in details in Appendix A.

2) The Temperature Loads

The computer program FELARC is capable of solving for temperature loads of any distribution through the thickness. As input, the temperatures at mid surfaces of each layer at the integration point of each element are required (Fig. 4.4).

3) Prestressing Forces

As mentioned in Section 2.5.1 the conventional distribution of circumferential prestressing is used. At the location of each prestressing tendon a line load is acting perpendicular to the surface of the wall; on a strip of unit width, the force is:

$$Q = \frac{P}{r} \tag{4.2}$$

where, P is the prestressing force per tendon and r is the radius of the tank.

However, the perpendicular force F is transmitted to the corner nodes of the corresponding elements proportionally, as shown in Fig. 4.5.

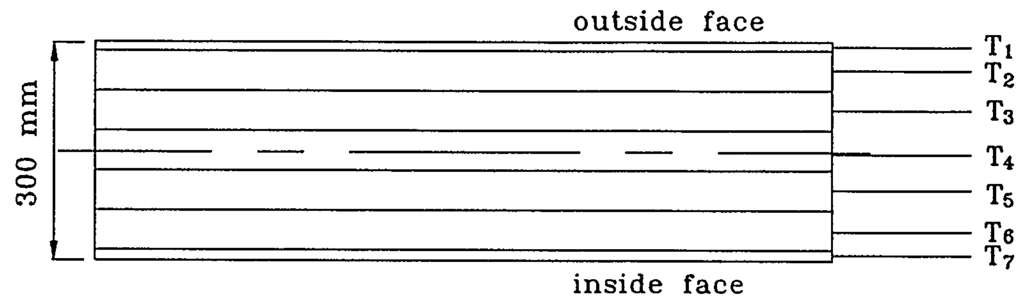

Figure 4.4 The input of the temperature variation through the thickness

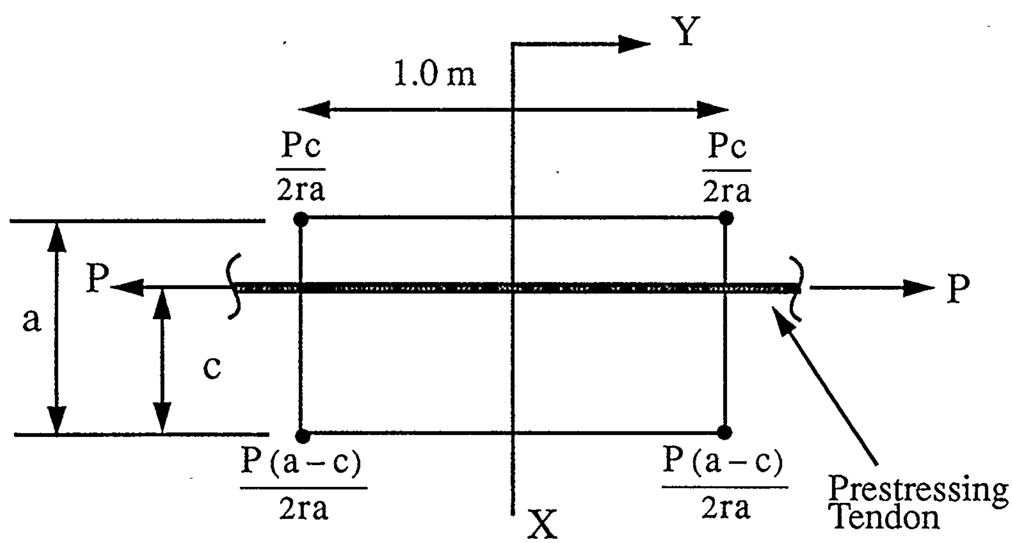

Figure 4.5 Element nodal forces in the Z-direction, representing the effect of a circumferential prestressing tendon

4.4 VERIFICATION OF THE AXI-SYMMETRICAL MODEL

In order to verify the previously proposed axi-symmetrical model, a linear finite element analysis is carried out using FELARC and compared with the elastic finite difference analysis by PCT (Section 2.4) for Tank 1. The comparison is based on the internal forces of two cases of loading, namely:

1) the liquid load: $q_{max} = 67.7$ kN/m^2

2) the temperature rise with a linear variation through the thickness:

$T_o = 45°C$ and $T_i = 15°C$.

A fair agreement is observed for the M_x-, N_ϕ- and M_ϕ-diagrams of both cases of loading (Figs. 4.6 to 4.11).

4.5 PROBLEM DESCRIPTION

Tanks 1 and 2, which were used for the linear analysis in Chapter 2 are analyzed using the nonlinear finite element analysis due to the following loadings:

1) Loading Case A:

. Liquid load + temperature rise ($T_o = 45°C$ and $T_i = 15°C$) for Tank 1.

. Vertical and circumferential prestressing (Section 2.5) + liquid load + temperature rise ($T_o = 45°C$ and $T_i = 15°C$) for Tank 2.

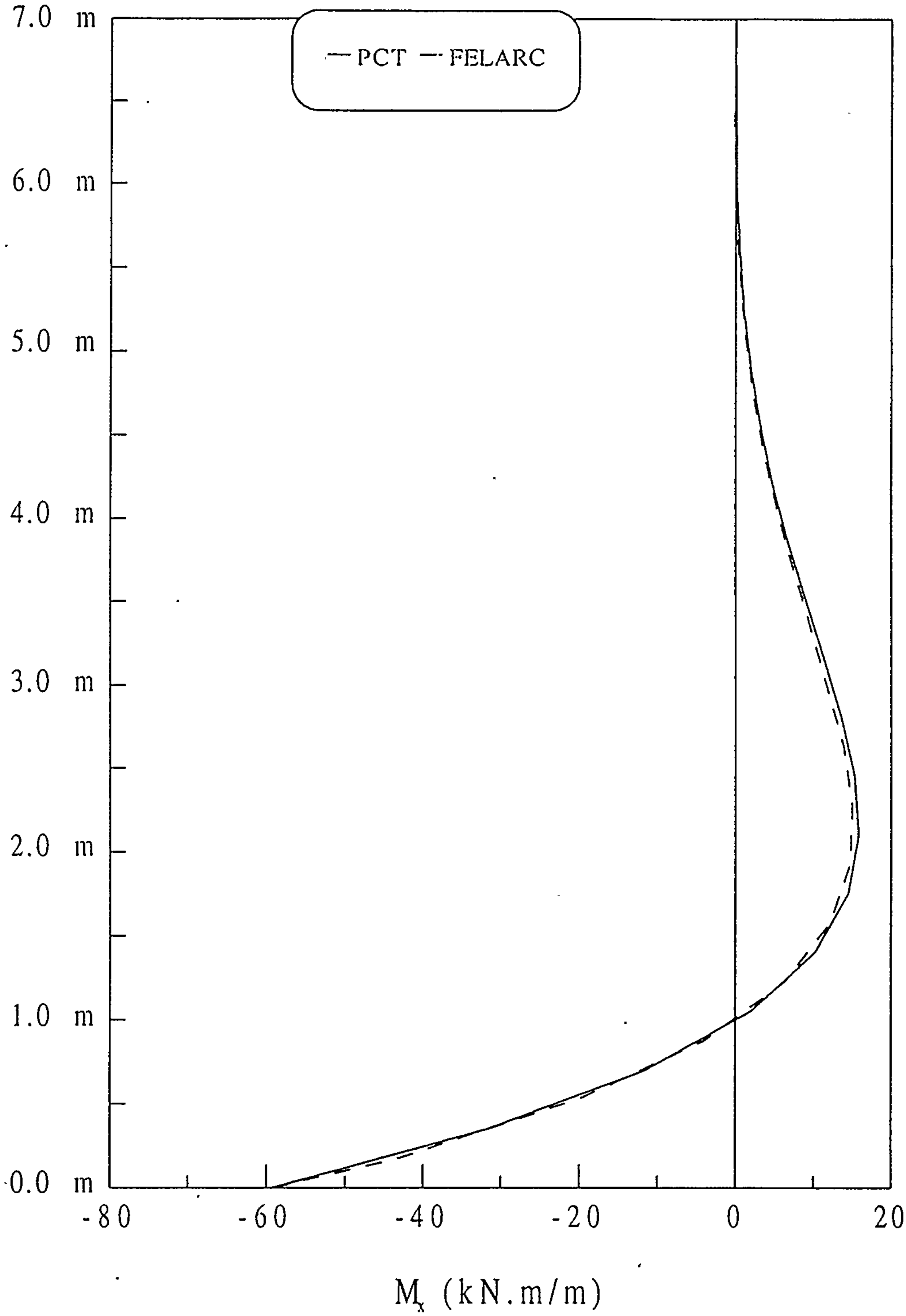

Figure 4.6 Comparison of M_x due to liquid load load according to PCT and FELARC using linear analysis.

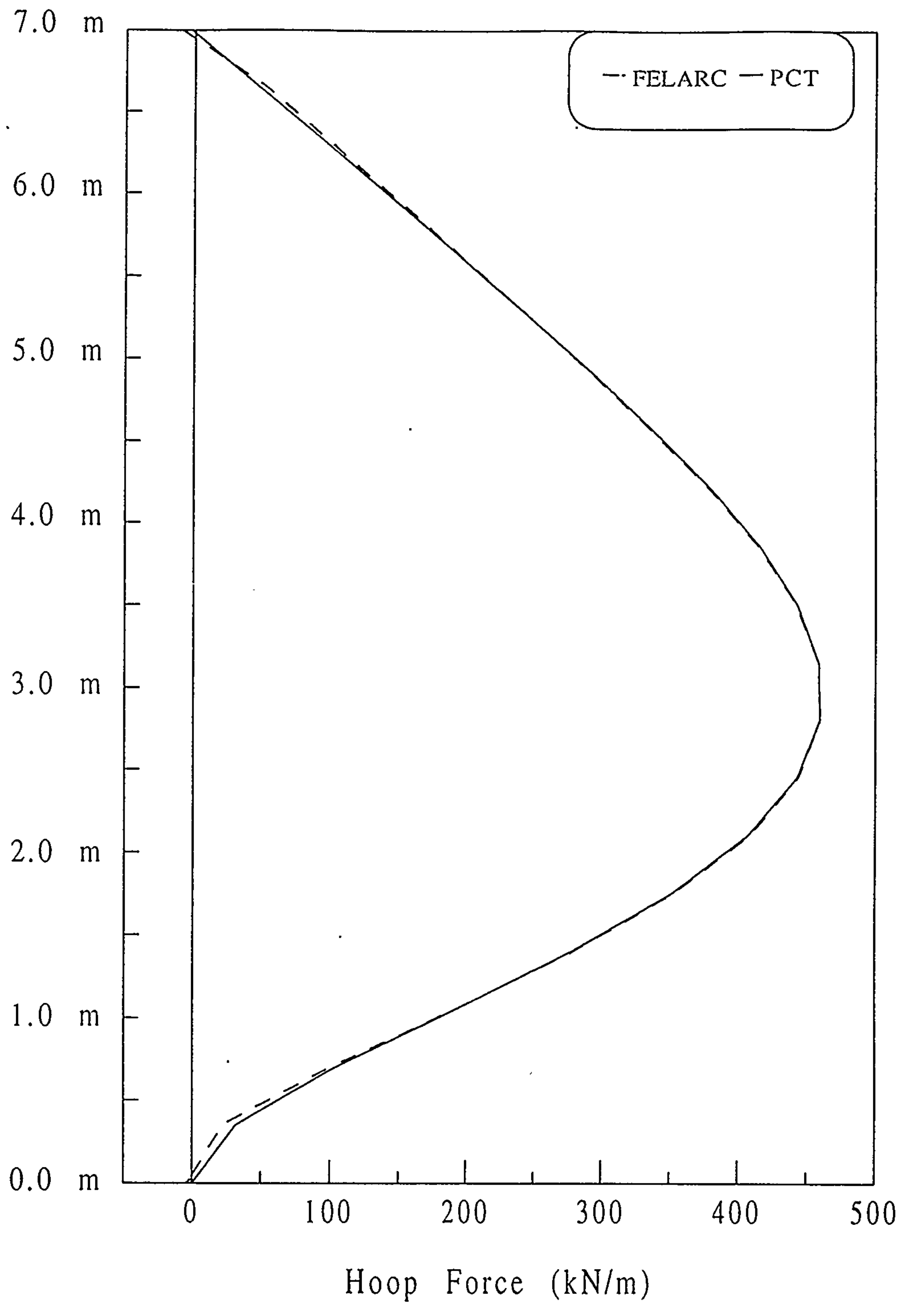

Figure 4.7 Comparison of N_ϕ due to liquid load according to PCT and FELARC using linear analysis

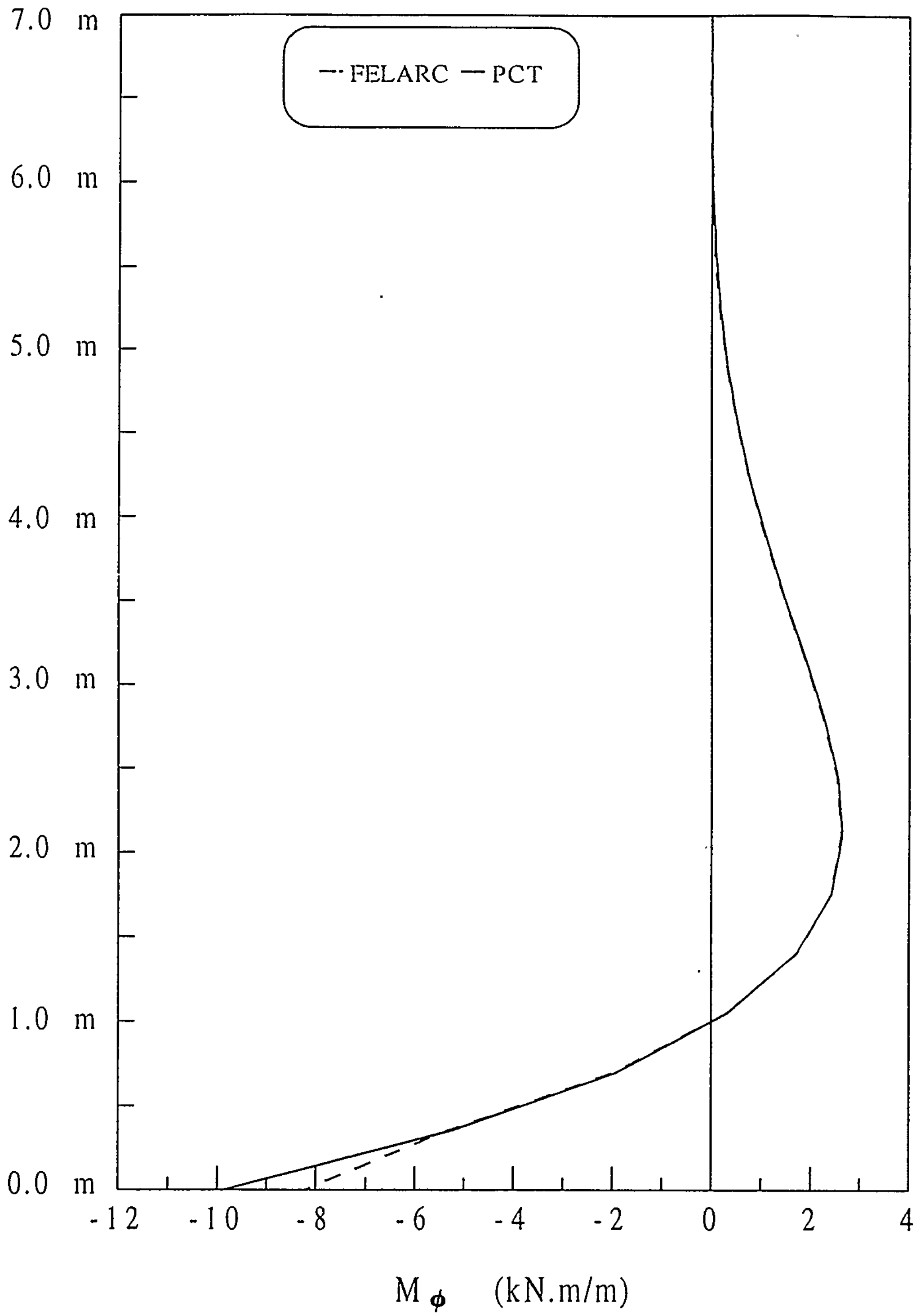

Figure 4.8 Comparison of M_ϕ due to liquid load according to PCT and FELARC using linear analysis.

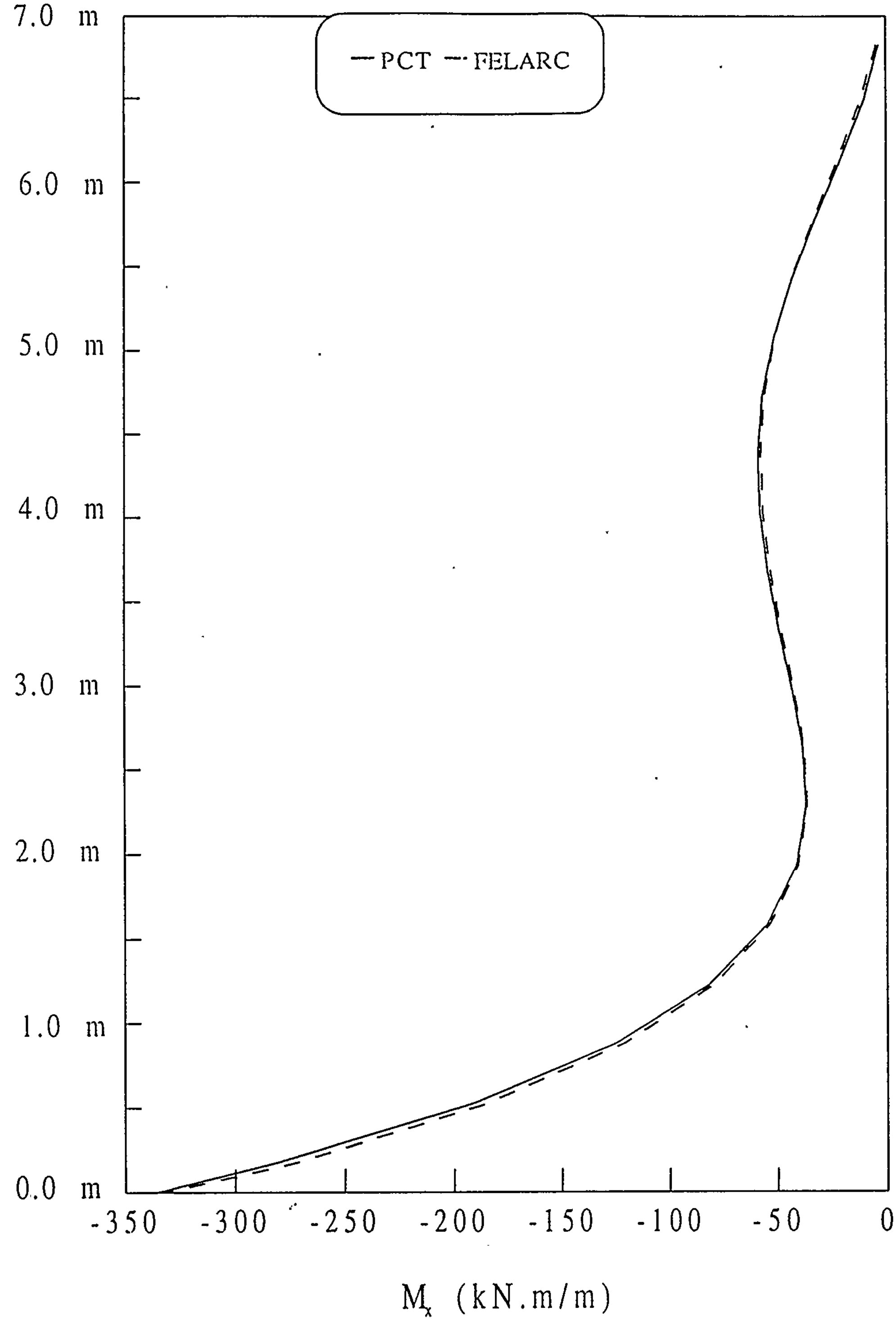

Figure 4.9 Comparison of M_x due to temperature rise according to PCT and FELARC using linear analysis

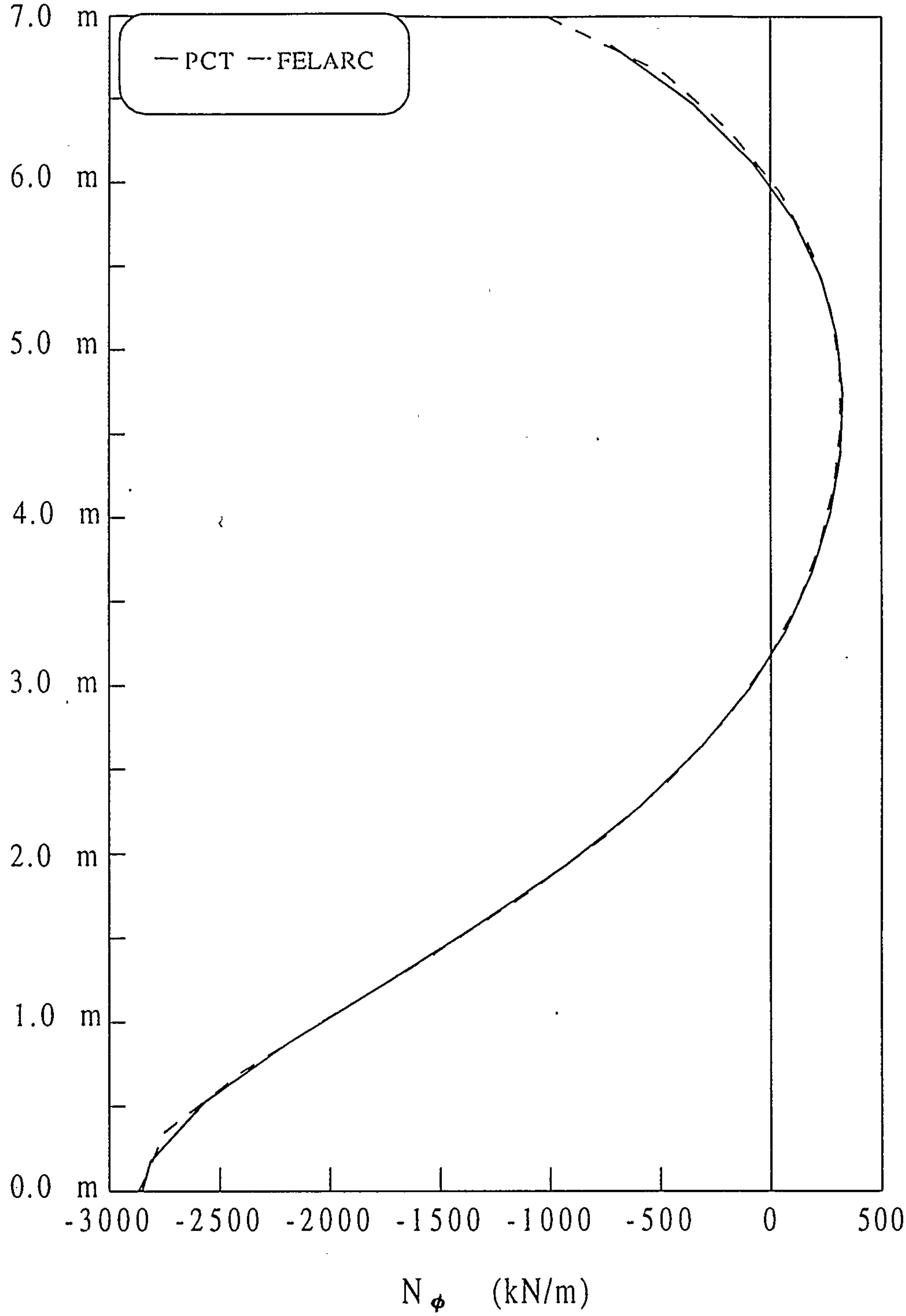

Figure 4.10 Comparison of N_{ϕ} due to temperature rise according to PCT and FELARC using linear analysis (T_o = 45 °C, T_i = 15 °C).

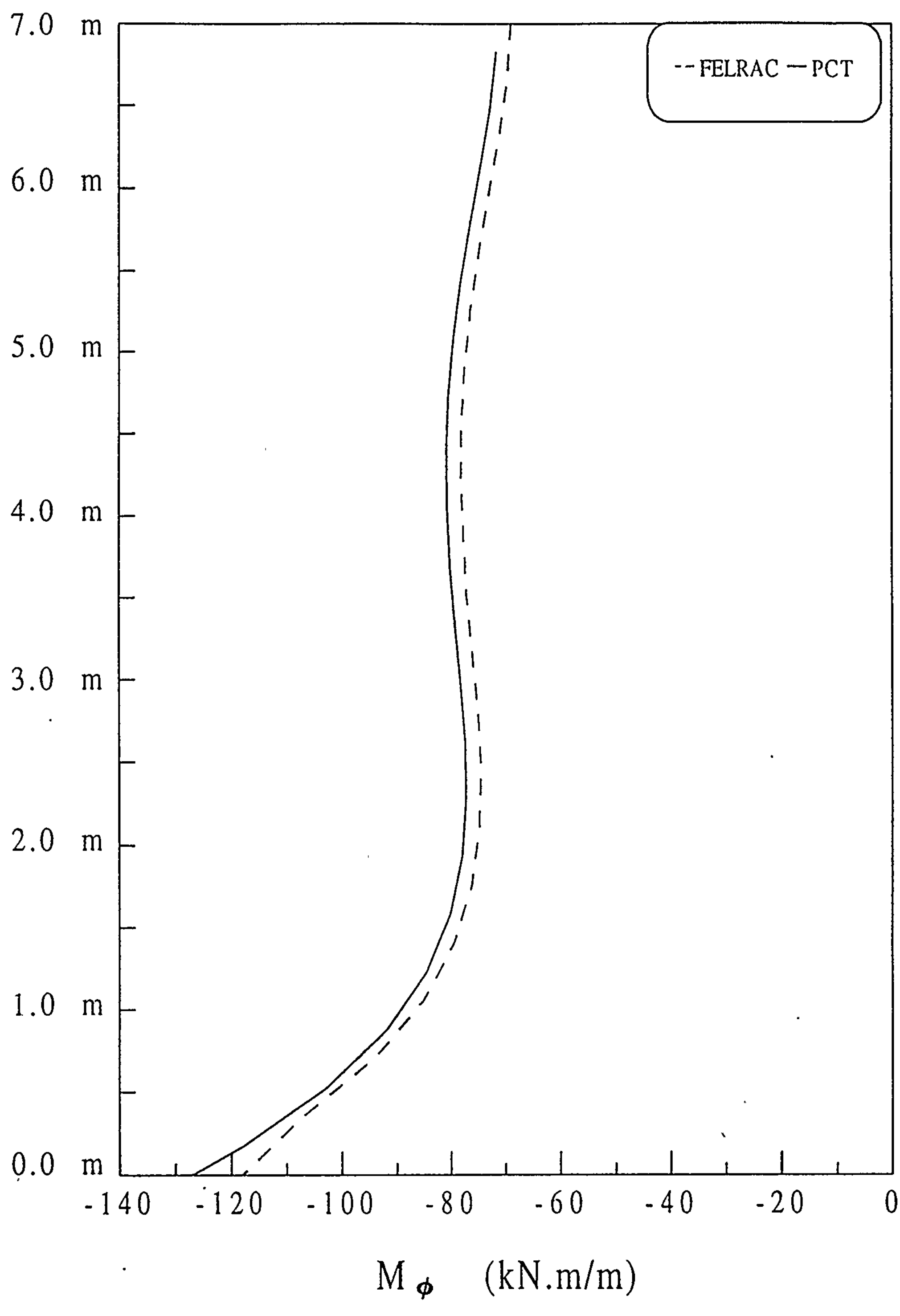

Figure 4.11 Comparison of M_ϕ due to temperature rise according to PCT and FELARC using linear analysis (T_o = 45 °C, T_i = 15 °C).

2) Loading case B:

. Temperature drop (T_o = -20°C and T_i = 5°C) for Tank 1.

. Vertical and circumferential prestressing + temperature drop (T_o = -20°C and T_i = 5°C) for Tank 2.

It is to be noted that the variation of the temperature through the thickness is linear for both cases.

The details of the non-prestressed and prestressed reinforcements are shown in Figs. 2.3 -2.6 and in Table 2.2.

4.6 RESULTS AND DISCUSSION

A nonlinear analysis of cylindrical reinforced concrete tanks was carried out by Elliott (1989). The study of Elliott included the effect of liquid load using the beam-on-elastic-foundation model. A substantial drop in the vertical bending moment and an increase in hoop forces were noticed after cracking. Cracking was due to vertical stresses only. The effect of the vertical cracks due to N_ϕ and M_ϕ was not included in the study.

A similar study is carried out in the present work to investigate the effects of temperature loads. Figures 4.13 - 4.23 illustrate a comparison of the results of the nonlinear analysis and the elastic linear analysis performed by FELARC and PCT, respectively.

A certain vertical non-prestressed steel ratio ($\rho_{iv} = \rho_{ov}$ = 1.0 %) is chosen for the study presented in this chapter. However, the nonlinear vertical moment is dependent on the vertical steel ratio as can be seen in Fig. 4.12.

Tank 1 - Case A:

Figs. 4.13 - 4.15 show the M_x-, N_ϕ- and M_ϕ-diagrams. A substantial drop in M_x (45 %) is observed at base due to the circumferential cracking (Fig. 4.13). Meanwhile, vertical cracks occur at the point of maximum N_ϕ and propagate. As a result a drop in the hoop forces can be seen (Fig. 4.14).

The development of vertical cracks near midheight is accompanied by a substantial reduction in M_ϕ (Fig. 4.15). It is to be noted that all M_ϕ values given in this thesis, represent stress resultants at the wall middle surface, which does not always coincide with the cross-section centroid, particularly after cracking. Cracking causes sudden change in the centroid of the effective section; thus when a section is subjected to N_ϕ, the shift in centroid location causes sudden change in moment. This may be the reason for the kink in the curve in Fig. 4.15 presented below.

Tank 1 - Case B:

The maximum tensile stresses occur at the base at the outer face of the tank wall in the circumferential and vertical directions. Consequentially, substantial drops in M_x, N_ϕ and M_ϕ result (Figs. 4.16, 4.17 and 4.18).

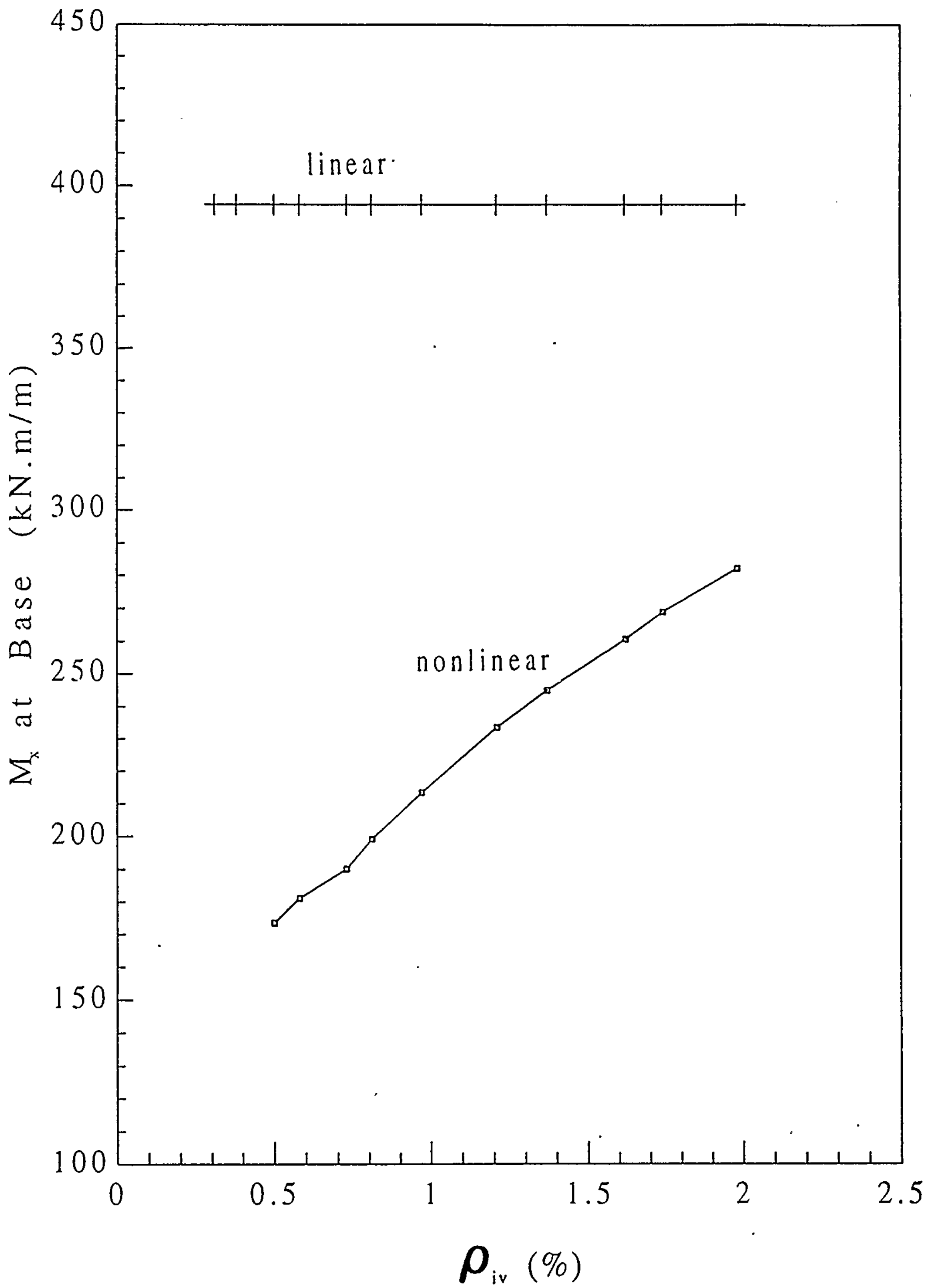

Figure 4.12 Effect of ρ_{iv} ratio on the nonlinear vertical moment at base for load case A.

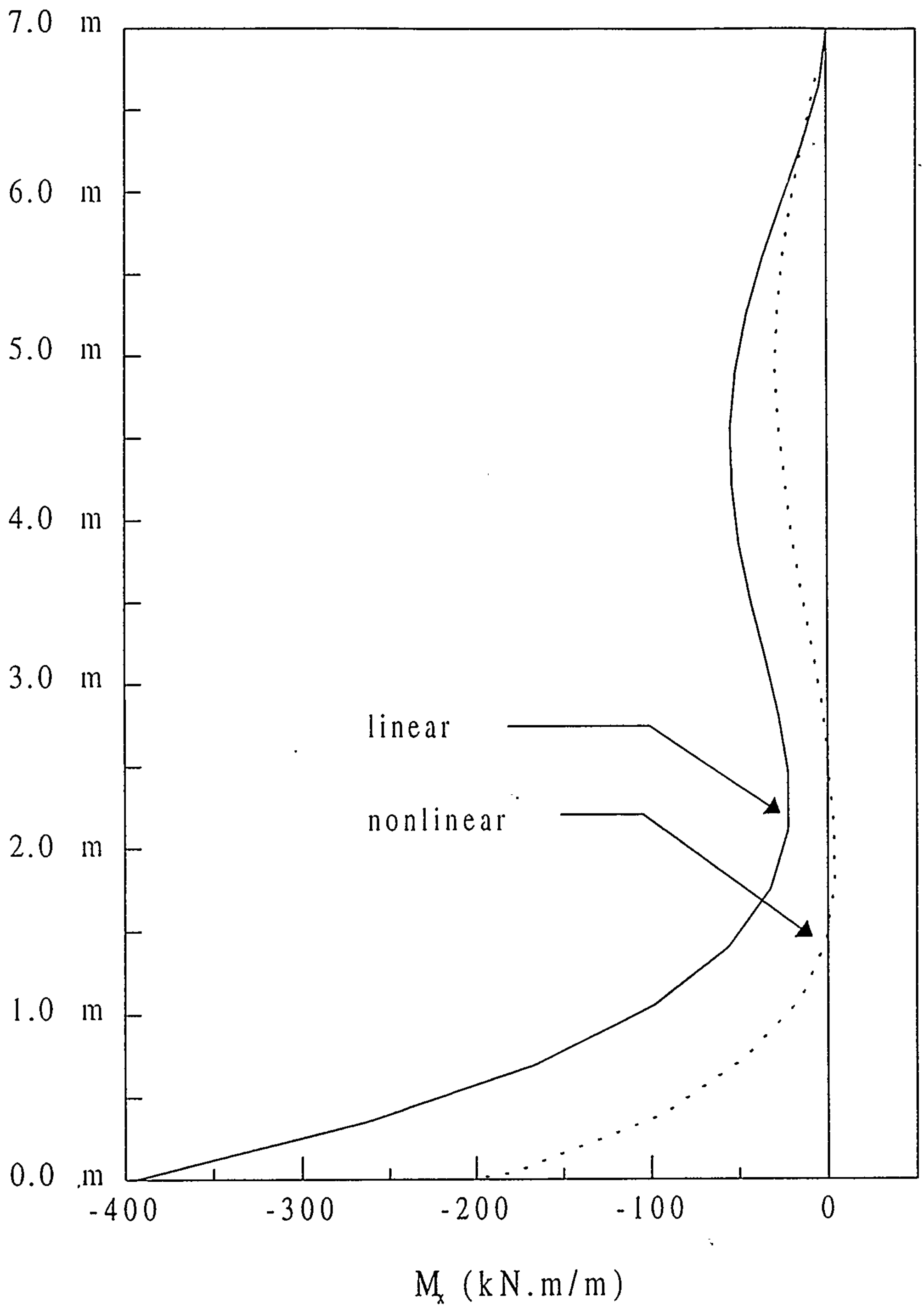

Figure 4.13 M_x-diagram for Tank 1 according to the linear and nonlinear analysis. Case of liquid load + temperature rise (T_o = 45 °C, T_i = 15 °C).

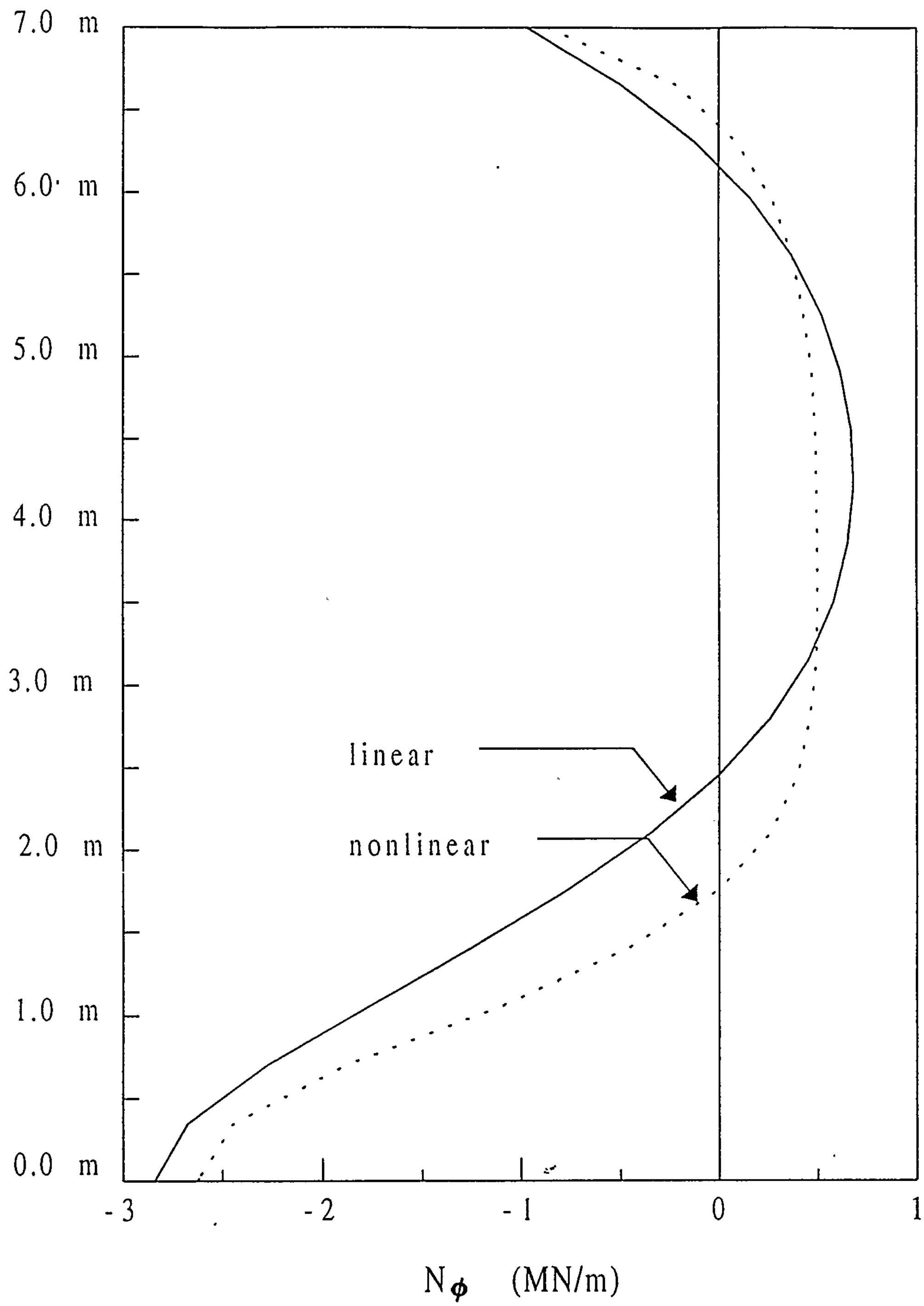

Figure 4.14 N_ϕ -diagram for Tank 1 according to the linear and nonlinear analysis. Case of liquid + temperature rise (T_o = 45 °C, T_i = 15 °C)

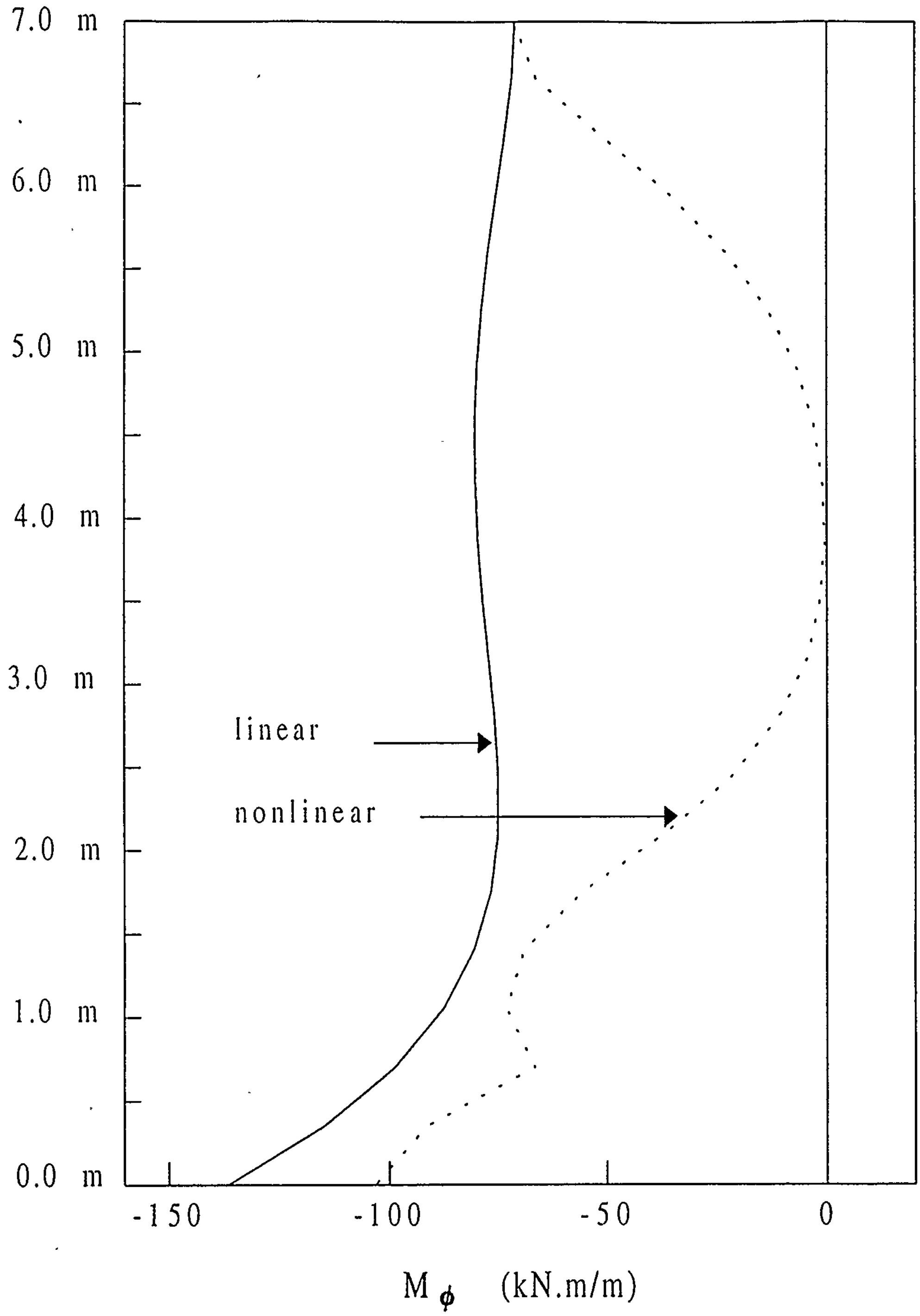

Figure 4.15 M_ϕ -diagram for Tank 1 according to the linear and nonlinear analyses. Case of liquid load + temperature rise (T_o = 45 °C, T_i = 15 °C).

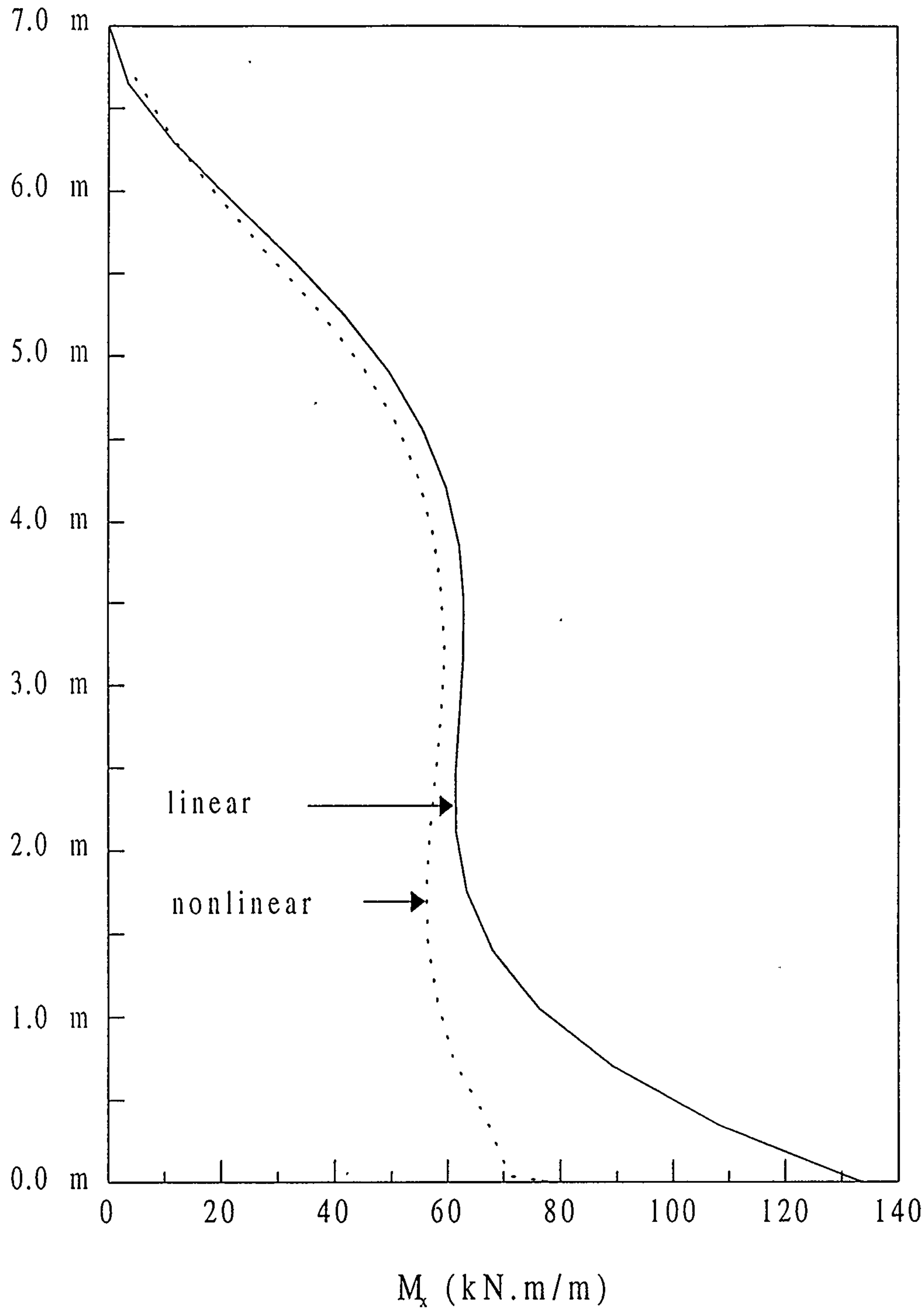

Figure 4.16 M_x-diagram for Tank 1 according to the linear and nonlinear analyses. Case of temperature drop (T_o = -20 °C, T_i = 5 °C).

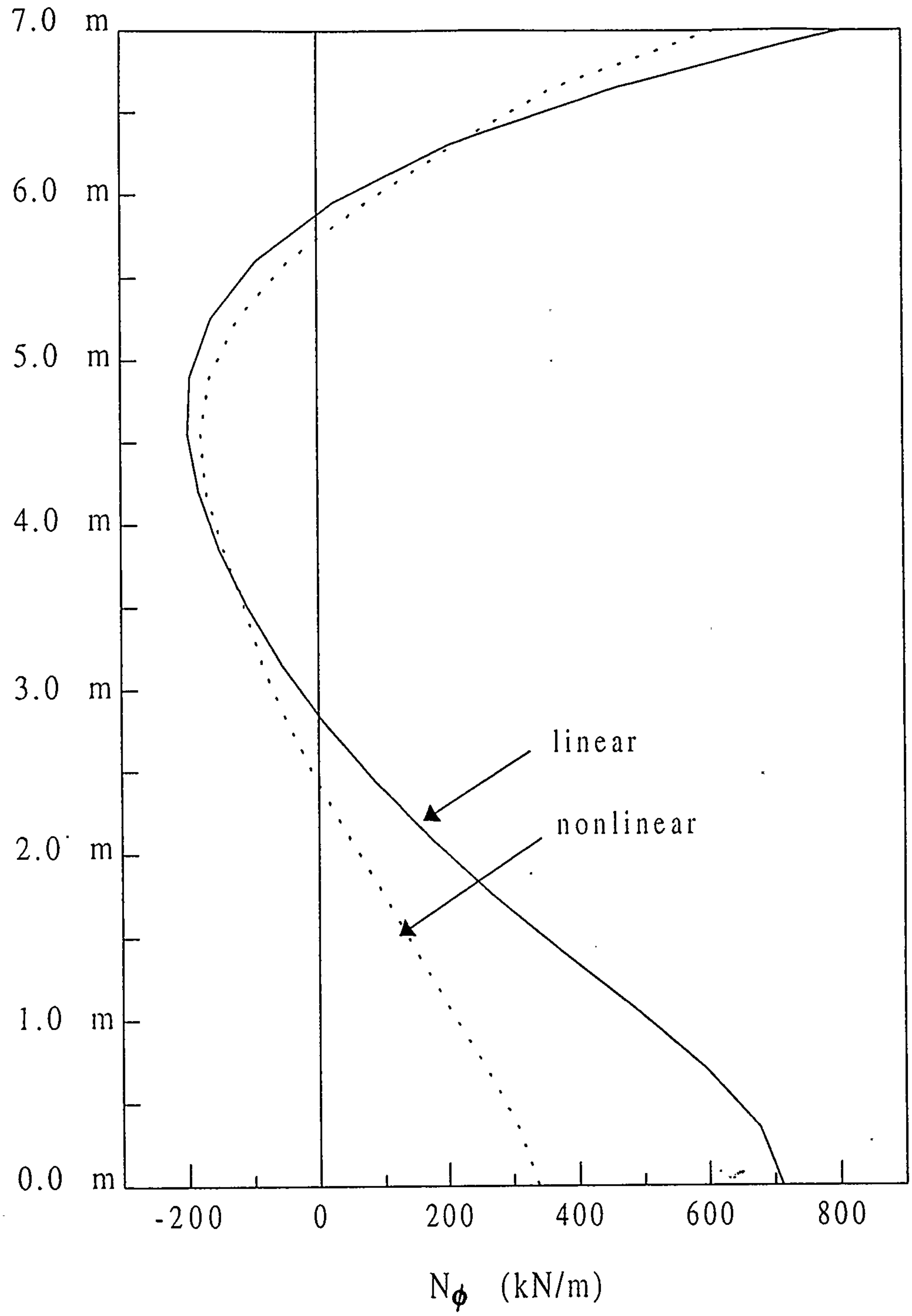

Figure 4.17 N_ϕ -diagram for Tank 1 according to the linear and nonlinear analyses. Case of temperature drop (T_o = -20 °C, T_i = 5 °C).

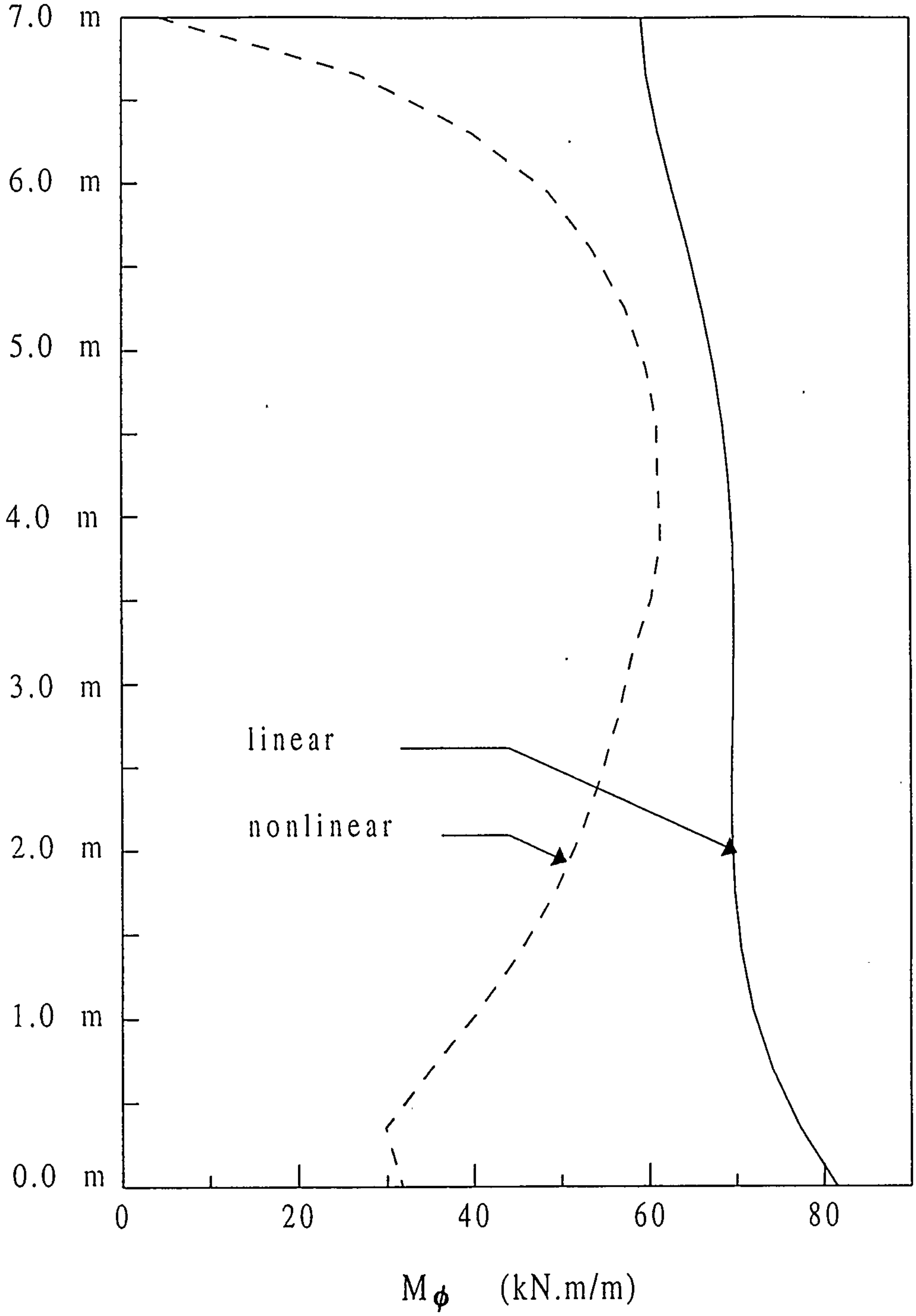

Figure 4.18 M_ϕ -diagram for Tank 1 according to the linear and nonlinear analyses. Case of temperature drop (T_o = -20 °C, T_i = 5 °C).

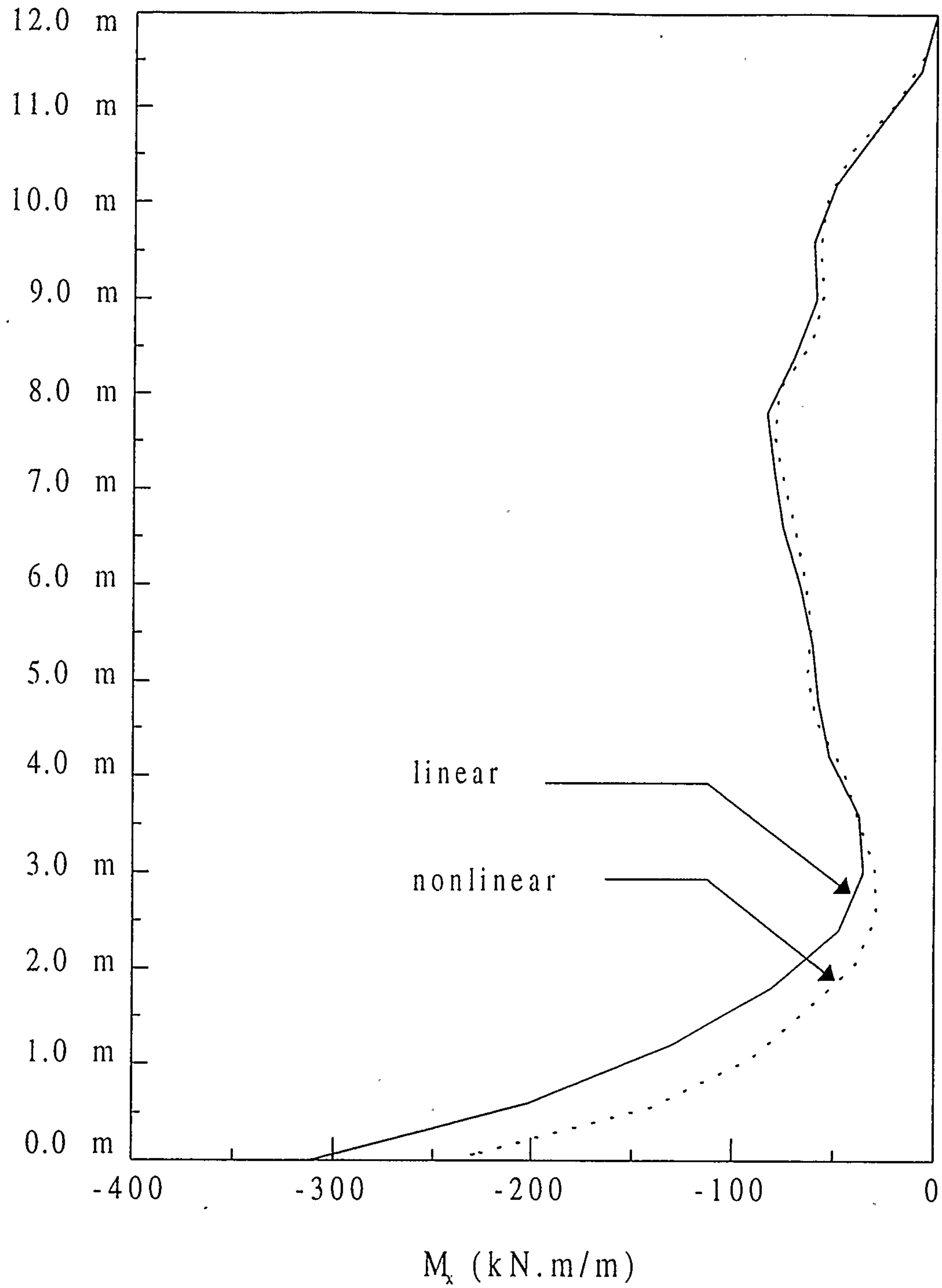

Figure 4.19 M_x-diagram for Tank 2 according to the linear and nonlinear analyses. Case of liquid load + prestressing + temperature rise (T_o = 45 °C, T_i = 15 °C).

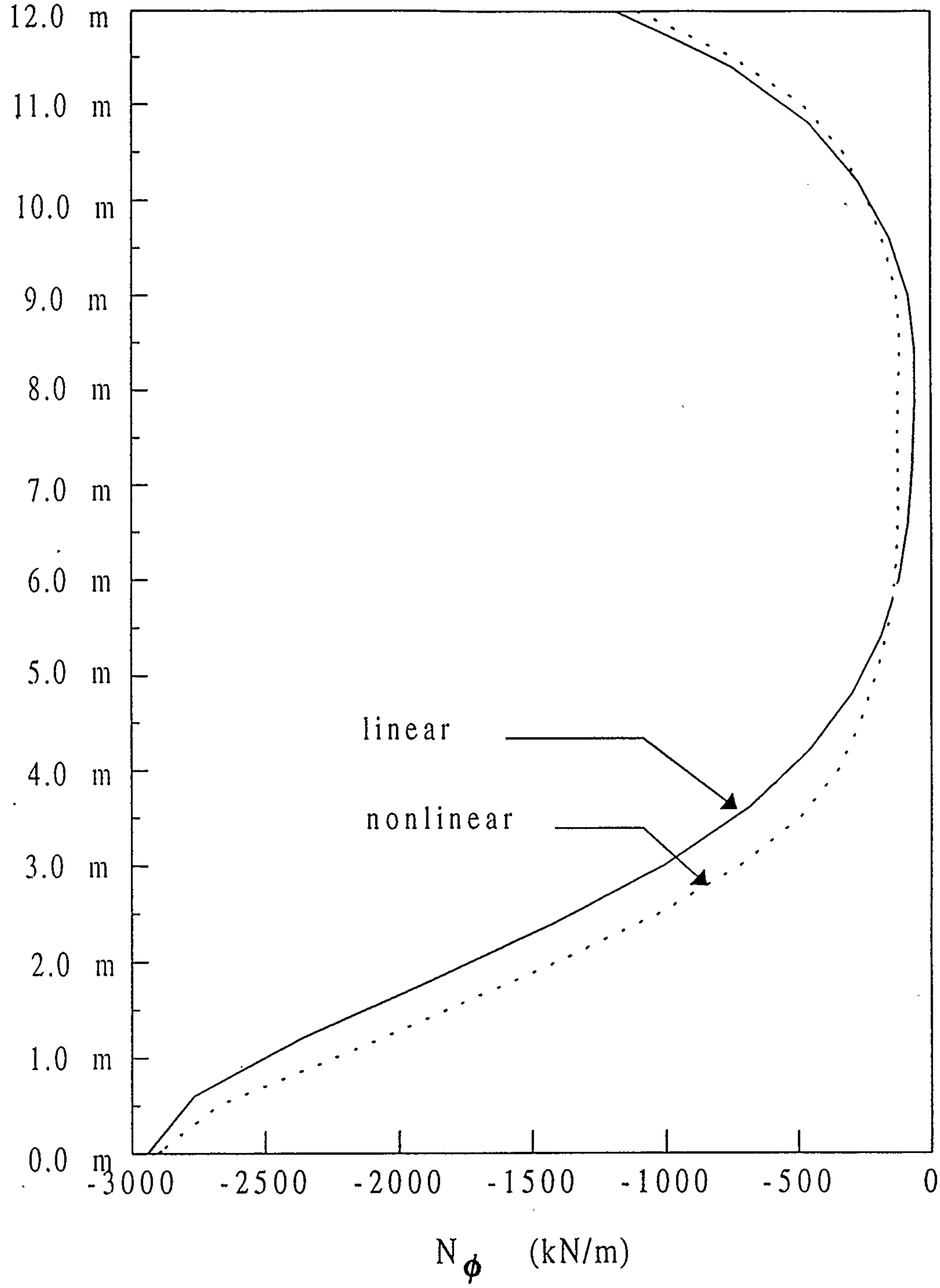

Figure 4.20 N_ϕ -diagram for Tank 2 according to the linear and nonlinear analyses. Case of liquid load+prestressing+temperature rise (T_o = 45 °C, T_i = 15 °C).

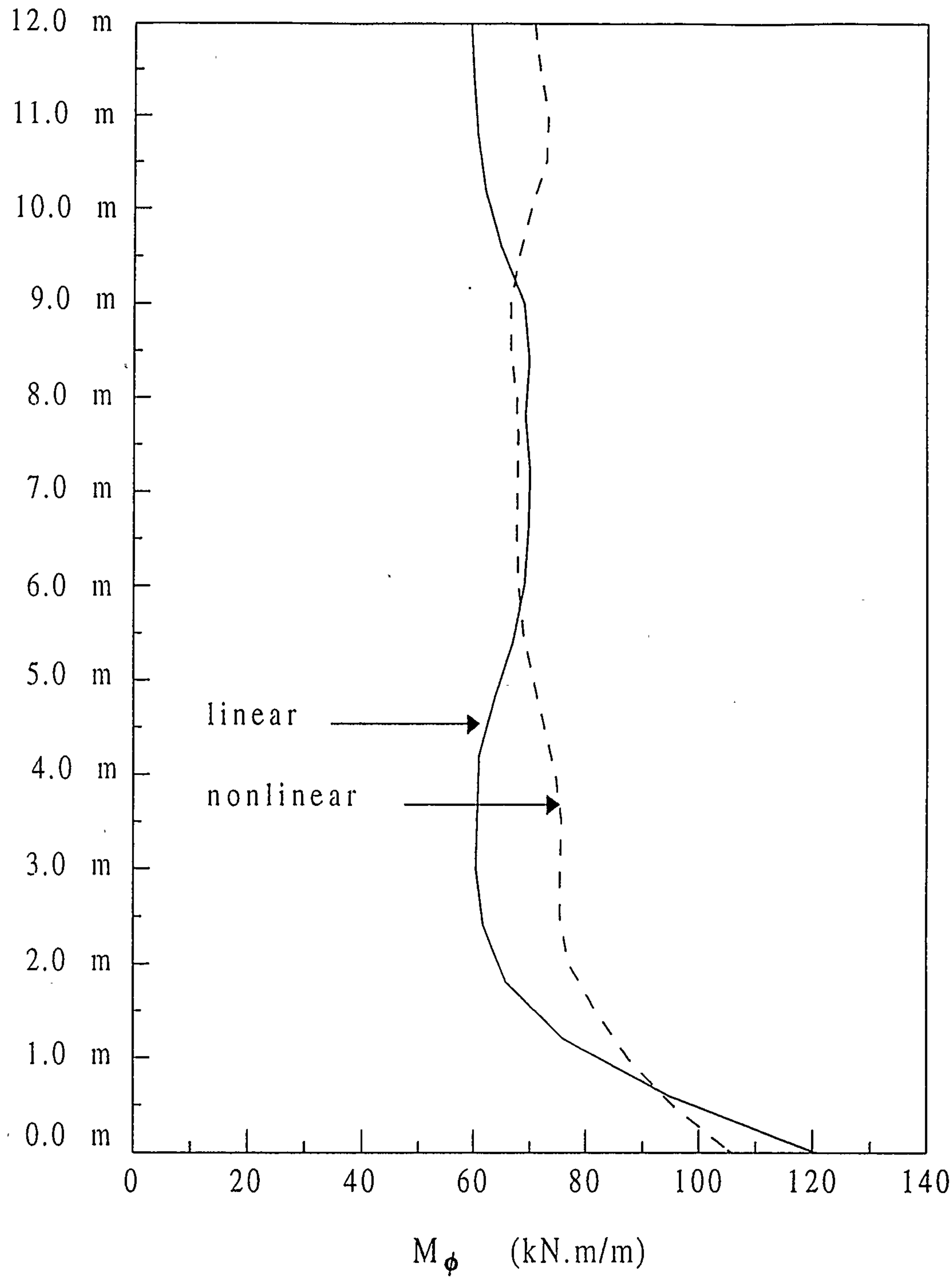

Figure 4.21 M_ϕ -diagram for Tank 2 according to the linear and nonlinear analyses. Case of liquid load + prestressing + temperature rise (T_o = 45 °C, T_i = 15 °C).

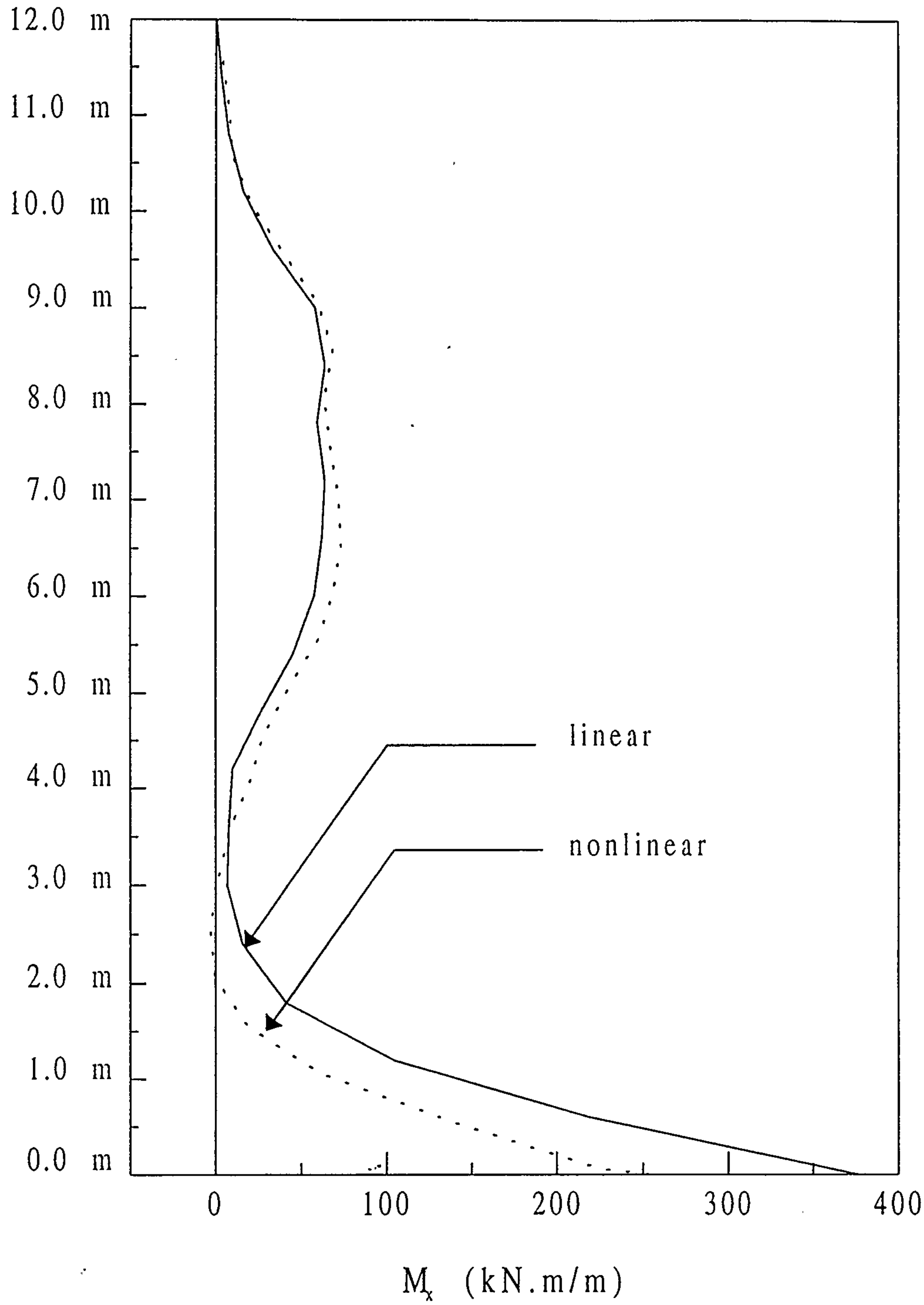

Figure 4.22 M_x-diagram for Tank 2 according to the linear and nonlinear analyses. Case of prestressing + temperature drop (T_o = -20 °C, T_i = 5 °C).

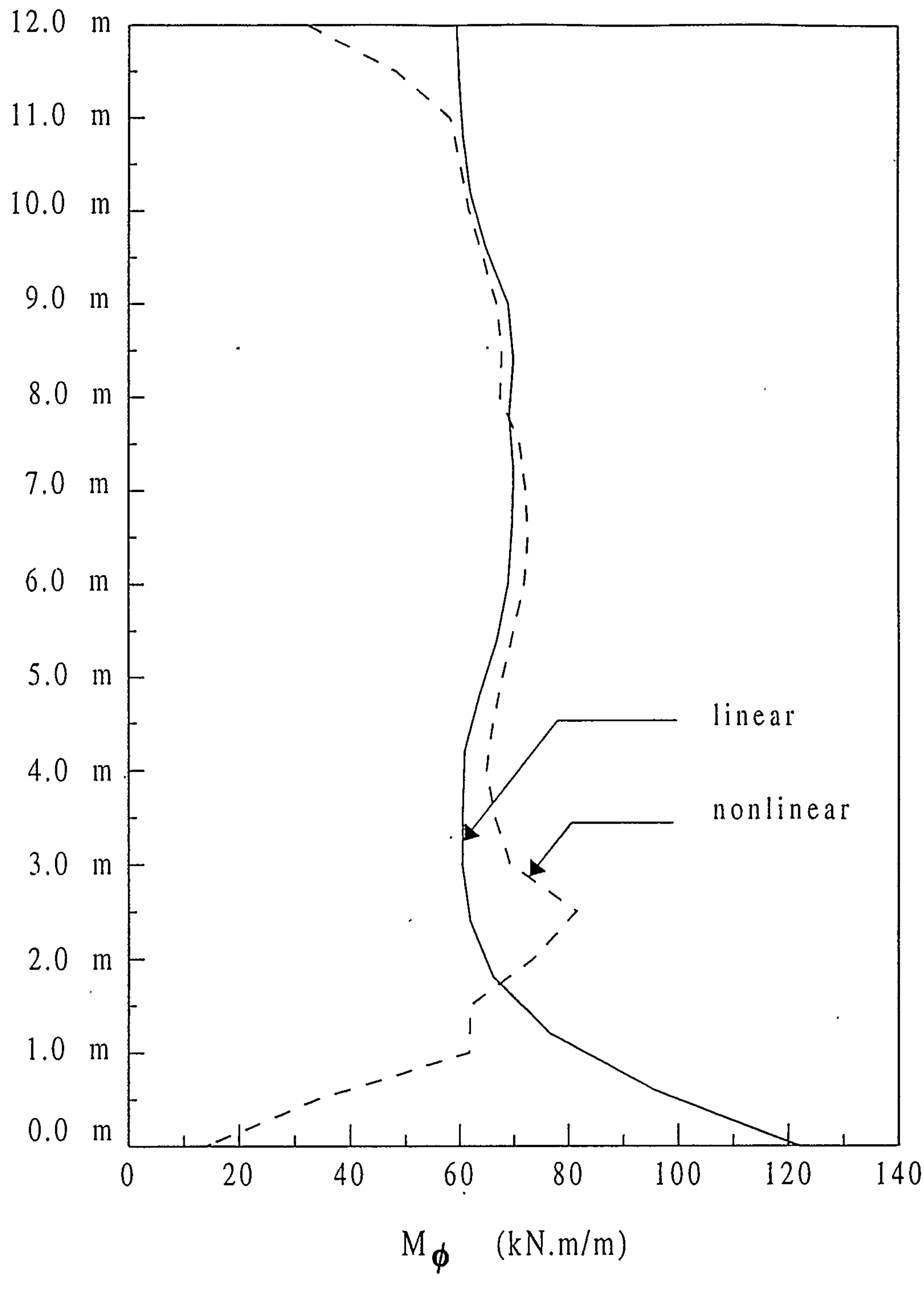

Figure 4.23 M_ϕ -diagram for Tank 2 according to the linear and nonlinear analyses. Case of prestressing + temperature drop (T_o = -20 ° C, T_i = 5 °C)

Tank 2 - Case A:

The situation becomes less severe by adding circumferential and vertical prestressing, as it is the case for Tank 2. A drop of 25 % in M_x occurs at bottom (Fig. 4.19). Although N_ϕ is compressive along the height of the Tank, vertical cracking takes place due to the tensile stresses produced by M_ϕ at the inner face of the tank wall. This explains the slight drop in hoop forces (Fig. 4.20). The M_ϕ-distribution shown in Fig. 4.21 results mainly from the eccentricity of N_ϕ with respect to the reference plane.

Tank 2 - Case B:

This case is comparable to the same case for Tank 1 (Figs. 4.22 and 4.23).

4.7 CONCLUDING REMARKS

Allowing for cracking in cylindrical concrete tanks subjected to temperature loads relieves the induced thermal stresses and reduces the stiffness of the tank wall. Thus, a drop in the internal forces results and a more economic cross-section could be attained.

The next chapter deals with the nonlinear behavior of reinforced tanks for a wide range of temperature changes. Crack widths and the amount of non-prestressed steel required in the control of cracking will be discussed in Chapter 6.

CHAPTER 5

NONLINEAR BEHAVIOR OF NON-PRESTRESSED TANKS UNDER THERMAL LOADS ONLY

5.1 GENERAL

Thermal stresses induced in circular tanks by daily fluctuations of ambient conditions have generally been ignored or calculated in an approximate way by designers in the belief that they are of insignificant magnitude compared with the actions of water load and prestressing. However, it has been shown in Chapter 2 that the stresses produced by those ambient thermal stresses are of a significant magnitude, which justified a detailed study of thermal effects on tanks.

Recently Elbadry (1989) investigated the nonlinear behavior of a continuous beam subjected to thermal loads. A temperature rise varying linearly over the depth is assumed. The difference in temperature between the top and the bottom surfaces, ΔT is gradually increased. The variation of the continuity moment M with ΔT is plotted as shown in Fig. 5.1.

As the tensile strength of concrete is reached, the first crack takes place accompanied by a sudden drop in M. The drop in M is caused by a reduction of the flexural rigidity. Further increase of ΔT increases M again up to the formation of a new crack. The same process continues until a stabilized crack pattern is attained.

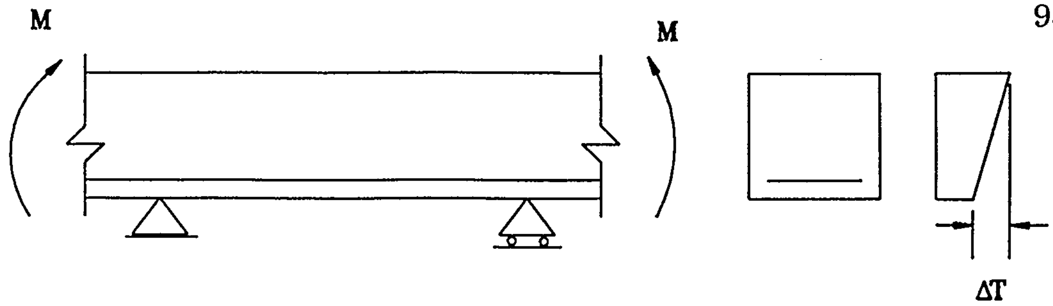

a) An interior span of a continuous beam subjected to temperature rise

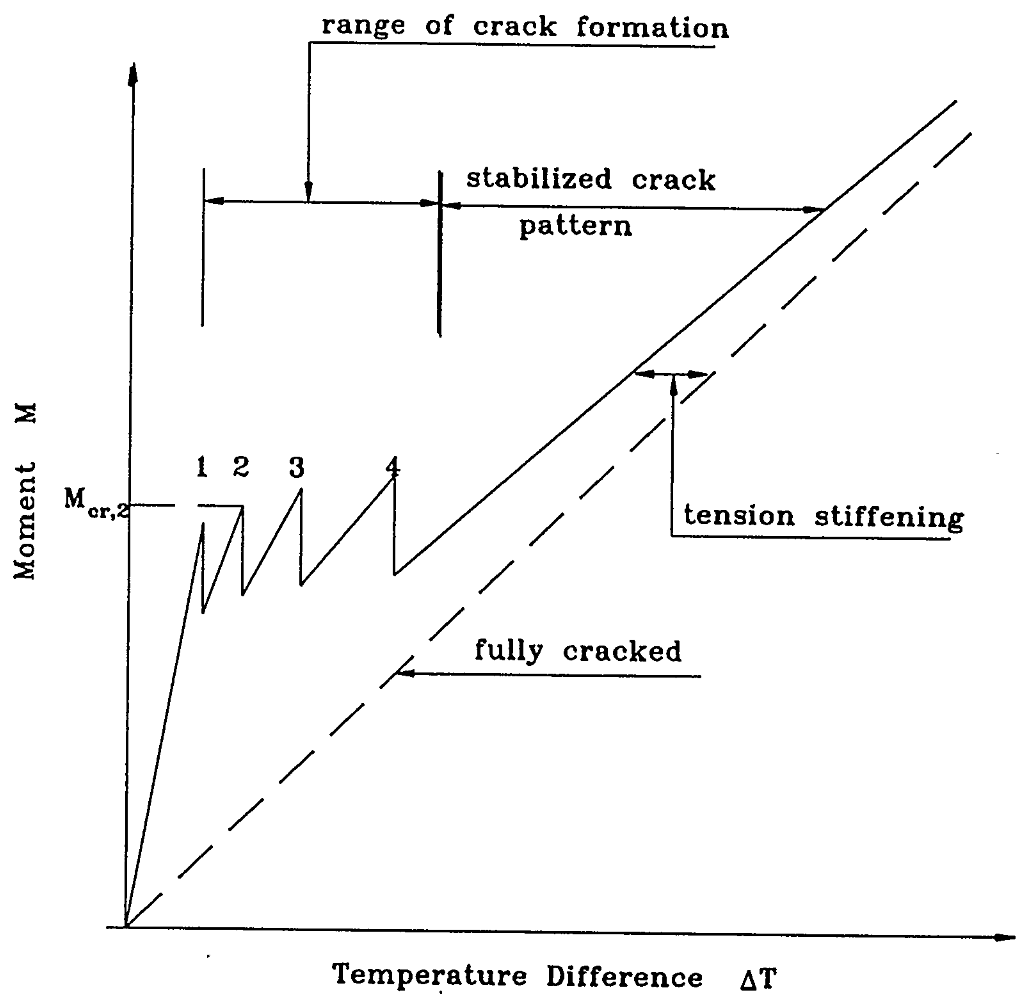

Figure 5.1 The thermal response of a continuous concrete beam (according to Elbadry).

Elbadry concluded that the largest moment occurring during the development of the cracking pattern is equal to the cracking moment of the section for a continuous beam.

In order to check the applicability of the latter conclusion for circular tanks, a study of the effects of cracking on the thermal response of a cylindrical concrete tank is conducted. The computer program FELARC is used to perform the nonlinear analysis using the same model explained in the previous chapter. Two cases are studied, in which linear temperature change is applied between T_o and T_i degrees Celsius at the outer and inner surfaces of the wall, respectively:

Case A: monotonic increase of T_o by an increment of 2°C and up to 48°C, while T_i=0.0.

Case B: monotonic decrease of T_o by an increment of -2°C and down to -62°C, while T_i=0.0.

The analyzed tank (Tank 1) is non-prestressed and has the following data:

r = 12.5 m,

H = 7.0 m,

t = 0.3 m,

A_{siv} = 1500 mm^2/m (ρ = 0.60 %) for Case A,

= 2100 mm^2/m (ρ = 0.80 %) for Case B,

A_{sov} = 600 mm^2/m (ρ = 0.25 %) for Case A,

	=	$2100\ mm^2/m$ for Case B,
A_{sih}	=	$600\ mm^2/m$ for Cases A and B,
A_{soh}	=	$600\ mm^2/m$ for Cases A and B,
c	=	30 mm,
f_t'	=	2.5 MPa,
α_c	=	10 E-6,
ν	=	1/6,

where c, f_t', α_c and ν are the clear concrete cover, the tensile strength, the thermal coefficient and Poisson's ratio of concrete, respectively. The subscripts used are:

siv	=	the vertical steel at the inner face of the tank wall,
sov	=	the vertical steel at the outer face of the tank wall,
sih	=	the horizontal steel at the inner face of the tank wall,
soh	=	the horizontal steel at the outer face of the tank wall.

The steel arrangement is the same as illustrated previously in Figs. 2.3 and 2.5.

Low steel ratios are chosen to point out the nonlinear behavior due to the thermal loads. Higher steel ratios are chosen for Case B to enable a reliable study of the progressive cracking of the concrete layers, especially because the cracking in the vertical and circumferential directions coincide at base.

The following assumptions are made to simplify the analysis:

- The concrete properties do not change in either in high or low temperatures.
- There is no ice formation taking place down to -62 °C.

5.2 ANALYSIS FOR LOADING CASE A

The elastic distributions of the internal forces are shown in Fig. 5.2 for $T_o = 10°C$ and $T_i = 0°C$. Two critical cross-sections are focused on, at which the maximum internal forces take place. The sections are:

1) the section at base, where the maximum negative M_x takes place,
2) the section at x = 4.2 m, where x is measured vertically from the base point, where the maximum positive N_ϕ takes place.

Tensile hoop forces and moments producing tension on the outer face of the tank wall are considered positive.

Figure 5.3 depicts the variation of M_x and f_{siv} at base versus T_o, where f_{siv} is the vertical steel stress at the inner face of the tank wall. At $M_x = M_{x,cr}$ = 41 kN.m/m circumferential cracking occurs, and hence a nonlinear increase of M_x takes place up to M_x = 77 kN.m/m corresponding to T_o = 14 °C. A further increase in T_o up to 18 °C results in a drop of M_x. The reason for that drop is as follows: the cross-section of the tank wall is divided into 7 concrete layers (Fig. 4.2). Three layers reached the state of total crack, i.e. the tension stiffening is overcome by the increasing tensile stresses. This results in a drop in wall stiffness accompanied by a drop in M_x and a substantial increase in

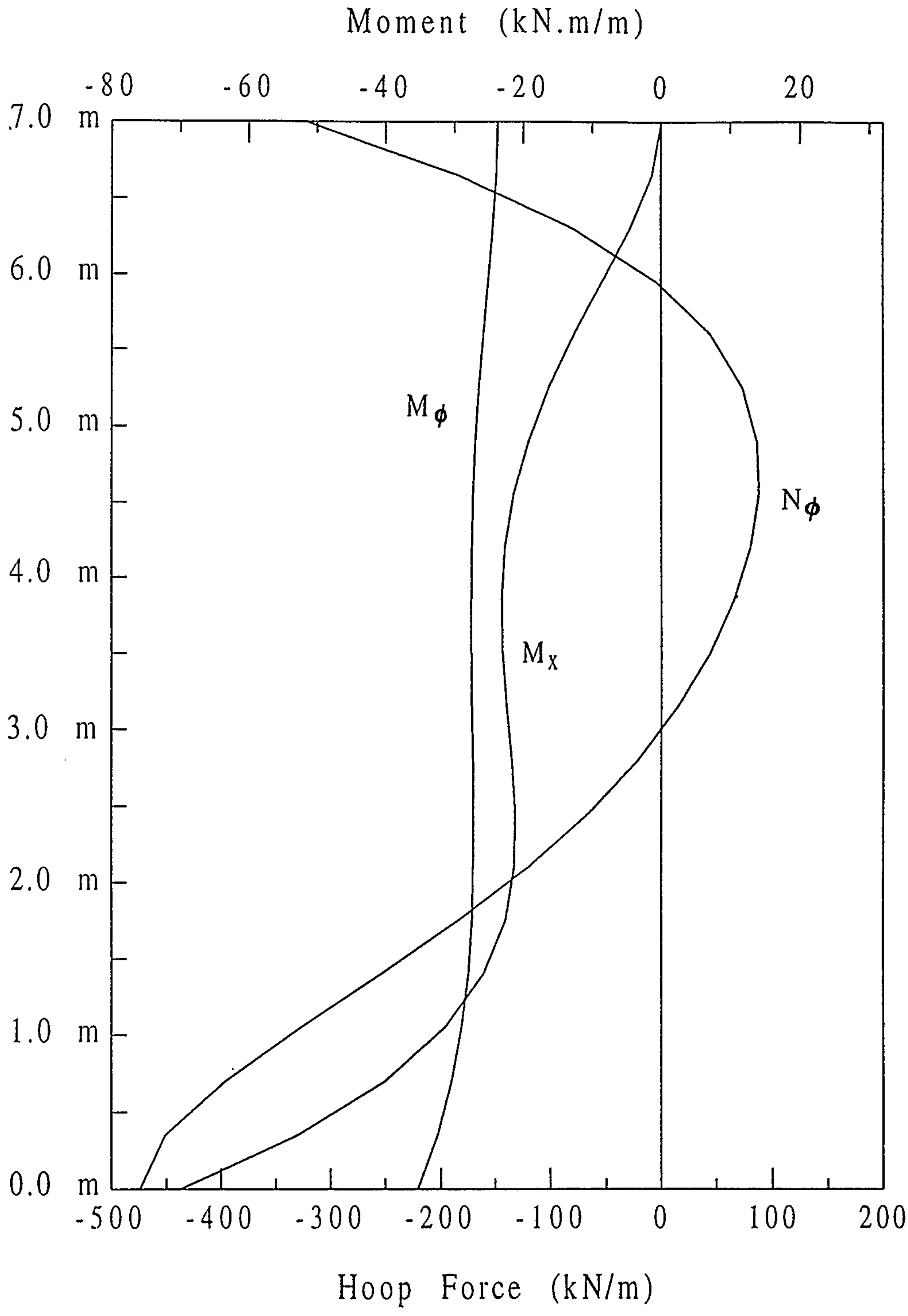

Figure 5.2 The internal forces produced due to a temperature rise (T_o = 10.0 °C, T_i = 0.0 °C)

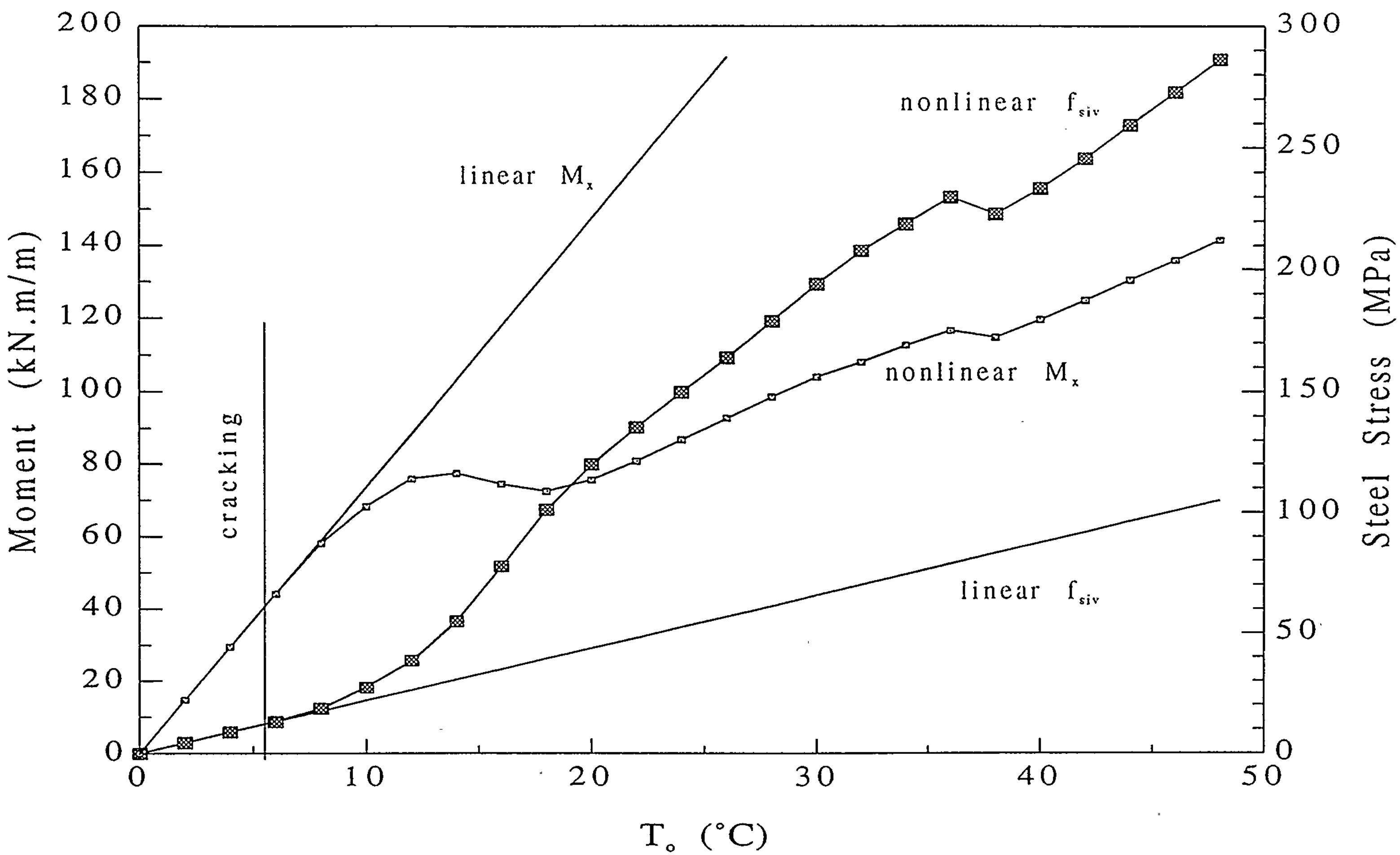

Figure 5.3 The variation of M_x and f_{siv} with T_o for Loading Case A at base.

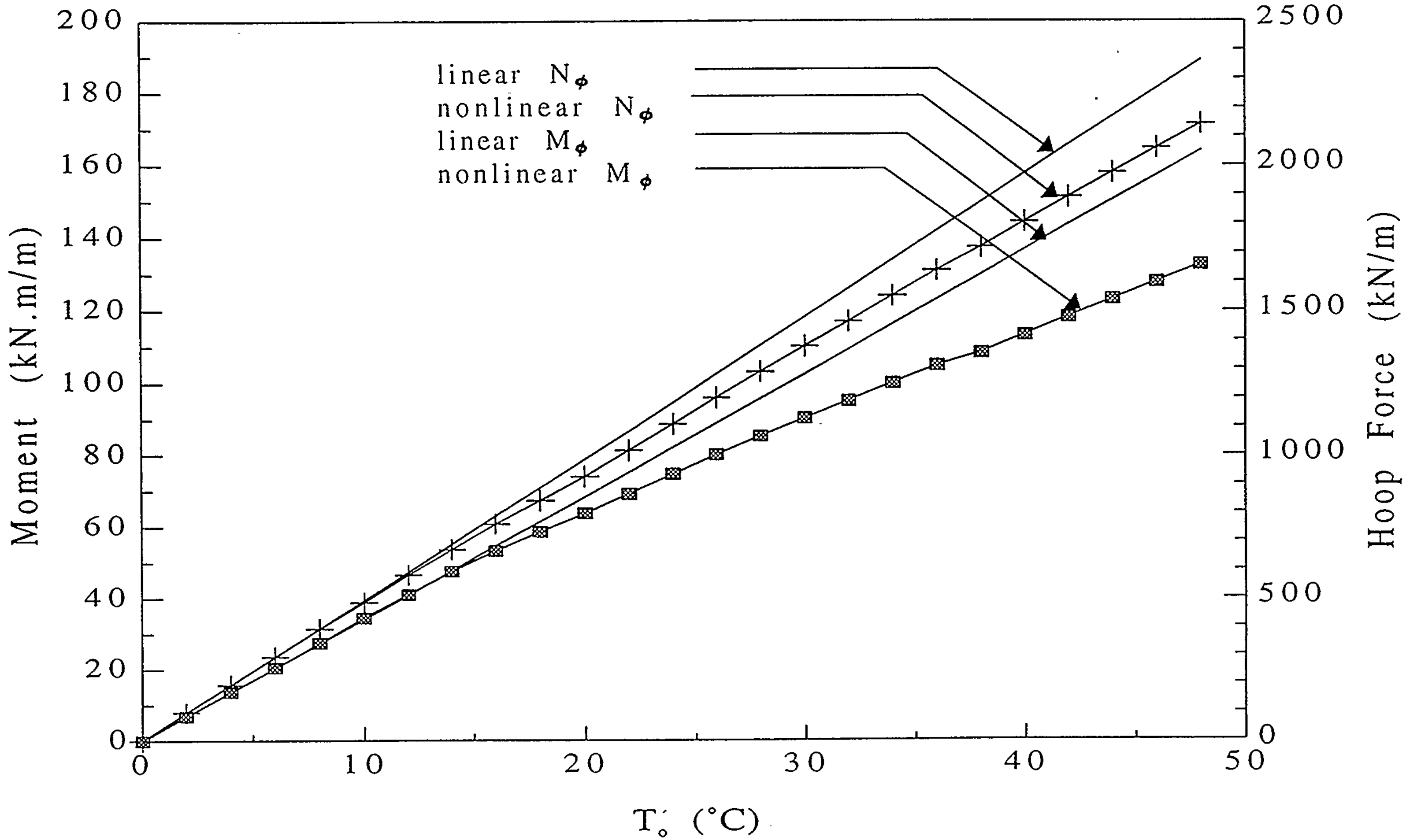

Figure 5.4 The variation of M_ϕ and N_ϕ with To for loading case A for Loading Case A at base.

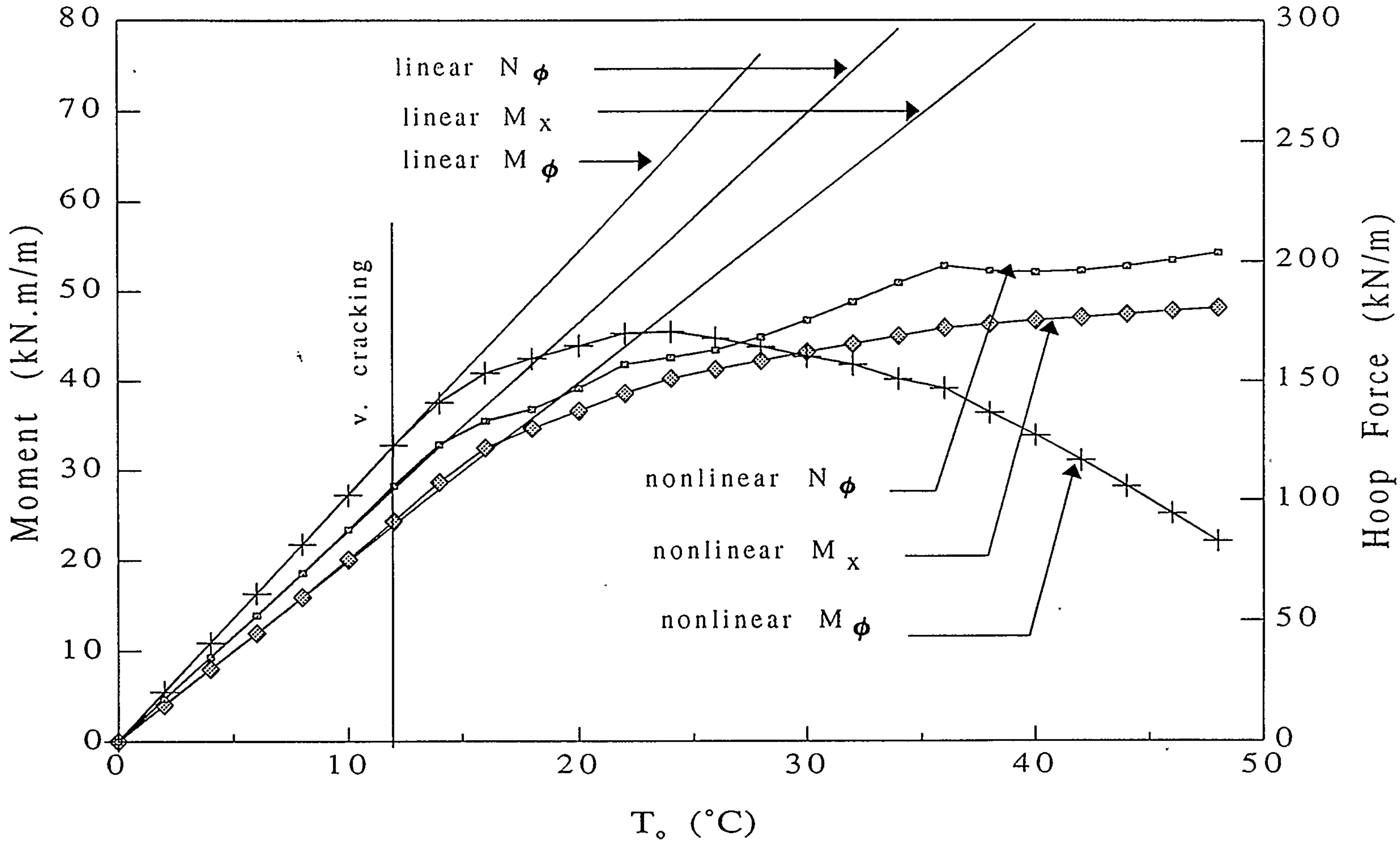

Figure 5.5 The variation of N_ϕ, M_ϕ and M_x with T_o for Loading Case A at x = 4.2 m.

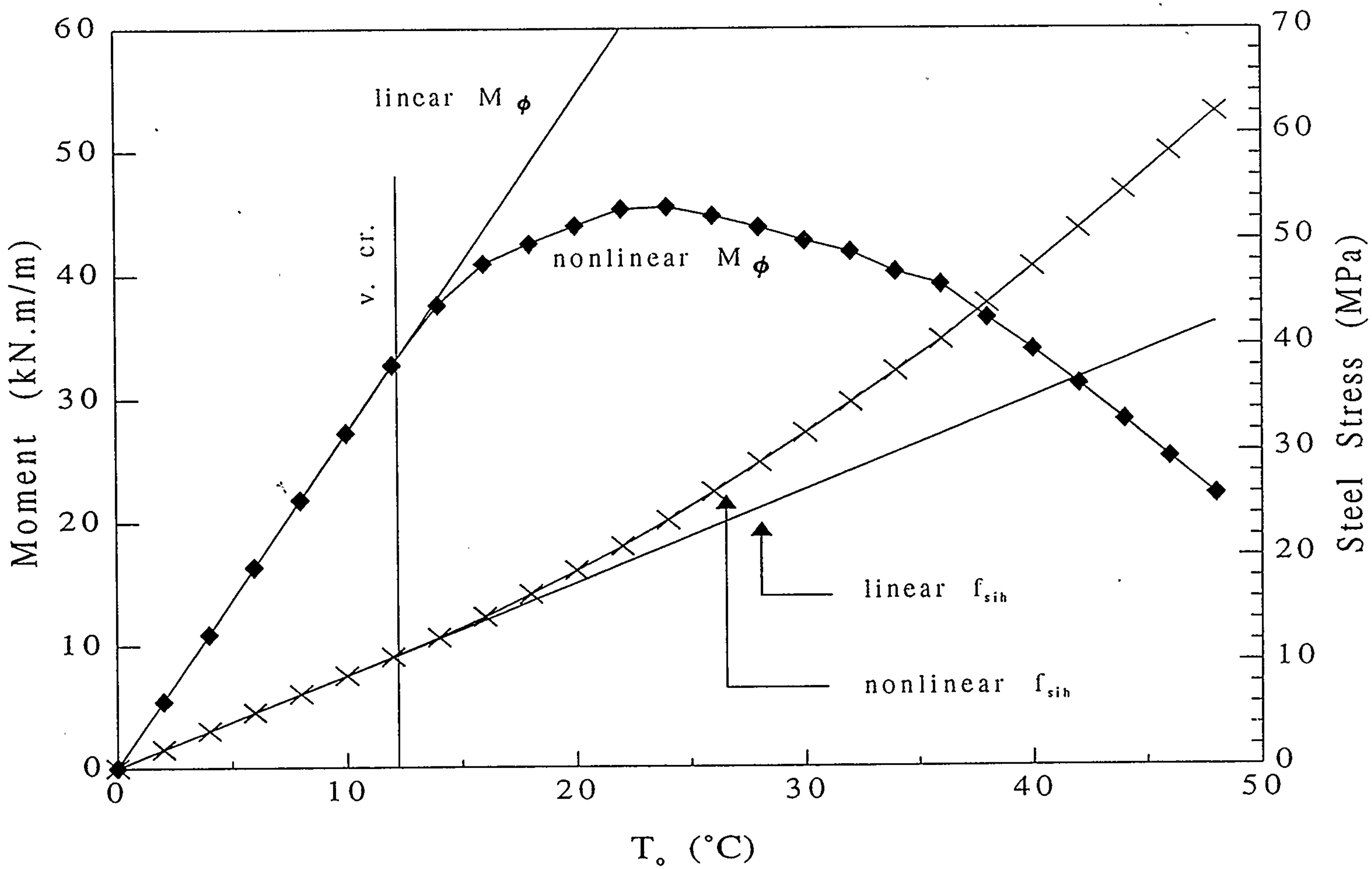

Figure 5.6 The variation of M ϕ and f_{sih} with T_o for Loading case A at x = 4.2 m.

slope of the curve for f_{siv} in the same region. For $T_o > 18°C$ M_x and f_{siv} increase up to the point of steel yielding.

A reduction in the values of N_ϕ and M_ϕ is noticeable at base, although no vertical cracks occur (Fig. 5.4). This reduction is due to the weakening of the wall cross-section because of the circumferential cracking. According to Elliott (1989) a reduction of M_x is accompanied by an increase of N_ϕ for the case of liquid load. However, this does not apply for the case of thermal loads, since cracking of concrete alleviates the induced thermal stresses.

The first vertical crack occurs at the point of maximum N_ϕ at $x = 4.2$ m, where $N_{\phi,cr}$ and $M_{\phi,cr}$ are 107 kN/m and 33 kN.m/m, respectively, corresponding to $T_o = 12$ °C. After cracking a nonlinear increase in both N_ϕ and M_ϕ takes place due to the increase of T_o (Fig. 5.5). For $T_o > 24$ °C the M_ϕ-curve descends, while the N_ϕ-curve is still ascending. The decrease of the M_ϕ-curve is attributed to eccentricity of N_ϕ with respect to the reference plane (the mid-layer) after cracking. The M_x-curve at the same section indicates a nonlinear behavior, although horizontal cracking does not occur. It is similar to the behavior of N_ϕ and M_ϕ at base.

On the other hand, the slope of the f_{sih}-curve increases as a result of cracking, where f_{sih} is the stress of the horizontal steel, as shown in Fig. 5.6.

5.3 THE ANALYSIS FOR LOADING CASE B

Figure 5.7 shows the elastic distributions of the internal forces of the

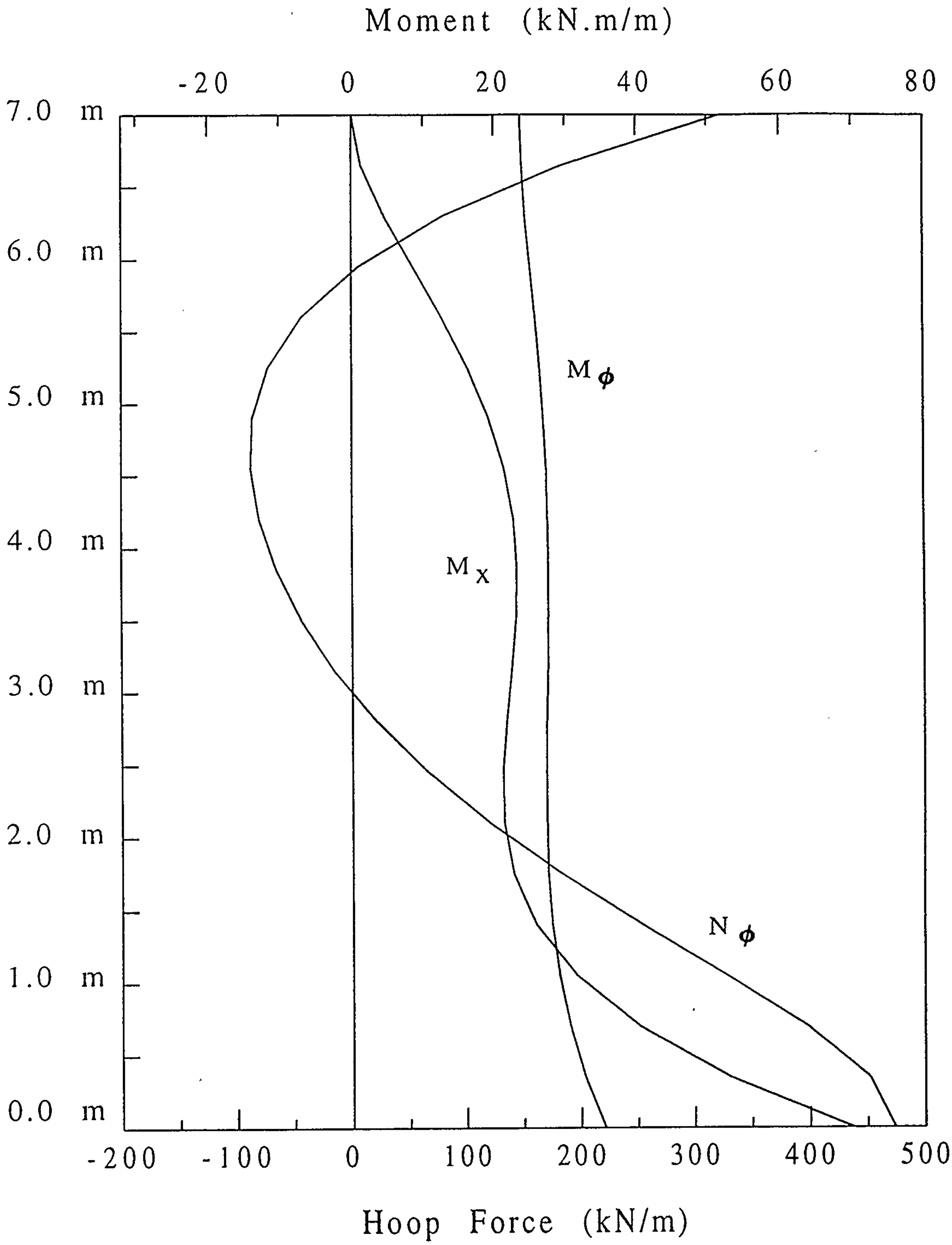

Figure 5.7 The internal forces produced due to a temperature drop (T_o = -10.0 °C, T_i = 0.0 °C)

following thermal loading: T_o = -10°C and T_i = 0°C. As for the previous case, two critical cross-sections are focused on, at which the maximum internal forces take place. The sections are:

1) the section at base, where the maximum negative M_x and the maximum positive N_ϕ take place,
2) the section at top, where a high value of positive N_ϕ takes place.

In Fig. 5.8 the variations of M_x, N_ϕ and M_ϕ at base with T_o are plotted. Vertical and circumferential cracking occur simultaneously at T_o = -6°C. After cracking the M_x- and N_ϕ-curves ascend up to T_o = -16°C, where N_ϕ-curve starts to descend while M_x-curve continues up. At T_o = -18°C the circumferential stiffness of the tank is substantially affected since all elements are vertically cracked. That is most probable reason for the drop of N_ϕ.

At T_o = -40°C two concrete layers out of the seven layers, of which the cross-section is composed, reach the state of full cracking due to the vertical tensile stresses. Consequently, M_x-curve experiences a sudden drop associated by a sudden jump in the f_{sov}-curve, as shown in Fig. 5.9, where f_{sov} is the stress of the vertical steel at the outer face of the tank wall. For the range of T_o = -40 to -50°C, M_x increases again. At T_o = -50°C another drop in M_x occurs as a result of full cracking of a third concrete layer.

At the top of the tank N_ϕ and M_ϕ cause the tank to crack vertically, while no circumferential cracking takes place, for M_x = 0.0 at top. Cracking occurs at T_o = -8°C, afterwards a nonlinear increase of N_ϕ takes place up to

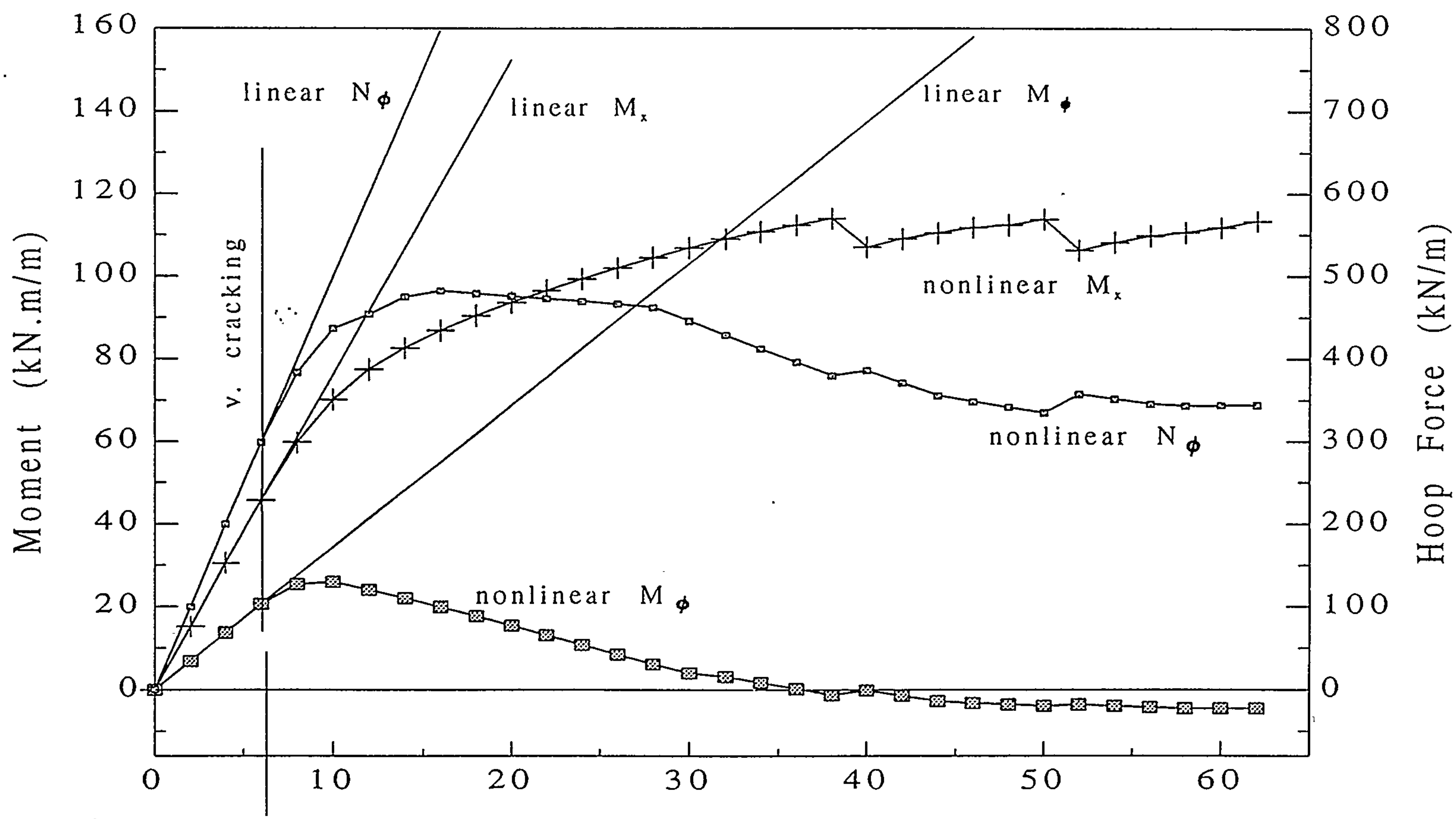

Figure 5.8 The variation of N_ϕ, M_x and M_ϕ with T_o for Loading Case B at base.

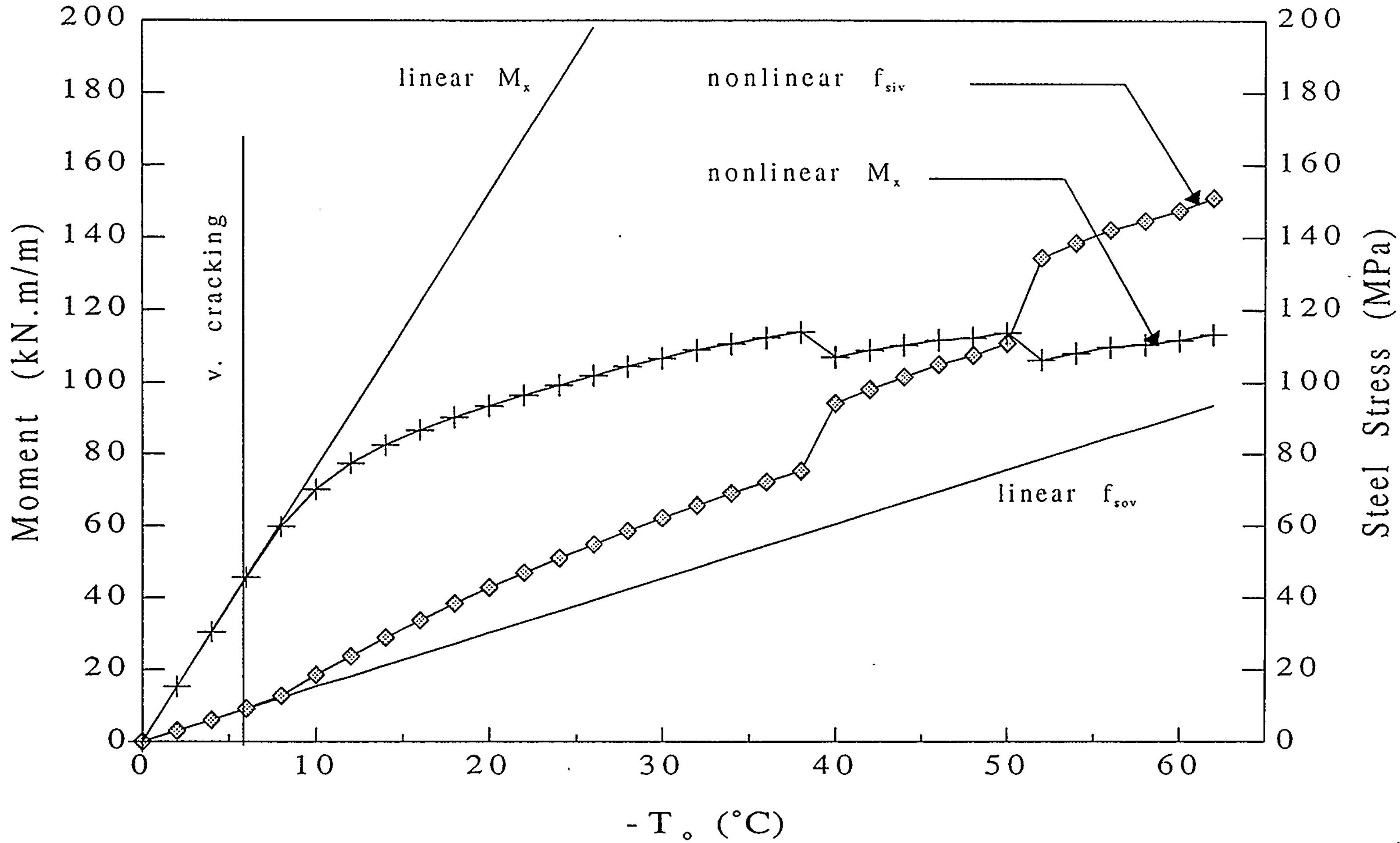

Figure 5.9 The variation of M_x and f_{sov} with T_o for Loading Case B at base.

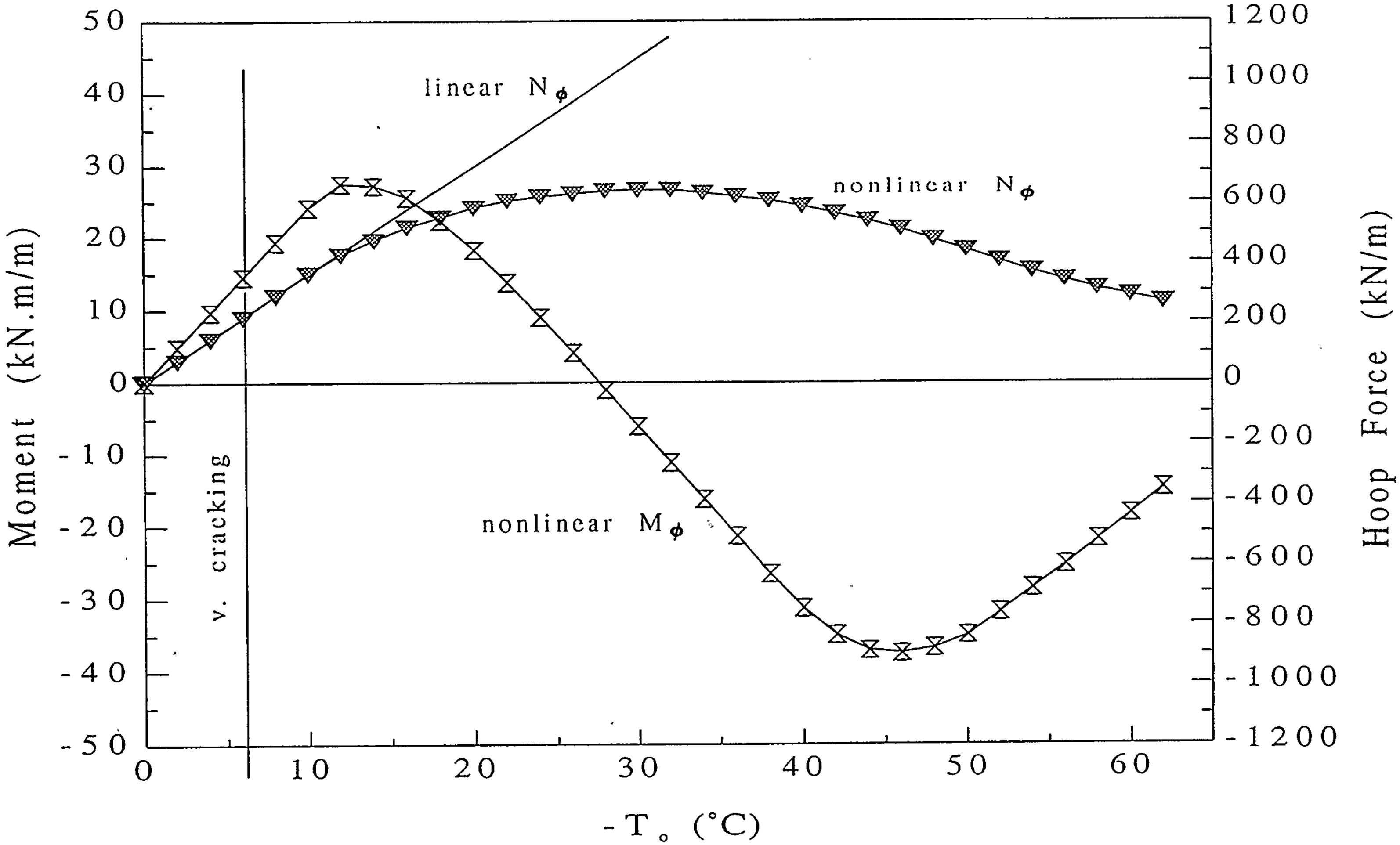

Figure 5.10 The variation of N_ϕ and M_ϕ with T_o for Loading Case B at top.

T_o = -34°C (Fig. 5.10). The distribution of M_ϕ is caused by the eccentricity of N_ϕ with respect to the reference plane.

5.4 CONCLUSION

The conclusions of Elbadry mentioned above was applied to a concrete beam subjected to a constant moment. The tensile strength of concrete was assumed variable along the length of the beam. However, in the present study a different case is examined. The magnitudes of the internal forces are variable and the tensile strength of the concrete is assumed constant along the height of the tank wall. On the other hand, the analysis using the computer program FELARC assumes a cracked concrete layer at the position of cracking and not a single individual crack. For these reasons once a section is cracked the stabilized condition is assumed without undergoing the phase of multiple drops illustrated in Fig. 5.1. This is why the vertical moments exceed the cracking moment for both examined cases.

Another point concluded by the present study, is that the cracking of concrete due to thermal loads in one direction affects the other perpendicular direction and causes the internal forces in the second direction to drop. This agrees with Elbadry, that the cracking of concrete alleviates the thermal stresses. However, this does not apply to the case of liquid load, since the cracking of concrete due to the vertical moments produced by the liquid load causes the hoop forces to increase Elliott (1989).

liquid load, since the cracking of concrete due to the vertical moments produced by the liquid load causes the hoop forces to increase Elliott (1989).

In the previous and present chapters the relief of thermal stresses due to the concrete cracking has been emphasized in order to design the cylindrical concrete tank wall with an economic cross-section. The next chapter deals with the control of crack width by means of the non-prestressed steel ratio to ensure a safe design.

CHAPTER 6

CRACK CONTROL IN CIRCULAR CONCRETE TANKS

6.1 GENERAL

In the previous chapters it was shown that the temperature load is one of the governing loadings for the design of circular tanks. It was also shown that the cracking of the concrete relieves the thermal stresses. The relief of internal forces and stresses should be accounted for in design so that more economic cross-sections can be employed.

ACI Committee 350 (1989) controls cracking of reinforced concrete cylindrical tanks by specifying a low steel tensile stress. Similarly, ACI Committee 344 (1988) and the British Code BS 8007 (1989) specify a low tensile stress in the non-prestressed steel for cylindrical prestressed tanks (see Chapter 2). The design using these codes is commonly based on linear elastic analysis.

In this chapter the control of crack width is examined based on results of nonlinear analyses. Crack widths in the range of 0.1 - 0.2 mm are admitted for the present study. This range is in accordance with the specifications of the different codes, namely CEB-FIB 1990, ACI 350-89 and BS 8007 1989.

On the other hand, some researchers justified the design allowing cracking in water retaining structures. Cordes et al (1991) and Clear (1985) conducted some research on the phenomena of autogenous healing of fine conducted some research on the phenomena of autogenous healing of fine cracks. They investigated crack widths in the range of 0.15 - 0.25 mm subjected to a head of water of 20 m. It was concluded that after a period less than 7 days of exposure, autogenous (self-produced) healing takes place caused by certain mechanical, physical and chemical processes. The same phenomenon was mentioned by Beeby (1978).

The present study emphasizes two factors as means to control the crack width, which are as follows :

- the vertical non-prestressed steel ratio,
- the vertical prestress.

6.2 CRACK WIDTH CALCULATION IN DIFFERENT CODES

There are many factors influencing the magnitude of crack width for prestressed members; the most important of which are:

- the steel stress in the non-prestressed steel,
- the diameter and the type of the non-prestressed reinforcement bars,
- the concrete cover,
- the location of the neutral axis,
- the tension stiffening of concrete,
- the bond properties.

There are two approaches in order to estimate the magnitude of the crack width. The first is a theoretical approach based mainly on the bond properties of concrete, as in the case of the European code CEB-FIP (1990). The second approach is based on experimental and statistical analyses as used for the ACI code. However, the British Code BS 8110 employs a formula, which is a combination of the theoretical and the experimental approaches.

6.2.1 CEB-FIP Code 1990

The equations given in the CEB-FIP Code 1990 are mainly based on the bond behaviour at the cracks. As the crack occurs, the steel overtakes the tension forces developed in the concrete. A relative displacement between concrete and steel takes place, which results in loss of bond stresses.

The relation between bond and slip is demonstrated in Fig. 6.1. The ascending part of the curve represents the stage of local crushing and micro-cracking associated with the penetration of the ribs on the surface of the deformed bars into the mortar matrix. The residual bond-capacity, which is maintained by virtue of a minimum transverse reinforcement keeps the maximum bond stress value, τ_{max} constant from s_1 to s_2. As the surface crack widens, the bond stress drops until the state of total cracking is reached ($s = s_3$).

In Fig. 6.2 the distribution of steel and concrete strains and bond stresses in the vicinity of a crack are illustrated.

Crack width study is basically valid for beams subjected to pure tension, however same formulae are applicable for flexure members after replacing the area of concrete in tension by an effective area, $A_{c,ef}$.

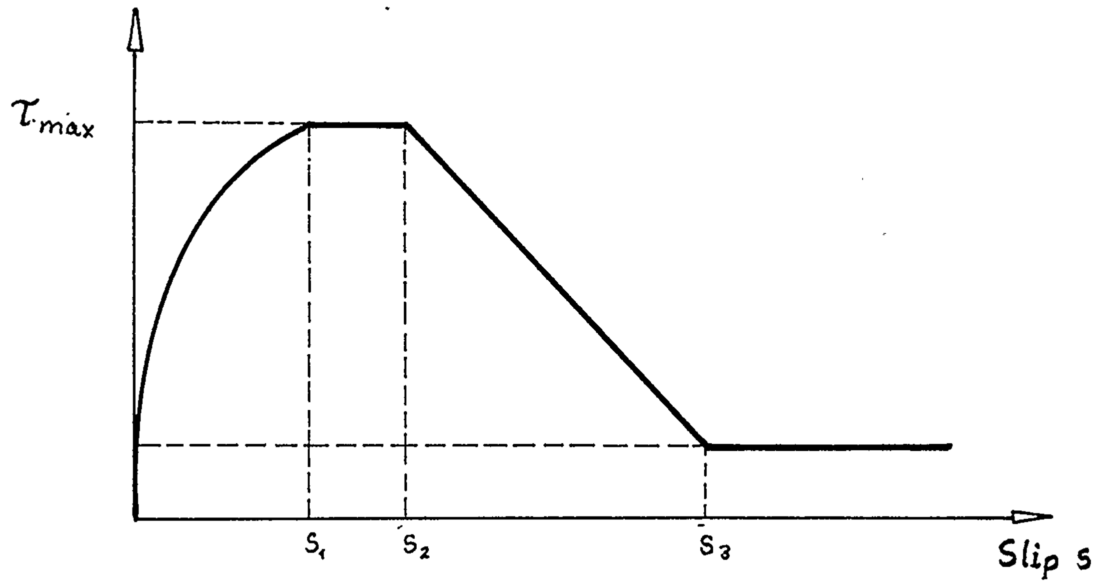

Figure 6.1 Bond stress - slip relationship (according to CEB-FIP 90)

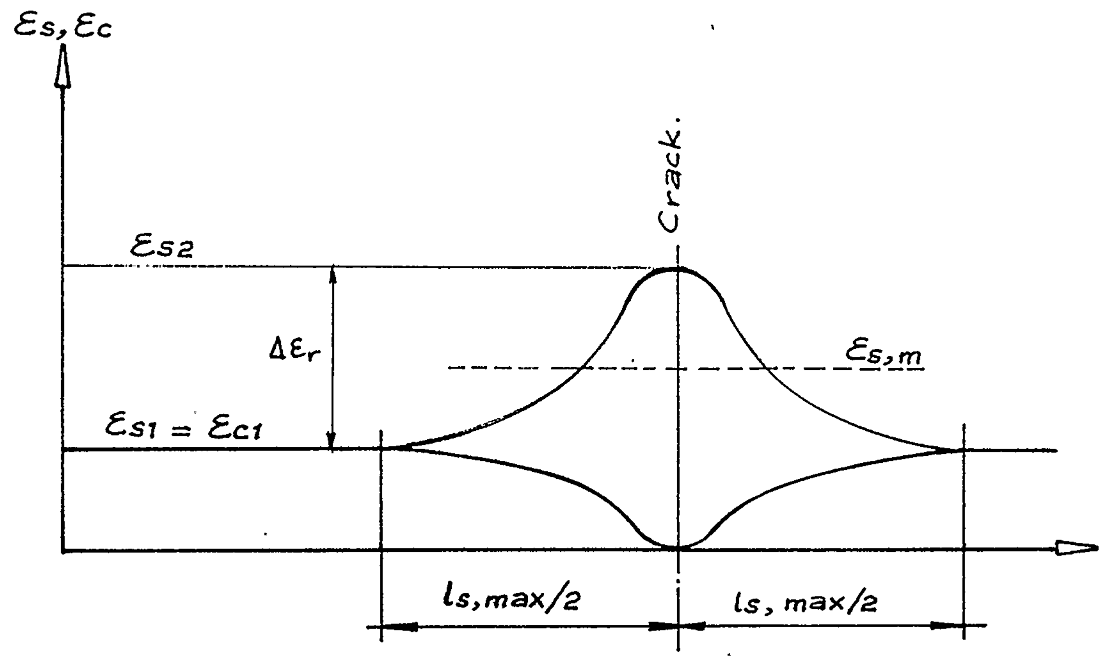

Figure 6.2 The Distribution of Steel and Concrete Strains within $l_{s,max}$

The design crack width is calculated according to the following expression:

$$w_{CEB} = l_{s,max}\,(\varepsilon_{sm} - \varepsilon_{cm} - \varepsilon_{cs}) \tag{6.1}$$

where,

$l_{s,max}$ is the length over which slip between steel and concrete occurs,

ε_{sm} is the average steel strain within $l_{s,max}$,

ε_{cm} is the average concrete strain within $l_{s,max}$,

ε_{cs} is the strain of concrete due to shrinkage.

The code differentiates between two conditions:

1) the single crack condition,

2) the stabilized cracking condition.

If $(\rho_{s,ef} \cdot \sigma_{s2} > f_{ctm}\,(1+\alpha_e\,\rho_{s,ef})$ the stabilized condition is assumed, otherwise the single crack formation is considered. Where,

f_{ctm} is the mean value of the tensile strength of the concrete at the time when the crack appears,

α_e is the ratio E_s/E_c,

$\rho_{s,ef}$ is the effective reinforcement ratio $A_s/A_{c,ef}$,

σ_{s2} is the steel stress at the crack.

The single crack condition is defined as the condition at the time of formation of the crack, when the tensile stress in the effective tension zone is equal to the tensile strength of the concrete f_{ctm}.

$A_{c,ef}$ is assessed according to Fig. 6.3. The symbols used in the figure are defined below:

x_n is the depth of the neutral axis,

c is the clear concrete cover,

ϕ_s is the bar diameter.

For the calculation of $l_{s,max}$ the bond equilibrium equation is used as follows (König and Fehling 1988):

$$F_s = \tau_{bk} \frac{l_{s,max}}{2} \Sigma O \tag{6.2}$$

where,

F_s is the force in the reinforcement steel,

τ_{bk} is the lower fractile value of the average bond stress,

ΣO is the summation of the perimeters of the rebars.

and hence,

$$l_{s,max} = 2 \frac{\sigma_{s2} - \sigma_{sE}}{4\tau_{bk}} \phi_s \tag{6.3}$$

$$l_{s,max} = \frac{\sigma_{s2} \phi_s}{2 \tau_{bk} (1 + \alpha_e \rho_{s,ef})} \quad \text{for single crack formation} \tag{6.4}$$

$$l_{s,max} = \frac{\phi_s}{3.6 \rho_{s,ef}} \quad \text{for stabilized cracking} \tag{6.5}$$

where,

σ_{sE} is the steel stress at the point of zero slip

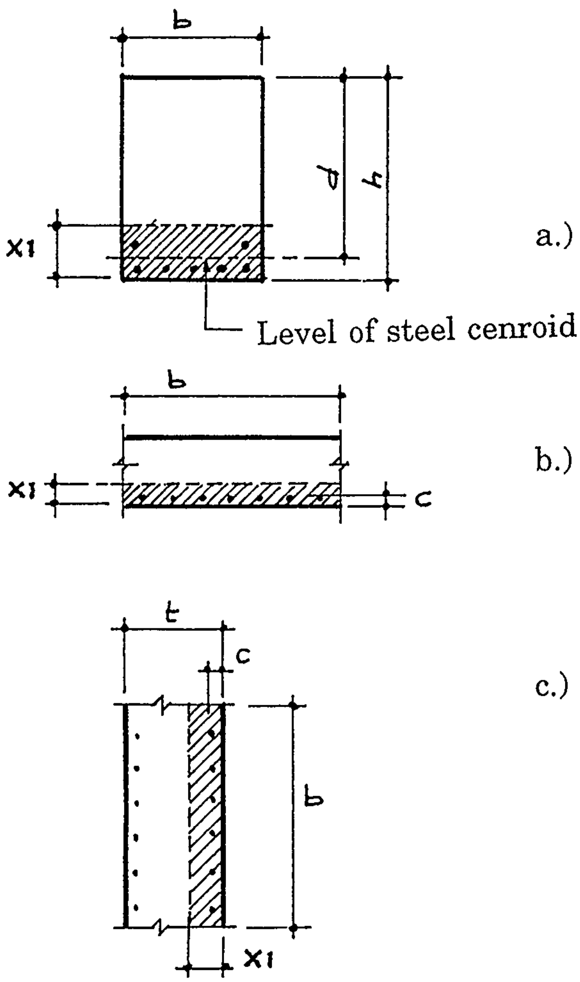

a.) <u>Beam.</u>
Effective tension area = b x_1
x_1 = 2.5 (h-d) < h-x/3

b.) <u>Slab.</u>
Effective tension area = b x_1
x_1 lesser of 2.5 (c+ /2)
or (h-x)/3

c.) <u>Member in tension.</u>
Effective tension area = b x_1
x_1 lesser of 2.5 (c+ /2)
or t/2

Figure 6.3 The Effective Tension Area

Table 6.1 Values for β_a and τ_{bk}

	Single crack formation	Stabilized cracking
Short term/ Instantaneous loading	β_a=0.6 τ_{bk}=1.8·f_{ctm}	β_a=0.6 τ_{bk}=1.8·f_{ctm}
Long term/ Repeated loading	β_a=0.6 τ_{bk}=1.35·f_{ctm}	β_a=0.38 τ_{bk}=1.8·f_{ctm}

The term $(\varepsilon_{sm}-\varepsilon_{cm})$ to be used in Eq. 6.1 is obtained by means of an empirical averaging factor β_a as follows:

$$\varepsilon_{sm} - \varepsilon_{cm} = (\varepsilon_{s2} - \beta_a \, \Delta\varepsilon_{sr}) = \varepsilon_{s2} - \beta_a \, \varepsilon_{sr2} \tag{6.6}$$

with

$$\varepsilon_{sr2} = \frac{f_{ctm}}{\rho_{s,ef} \, E_s} (1 + \alpha_e \rho_{s,ef}) \tag{6.7}$$

where,

ε_{s2} is the steel strain at the crack (Fig. 6.2).

ε_{sr2} is the steel strain at the crack due to forces causing f_{ctm} within $A_{c,ef}$. If the internal forces are lower than these forces, then $\varepsilon_{sr2}=\varepsilon_{s2}$.

ε_{sr1} is the steel strain at the point of zero slip under cracking forces reaching f_{ctm}.

$\Delta\varepsilon_{sr}$ is the difference of ε_{sr2} and ε_{sr1}.

β_a denotes an empirical factor depending on the type of loading and the condition of cracking. The values for β are shown in Table 6.1.

In order to use the output of the computer program FELARC for the calculation of crack width by the present formula, the term $(\beta_a\varepsilon_{sr2})$ in Eq. 6.6 is omitted. FELARC takes into account the tension stiffening effect and thus the resulting strain in steel is equivalent to the required strain $(\varepsilon_{sm}-\varepsilon_{cm})$.

6.2.2 ACI Committee 224

Requirements for crack control in beams and thick one-way slabs in the ACI Building Code (ACI 318) are based on the statistical analysis done by

Gergely and Lutz (1968). The main factors affecting the formulae are:

1) the stress in the steel,

2) the thickness of the concrete cover,

3) the area of concrete surrounding each reinforcing bar,

4) the strain gradient from the level of the steel to the tension face of the beam.

The crack width is calculated using the following equations:

$$w_b = (91x10^{-6}) \sqrt[3]{t_b A}\, \beta_s (f_s - 5) \tag{6.8}$$

$$w_s = (91x10^{-6}) \frac{\sqrt[3]{t_s A}}{1 + t_s / h_1} (f_s - 5) \tag{6.9}$$

where,

w_b is the most probable maximum crack width at bottom of the beam (in.),

w_s is the most probable maximum crack width at level of reinforcement (in.),

f_s is the reinforcing steel stress calculated by elastic cracked section theory (ksi),

A is the area of concrete symmetric with reinforcing steel divided by number of bars (in^2.),

t_b is the bottom cover to center of bar (in.),

t_s is the side cover to center of bar (in.),

β_s is the ratio of distance between neutral axis and tension face to distance between neutral axis and centroid of reinforcing steel,

h_1 is the distance from the neutral axis to the reinforcing steel (in.).

Simplification of Eq. (6.8) yields the following equation:

$$w_{ACI} = (76x10^{-6})\ \beta_s\ f_s\ \sqrt[3]{d_c\ A} \tag{6.10}$$

where,

w_{ACI} is the most probable crack width (in),

d_c is the thickness of cover from tension fiber to center of bar closest thereto (in).

6.2.3 The British Standards BS 8110 (1989)

Three main factors are governing the crack width calculation as introduced by the British Code, which are:

1) the relative position of the point, at which the crack width is calculated, to the reinforcing bars perpendicular to the cracks,
2) the distance from the neutral axis to the considered point,
3) the average surface strain at the considered point.

The design surface crack width, w_{BS} is calculated from the following equation, provided the strain in the tension reinforcement is limited to $0.8\ f_y/E_s$:

$$w_{BS} = \frac{3\ a_{cr}\ \varepsilon_m}{1+2\left(\dfrac{a_{cr}-c}{t-x_n}\right)} \tag{6.11}$$

where,

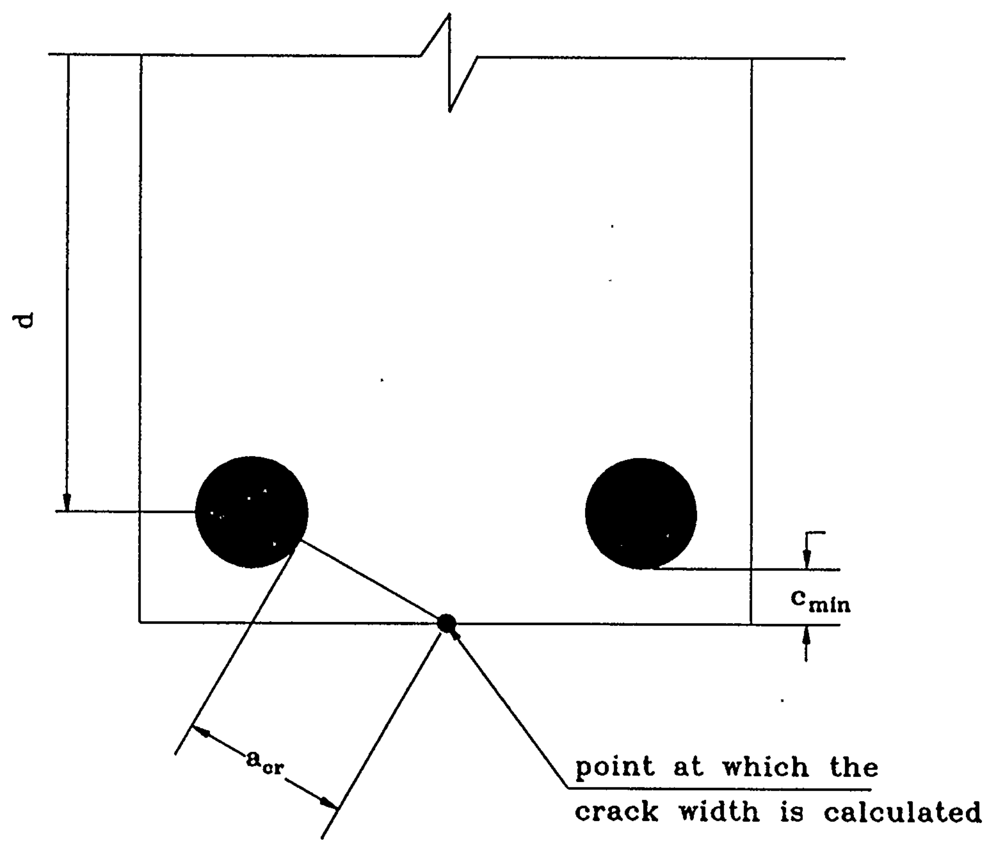

Figure 6.4 The Distance a_{cr} used in Eq. 6.11

a_{cr} is the distance from the point considered to the surface of the nearest longitudinal bar(m) (Fig. 6.4),

ε_m is the average strain in steel at the level where the cracking is being considered,

c is the minimum clear cover to the tension steel (m),

t is the overall depth of the member (m),

x_n is the depth of the neutral axis (m).

The average strain ε_m is calculated as the difference of the strain in the steel ε_1, calculated on the basis of a cracked section, and the strain produced by the tension stiffening of the concrete. The stresses in the concrete in tension are assumed to have a triangular distribution, having a value of zero at the neutral axis and a value at the centroid of the tension steel of 1.0 MPa. The total tensile force produced in concrete is divided by $(E_s A_s)$ to obtain the reduction in steel strain due to tension stiffening. Thus ε_m is calculated as follows:

$$\varepsilon_m = \varepsilon_1 - \frac{b_t\,(t-x_n)\,(a'-x_n)}{3\,E_s\,A_s\,(d-x_n)} \tag{6.12}$$

where,

ε_1 is the strain in the steel calculated on the basis of a cracked section,

b_t is the width of the section at the centroid of the tension steel (m),

a' is the distance from the compression face to the point at which the crack width is being calculated (m),

E_s is the modulus of elasticity of the reinforcement (MPa),

A_s is the area of tension reinforcement (m^2),

d is the effective depth (m).

As previously mentioned, in the analysis discussed below, ε_m is taken directly from the output of FELARC.

6.3 CRACK CONTROL IN CIRCULAR TANKS

It is apparent that the steel stress (or strain) is a common factor in the previously discussed formulae of crack width calculation. For this reason the present study focuses on the effect of the amount of the non-prestressed steel on the stress and on the crack width. One of the factors, which influence the stress in the non-prestressed steel is also included in the study, which is the vertical prestress.

As it is mentioned before in section 3.2, in the analysis using computer program FELARC, the concrete section is divided into several layers. As the stress in any layer reaches the tensile strength of the concrete, the whole layer is considered cracked. This implies a smeared crack representation. Thus, the calculated crack width based on strain calculated by FELARC, will present an average magnitude of the width of the actual cracks, without the need to account further for the effect of tension stiffening.

Crack widths of magnitudes in the range of 0.1-0.2 mm are assumed satisfactory for the CEB and BS codes, while a Z-factor of max 20.1 kN/mm (115 kips/in) is the limit for ACI code, where,

$$Z = f_s \sqrt[3]{d_c A} \tag{6.13}$$

f_s is the steel stress (ksi), d_c is the thickness of cover from tension fiber to center of the closest bar and A is the area of concrete symmetric with reinforcing steel divided by number of bars (in^2).

6.3.1 The Crack Control of Reinforced Concrete Tanks

A circular reinforced concrete tank, Tank 1 (Section 2.5) is used to accomplish this study. Variable vertical steel ratios are assumed at the inner and the outer faces of the tank wall; however the circumferential steel ratio is kept constant ($\rho_{ih} = \rho_{oh} = 0.25$ %).

Combinations of three loadings are applied to the tank to determine the maximum magnitudes of the crack widths in the circumferential and vertical directions as follows:

Loading Case (A):

The full liquid load in addition to a uniform temperature rise varying linearly through the thickness: T_o = 45°C, T_i = 15°C. This loading produces maximum width of the circumferential cracks at the inner face of the tank wall at base and the vertical cracks at the inner side of the tank wall at x = 4.2 m; where x is measured vertically from base.

Loading Case (B):

T_o = -20°C, T_i = 5°C with a linear variation through the thickness. This loading gives the maximum width of the circumferential cracks at the outer side of the tank wall at the base, in addition to the maximum width of the vertical cracks at the outer side of the tank wall at base and at top.

Loading Case (C):

The full liquid load only, to determine the maximum width of the vertical cracks at x = 2.8 m.

6.3.1.1 Circumferential Cracks

Since the examined tank is fixed at the base, the maximum vertical moment occurs at the fixation. Vertical reinforcement ratios, ρ_{iv} varying from 0.5 to 2.4% are provided on the inside face of the tank wall in order to control the width of the circumferential cracks at bottom. ρ_{iv} is equal to A_{siv}/bd, where A_{siv} is the area of tensile reinforcement per metre width, b is the width of the section (1.0 m) and d the effective depth of the section. The vertical steel ratio at the outside face of the tank wall, ρ_{ov} is taken equal to ρ_{iv}.

A new nonlinear analysis is performed for each value of ρ_{iv}. Each time A_{siv} and A_{sov} are changed and in order to keep a constant clear cover of 30 mm, the location of the steel layers are also changed. A fixed number of 5 bars is chosen for all steel ratios as shown in Table 6.2.

Table 6.2 Details of non-prestressed reinforcement

ρ_{iv} (ρ_{ov})* (%)	A_{siv} (A_{sov}) (mm^2)	Reinforcement† (per meter)
0.05**	100	1 # 10
0.20	500	5 # 10
0.25	600	6 # 10
0.30	800	2 # 10 + 3 # 15
0.40	1000	5 # 15
0.50	1300	2 # 15 + 3 # 20
0.60	1500	5 # 20
0.75	1900	3 # 20 + 2 # 25
0.80	2100	2 # 20 + 3 # 25
1.00	2500	5 # 25
1.20	3100	2 # 25 + 3 # 30
1.35	3500	5 # 30
1.60	4100	3 # 30 + 2 # 35
1.75	4400	2 # 30 + 3 # 35
2.00	5000	5 # 35
2.40	6000	6 # 35

* A clear concrete cover is maintained for all steel ratios.

** This steel ratio represents the case of full prestressing.

† For cross-section area of bars with designations # 10, # 20, ..., see Appendix B.

The arrangement of the reinforcement is previously shown in Figs. 2.3-2.6.

After each analysis the depth of the neutral axis and the stress in steel along with the already known steel ratio, steel location and number of reinforcement bars are used as input for the crack width calculation according to ACI 224-86, CEB-FIP MC90, BS 8110.

As it is previously shown in Chapter 4 (Fig. 4.12), the nonlinear vertical moment is almost linearly varying with the vertical steel ratio. This could be also seen in Table 6.3.

The resulted crack widths, as calculated by the ACI, CEB and BS Codes, the Z-factor, along with the stress in the inner vertical steel, f_{siv} and the compressive stress in concrete f_c are shown in Table 6.3 and plotted in Fig. 6.6.

The three codes vary in their estimates of the crack width. The ACI code

provides the most conservative estimates of ρ_{iv} necessary to limit the crack width between 0.1 and 0.2 mm (ρ_{iv} > 1.0 %). However, the curve of the CEB Code is the most sensitive to the variation of ρ_{iv}. This could be inferred from the three Eqs. 6.5, 6.10 and 6.11. At ρ_{iv} = 1.75 % the crack widths calculated by the BS and the CEB Codes are within the previously proposed range. However the ACI Code is only satisfied at ρ_{iv} = 2.40 %.

Another case is examined with the same thickness t = 300 mm and providing the same area of vertical steel at the inside and the outside faces of the tank wall ($\rho_{iv} = \rho_{ov}$).

Table 6.3 Analysis results of Tank 1, loading case A
t = 300 mm, variable ρ_{iv}

ρ_{iv} (%)	M_x (kNm/m)	f_s (MPa)	f_c (MPa)	w_{ACI} (mm)	w_{CEB} (mm)	w_{BS} (mm)	Z (kN/mm)
0.50	-173.5	399.8	19.64	0.445	0.607	0.376	33.80
0.60	-181.0	377.1	19.56	0.429	0.536	0.352	32.36
0.75	-190.0	316.7	19.33	0.374	0.395	0.291	27.82
0.80	-199.1	303.0	19.60	0.359	0.338	0.277	26.62
1.00	-213.3	281.0	19.90	0.345	0.290	0.254	25.25
1.20	-233.4	257.4	20.00	0.325	0.230	0.230	23.56
1.35	-244.9	245.7	20.00	0.319	0.209	0.218	22.88
1.60	-260.6	231.0	19.96	0.310	0.181	0.203	21.98
1.75	-268.8	224.9	19.93	0.303	0.164	0.197	21.40
2.00	-282.1	213.3	20.00	0.297	0.147	0.185	20.71

Table 6.4 Analysis results of Tank 1, loading case B
t = 300 mm, , variable ρ_{ov}

ρ_{ov} (%)	M_x (kNm/m)	f_{sov} (MPa)	f_c (MPa)	w_{ACI} (mm)	w_{CEB} (mm)	w_{BS} (mm)	Z (kN/mm)
0.30	46.5	114.20	7.25	0.146	0.202	0.105	11.07
0.40	51.3	105.80	7.26	0.139	0.172	0.096	10.43
0.50	57.6	94.40	7.15	0.127	0.128	0.085	9.42
0.60	61.5	85.51	7.04	0.117	0.108	0.076	8.63
0.75	69.9	69.20	6.94	0.099	0.075	0.060	7.12
0.80	72.5	65.60	6.90	0.094	0.064	0.057	6.75
1.00	76.7	59.90	6.85	0.089	0.054	0.051	6.28
1.20	82.8	52.80	6.74	0.081	0.040	0.044	5.61
1.35	85.9	49.87	6.69	0.079	0.036	0.042	5.38

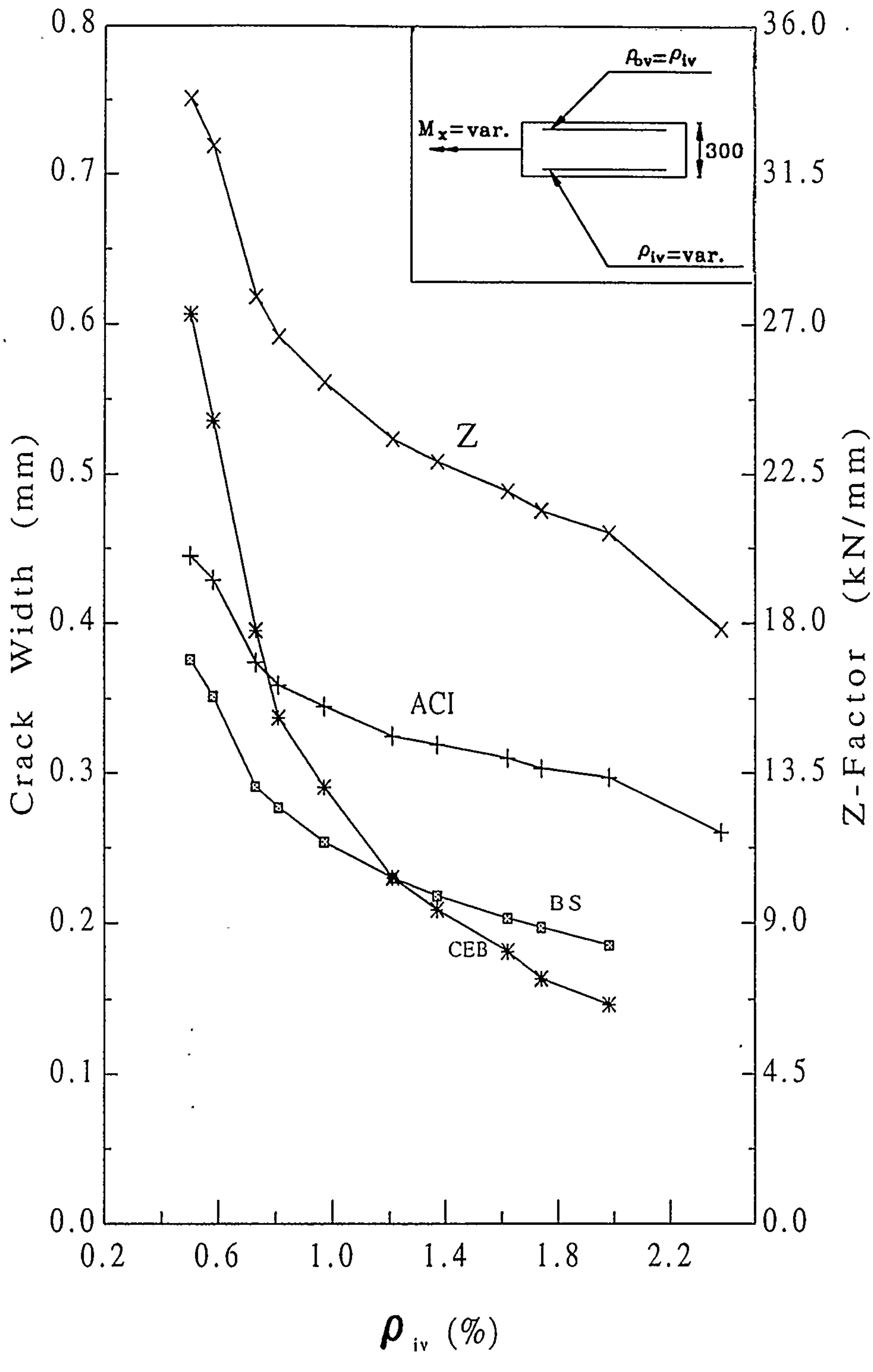

Figure 6.5 The variation of the crack width and the Z-factor versus ρ_{iv} for Tank 1 subjected to loading case A. (t = 300 mm)

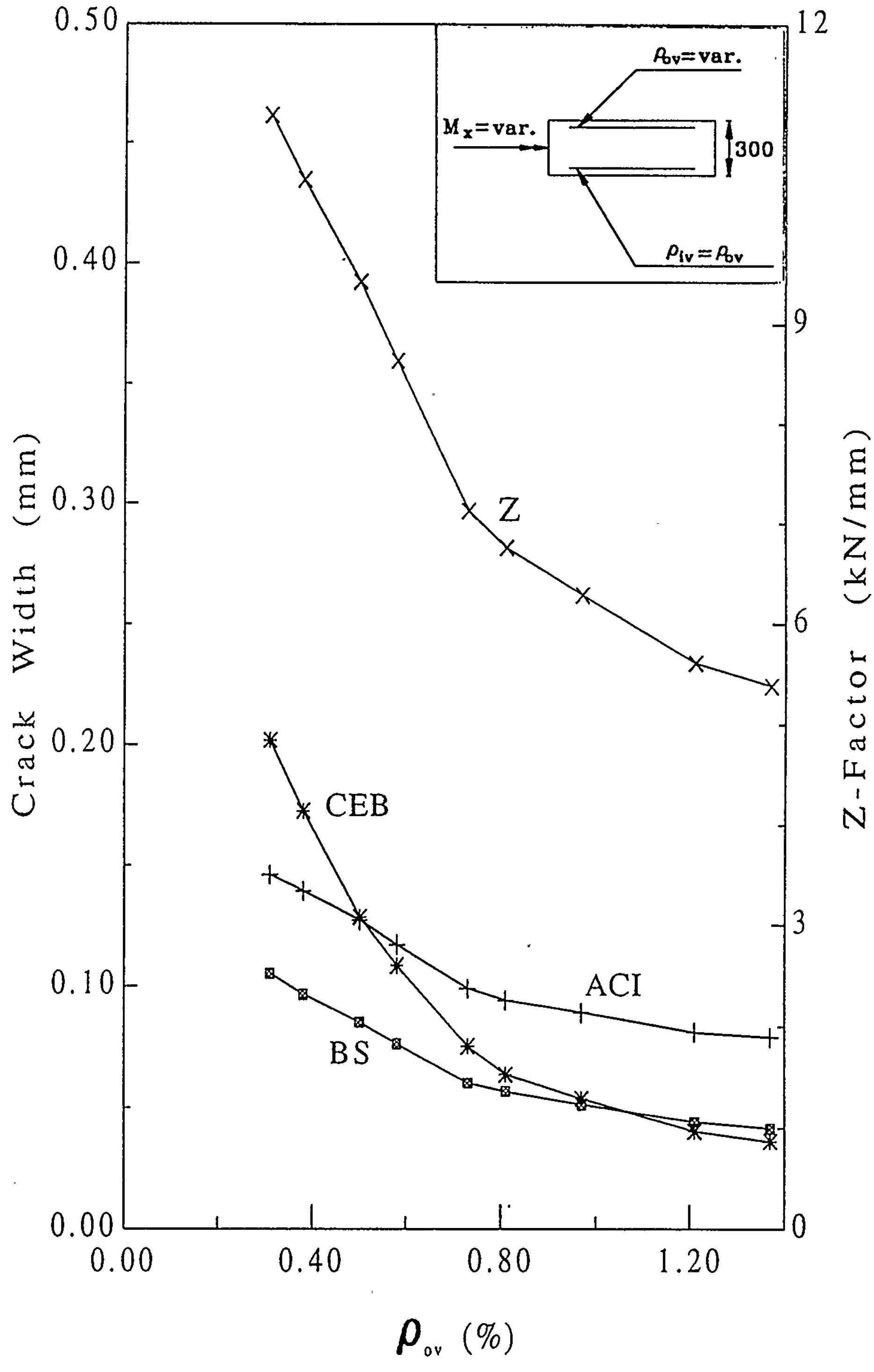

Figure 6.6 The variation of the crack width and Z-factor versus versus ρ_{ov} for Tank 1 subjected to loading case B. (t = 300 mm)

The tank is subjected to loading case B to examine the width of the circumferential cracks at the base at the outside face of the wall. The results are provided in Table 6.4 and plotted in Fig. 6.6. This case is less severe and a steel ratio ρ_{ov} = 0.30 % satisfy the crack width requirements.

6.3.2 Crack Control of Prestressed Tanks

A further step is made to investigate the variation of the circumferential and vertical crack widths for prestressed circular tanks as a function of the vertical non-prestressed steel ratios. In addition the effect of the vertical prestress σ_{vp} is also included as one of the main factors influencing the width of the circumferential cracks.

In order to conduct the aimed study, the behavior of Tank 2 (Section 2.5) is investigated under the loading cases A and B. The tank is circumferentially prestressed to counteract the liquid load in addition to a residual compression of 1.0 MPa, as explained in detail in Section 2.5.

Four variable parameters are introduced, which are:

ρ_{iv}, ρ_{ov} the vertical non-prestressed steel ratio at the inside and the outside face of the tank wall, associating the loading cases A and B, respectively.

σ_{vp} the vertical prestress at the centre of the cross-section.

t the thickness of wall.

Four dependent parameters are aimed to be determined each time, which are:

f_{siv}, f_{sov} the stress in the non-prestressed vertical steel at the inside and outside faces of the tank wall, respectively.

w the crack width at the critical positions according to the loading case. The formula of the ACI, CEB and BS are employed for the determination of w.

Z the parameter defined by Eq. 6.13.

f_c the maximum compressive stress in the concrete section.

The vertical cracks, caused by the hoop stresses, are found to be of negligible magnitudes (< 0.1 mm) for the considered loading cases. A steel ratio of 0.25 % is assumed for the circumferential non-prestressed steel on outer and inner faces of the wall. According to El Badry the minimum steel ratio in order to avoid the yielding of steel after first cracking for the case of pure flexure is :

$$\rho_{min} = 0.24 \frac{f'_t}{f_y} \tag{6.14}$$

For f'_t = 2.5 MPa and f_y = 400 MPa, ρ_{min} = 0.15 %.

6.3.2.1 The Effect of Vertical Prestress

The effect of the vertical prestress σ_{vp} is investigated for loading cases A and B. The following are the values of t, ρ_{iv}, and ρ_{ov} for each case:

	t (mm)	ρ_{iv} (%)	ρ_{ov} (%)
Loading Case A	300	0.60	0.25
Loading Case B	300	0.75	0.75

Tables 6.5 and 6.6 and Figs. 6.7 and 6.8, respectively, show the values and the variation of w, z, and f_s and f_c for each loading case.

Crack widths within the previously proposed range is obtained at σ_{vp} = 2.0 MPa, however the compression in concrete at the extreme fibre is equal to 21.9 MPa (0.55 f'_c) and 23.0 MPa (0.575 f'_c) for cases A and B, respectively. A desired value of the compression in concrete is 0.45 f'_c according to the ACI 318-89.

6.3.2.2 The Effect of Non-Prestressed Steel

For t = 300 mm and σ_{vp} = 2.0 MPa, variable ρ_{iv}, ρ_{ov} are provided for the cases A and B, respectively. A considerable decrease in crack width is apparent with the increase of ρ_{iv} and ρ_{ov}, however the compression in concrete is still higher than desired. (Figs. 6.9 and 6.10 and Tables 6.7 and 6.8).

The high compressive stresses developed at the concrete fibers are mainly produced by secondary effects, namely the thermal loads. Therefore, the allowable stresses could be increased (CEB-FIP MC90). This will satisfy the present design: σ_{vp} = 2.0 MPa, $\rho_{iv} = \rho_{ov}$ = 0.75 %.

Table 6.5 Analysis results of Tank 2, loading case A
t= 300 mm, ρ_{iv} = 0.60 %, ρ_{ov} = 0.25 %, variable σ_{vp}

σ_{vp} (MPa)	M_x (kNm/m)	f_{siv} (MPa)	f_c (MPa)	w_{ACI} (mm)	w_{CEB} (mm)	w_{BS} (mm)	Z (kN/mm)
0.0	-161.5	229.70	17.82	0.266	0.300	0.208	19.71
0.5	-175.8	219.20	18.70	0.256	0.278	0.196	18.81
1.0	-193.9	196.90	20.18	0.233	0.236	0.172	16.90
1.5	-203.9	191.70	20.97	0.228	0.225	0.166	16.45
2.0	-219.2	174.30	21.89	0.210	0.195	0.148	14.96
2.5	-246.0	139.50	22.53	0.173	0.142	0.114	11.97
3.0	-253.2	139.70	23.60	0.174	0.139	0.113	11.99
4.0	-269.6	127.10	24.99	0.162	0.118	0.099	10.91

Table 6.6 Analysis results of Tank 2, loading case B
t = 300 mm, $\rho_{ov} = \rho_{iv}$ = 0.75%, variable σ_{vp}

σ_{vp} (MPa)	M_x (kNm/m)	f_{sov} (MPa)	f_c (MPa)	w_{ACI} (mm)	w_{CEB} (mm)	w_{BS} (mm)	Z (kN/mm)
0.0	196.7	285.70	20.38	0.343	0.307	0.256	25.1
1.0	225.2	239.10	21.87	0.292	0.234	0.208	21.01
2.0	250.5	206.20	23.06	0.256	0.184	0.175	18.12
3.0	272.6	172.50	24.54	0.220	0.136	0.141	15.16
4.0	292.4	148.10	25.68	0.194	0.105	0.117	13.01

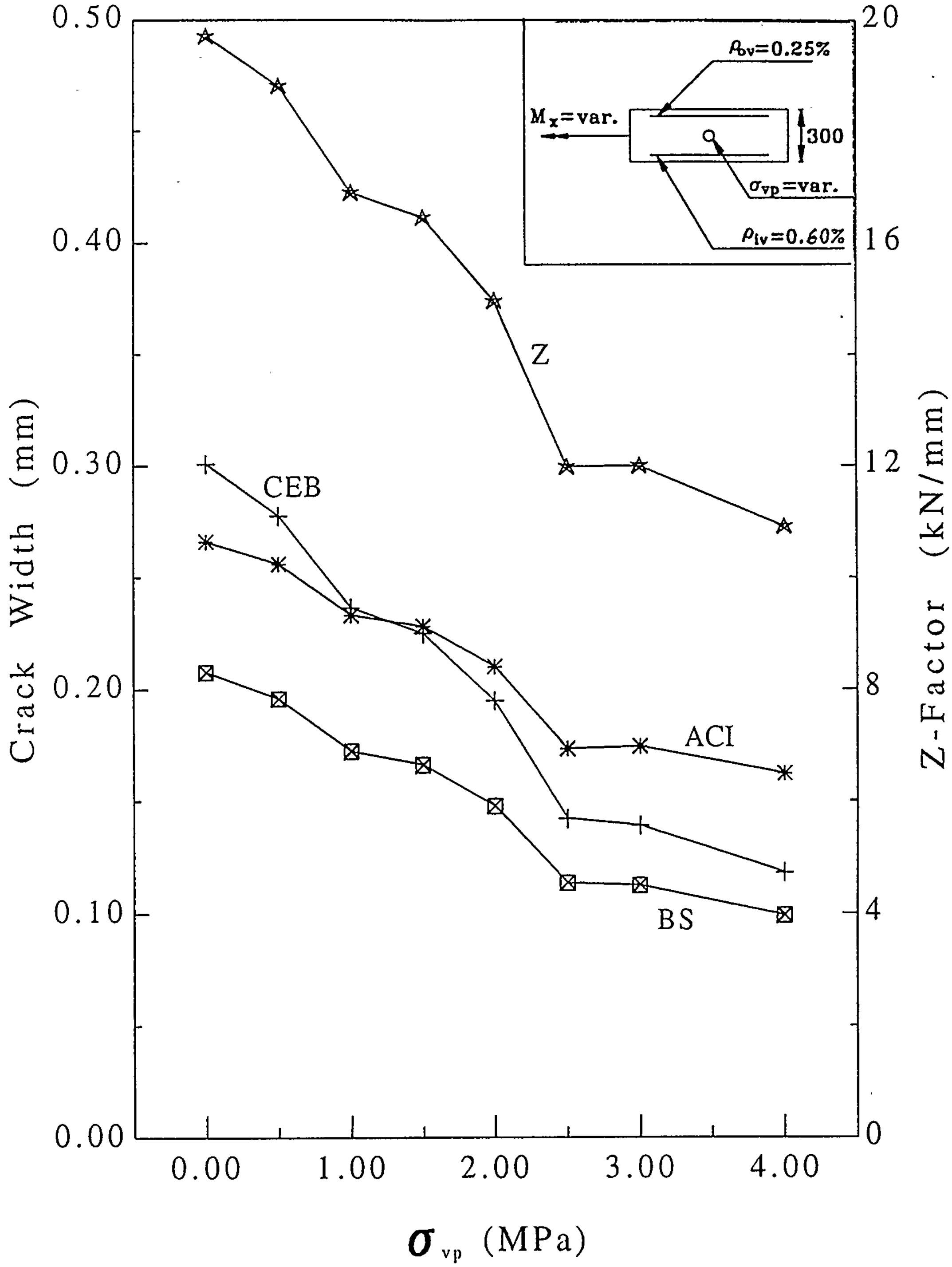

Figure 6.7 The variation of crack width and Z-factor versus σ_{vp} for Tank 2 subjected to loading case A. (t = 300 mm, ρ_{iv} = 0.60 %, ρ_{ov} = 0.25 %)

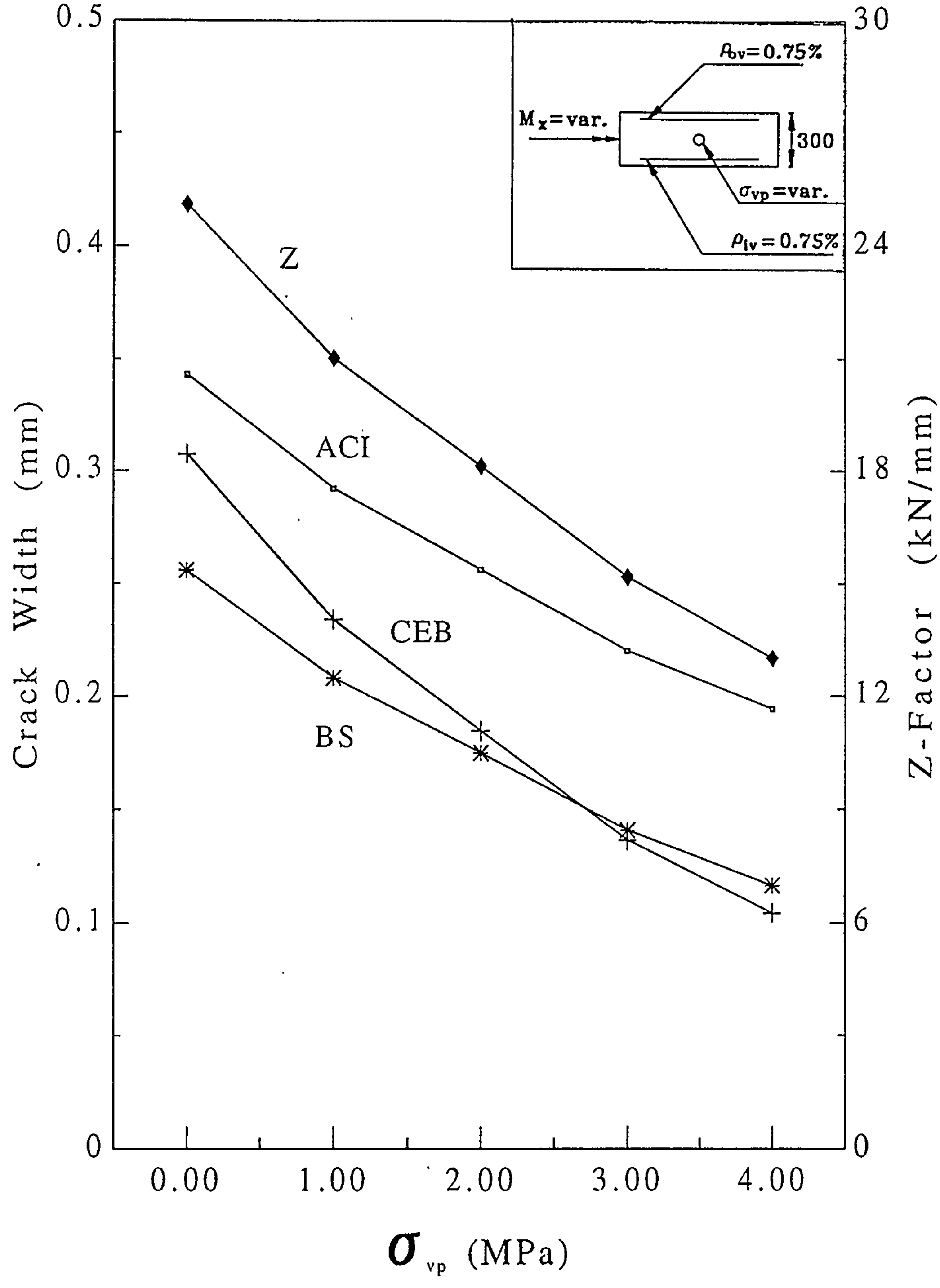

Figure 6.8 The variation of the crack width and Z-factor versus σ_{vp} for Tank 2 subjected to loading case B. (t = 300 mm, $\rho_{ov} = \rho_{iv}$ = 0.75 %)

Table 6.7 Analysis results of Tank 2, loading case A
t = 300 mm, σ_{vp} = 2.0 MPa, variable ρ_{iv}

ρ_{iv} (%)	M_x (kNm/m)	f_{siv} (MPa)	f_c (MPa)	w_{ACI} (mm)	w_{CEB} (mm)	w_{BS} (mm)	Z (kN/mm)
0.05	-190.6	242.7	23.81	0.258	0.486	0.216	19.31
0.20	-207.2	192.4	23.12	0.209	0.295	0.165	15.35
0.30	-210.1	181.7	22.52	0.204	0.264	0.155	14.82
0.40	-218.5	174.4	22.10	0.202	0.235	0.147	14.52
0.60	-219.2	174.3	21.89	0.210	0.195	0.148	14.96
0.75	-232.8	160.4	21.15	0.201	0.158	0.134	14.09
0.80	-239.5	155.1	20.87	0.195	0.137	0.129	13.63
1.00	-252.8	146.1	20.55	0.191	0.120	0.120	13.13
1.20	-258.1	135.6	20.51	0.184	0.096	0.110	12.41
1.35	-261.1	130.9	20.61	0.183	0.088	0.106	12.19

Table 6.8 Analysis results of Tank 2, loading case B
t = 300 mm, σ_{vp} = 2.0 MPa, variable ρ_{ov}

ρ_{ov} (%)	M_x (kNm/m)	f_{sov} (MPa)	f_c (MPa)	w_{ACI} (mm)	w_{CEB} (mm)	w_{BS} (mm)	Z (kN/mm)
0.25	197.5	265.6	24.19	0.285	0.558	0.233	21.20
0.30	207.9	262.8	22.90	0.289	0.416	0.232	21.43
0.40	216.9	249.6	22.94	0.284	0.365	0.218	20.79
0.50	229.5	234.1	22.98	0.273	0.287	0.203	19.79
0.60	236.4	224.4	23.02	0.268	0.258	0.193	19.26
0.75	250.5	206.2	23.06	0.256	0.210	0.175	18.12
0.80	256.3	199.5	23.10	0.249	0.181	0.168	17.53
1.00	265.7	185.9	23.32	0.241	0.156	0.155	16.71
1.20	276.9	171.3	23.16	0.230	0.124	0.141	15.68
1.35	283.4	161.9	23.21	0.225	0.111	0.131	15.08

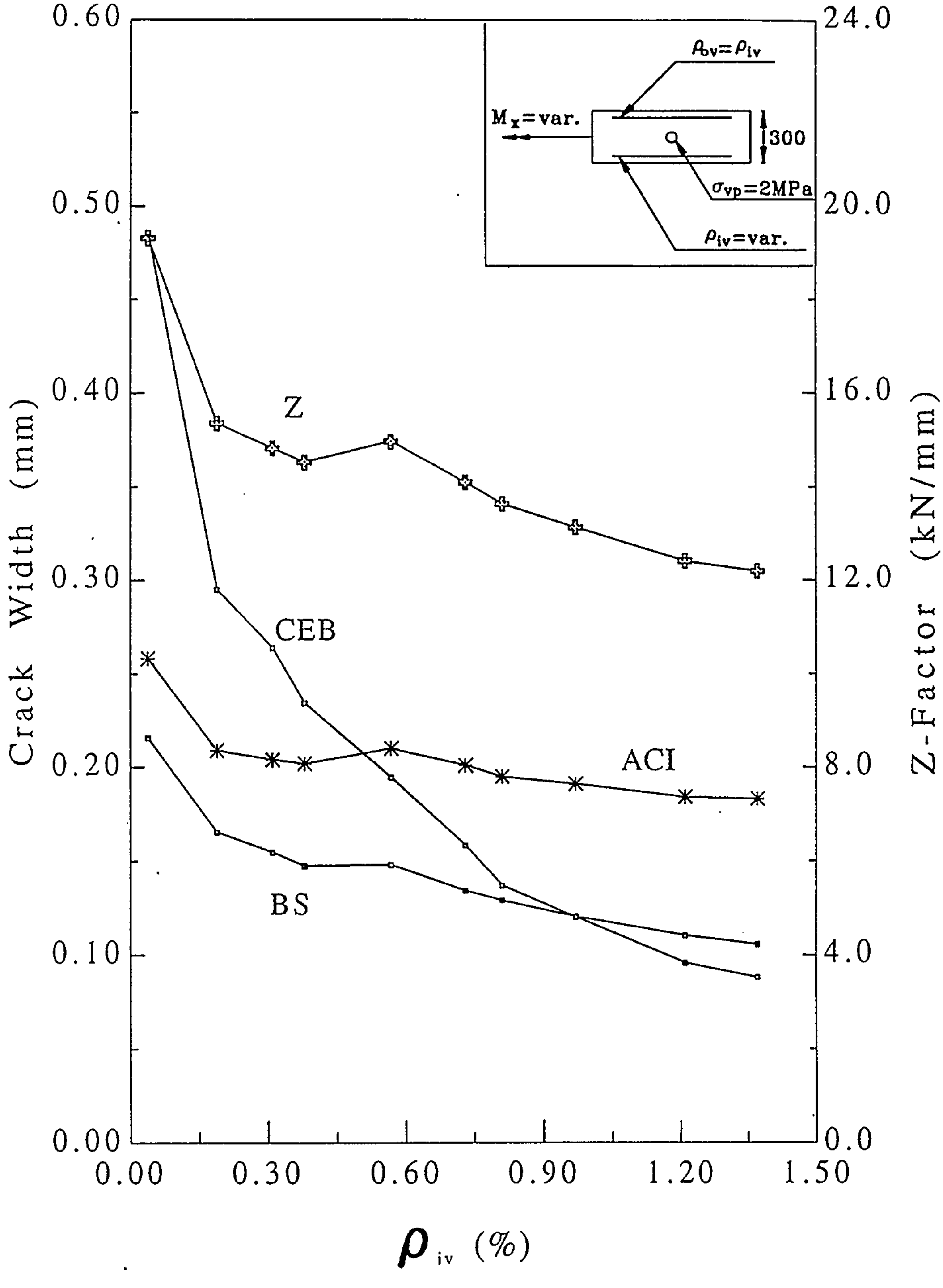

Figure 6.9 The variation of crack width and Z-factor versus ρ_{iv} for Tank 2 subjected to loading case A. (t = 300 mm, σ_{vp} = 2.0 MPa)

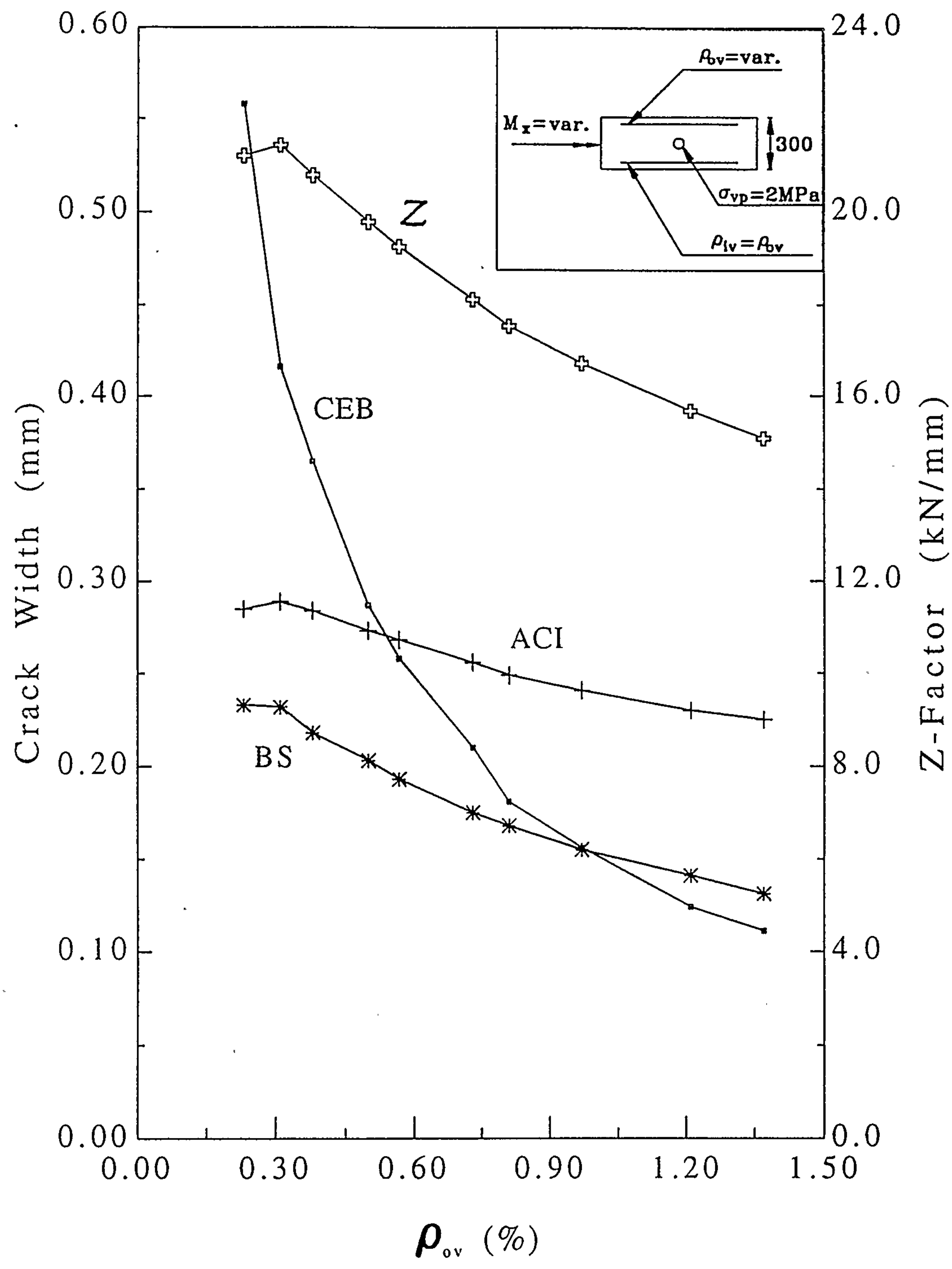

Figure 6.10 The variation of crack width and Z-Factor versus ρ_{ov} for Tank 2 subjected to loading case B. (t = 300 mm, σ_{vp} = 2.0 MPa)

6.4 DISCUSSION OF RESULTS

In Chapter 4 a design of Tanks 1 and 2 was done in accordance to the American and British Codes. The design took into account the internal forces caused by the thermal loads. It was based on the elastic analysis of circular tanks and resulted in large cross-sections for both tanks. However, in the present chapter it has been shown that by a nonlinear analysis of the same tanks and by the control of crack width a substantial reduction in the depth of the cross-sections is attainable. The crack control study for Tank 1 is applied on a wall thickness of 300 mm, which is 40 % less than the designed thickness according to ACI 350 and BS 8007 (Chapter 2). However, in order to keep the crack width within the previously proposed range, a high percentage of steel ratio is required.

High steel ratios are practically not preferred for two reasons. The first is, for shallow cross-sections the placing and compaction of cast-in-situ concrete may be affected. The second reason is the high concrete stresses due to shrinkage.

The high vertical moments at base could be reduced by assuming a partially fixed base instead of a totally fixed base. This presents a more realistic case, since a total fixation is never fully achieved. This will reduce the steel ratio to an acceptable limit. Another way to reduce the moment at the base is to introduce a partially fixed wall-base joint allowing for some rotation at base.

The PCA report (1993) recommends that one assumes the base to be hinged for the analysis of a fixed base tank.

A significant drop in the vertical moment at base is due to the nonlinear analysis (Chapter 4). Another drop is due to the partial fixation. Ideally, one can base the design on nonlinear analysis assuming partial fixity dependent upon the conditions of the tank being designed. However, for most engineers nonlinear analysis is considered not practical. In this case one can multiply the vertical moment at base obtained by elastic analysis by two reduction factors: the first is to account for the effect of nonlinearity due to cracking and the second is to account for the partial fixity. It is not simple to suggest values for these factors, because the first depends upon the amount of steel provided in the vertical direction and the second depends upon the soil conditions, floor thickness and joint detail (see Figs. 1.c and d). Therefore, it is left to the designer to choose the proper values.

With the joint detail in Fig. 1d, the partial fixity can be accounted for more accurately by the analysis of the wall continuous with a ring-shaped part of the base.

These recommendations are applicable for both prestressed and non-prestressed circular concrete tanks.

CHAPTER 7

CONCLUSIONS AND RECOMMENDATIONS

7.1 CONCLUSIONS

The main results of the present investigation can be briefly summarized as follows:

i. The structural design of circular reinforced and prestressed concrete tanks with a fixed base results in large cross-sections, when including the thermal load as one of the main loads and basing the design on linear analysis.

ii. The cracking of the cylindrical concrete tank alleviates the induced thermal stresses significantly and hence the design of economic cross-sections can be achieved.

iii. A drop of induced thermal stresses in one direction (vertical or circumferential) due to cracking of the circular concrete tank is associated with a drop of the thermal stresses in the perpendicular direction. This is unlike the effect of liquid loads, where the cracking due to the stresses in one direction causes an increase of the stresses in the perpendicular direction.

iv. The amount of bonded steel is the main factor for the control of crack width in reinforced and prestressed circular tanks.

v. The crack width calculation according to ACI 224 provides a conservative value in comparison to CEB FIP (1990) and BS 8110 (1987).

vi. For fixed base circular concrete tanks, the main circumferential cracks occur at base due to the liquid load and/or the thermal load. The vertical cracks produced by circumferential stresses are of negligible magnitudes for the same loading cases.

7.2 RECOMMENDATIONS FOR DESIGN

i. The non-linear analysis of circular concrete tanks is recommended in case of the inclusion of the thermal loads.

ii. A serviceability check is essential in case the design is based on a cracked section analysis.

iii. The use of partially fixed base instead of totally fixed is recommended in order to reduce the vertical moments at base.

iv. The allowance for higher compressive stresses in the concrete in the design for thermal loads can be necessary.

7.3 RECOMMENDATIONS FOR FURTHER RESEARCH

i. Experimental verification of the present analytical study.

ii. Extension of the present study to include the effects of creep, shrinkage and relaxation of prestressed steel.

iii. Extension of the present work to cover the actual nonlinear temperature variation through the wall thickness.

iv. Study the effects of the formation of an ice cap in cold regions.

REFEREMCES

ACI Committee 224, (1986), " Cracking of Concrete Members in Direct Tension, " Journal of the American Concrete Institute, 80(6) pp. 467-486.

ACI Committee 318, (1989), " Building Code Requirements for Reinforced Concrete (ACI 318-89) and Commentary (ACI 318R-89), " American Concrete Institute, Detroit, 353 pp.

ACI Committee 344, (1988), " Design and Construction of Circular Prestressed Concrete Structures with Circumferential Tendos. (ACI 344-88)," American Concrete Institute, Detroit, 42 pp.

ACI Committee 344, (1988), " Design and Construction of Circular Wire and Strand Wrapped Prestressed Concrete Structures (ACI 344-88)," American Concrete Institute, Detroit, 44 pp.

ACI Committee 350, (1989), " Environmental Engineering Concrete Structures (ACI 350R-89), American Concrete Institute, Detroit.

Beeby, A.W., (1979), " The Prediction of Crack Widths in Hardened Concrete," The Structural Engineer, 57A, No. 1, January, pp. 9 -17.

Beeby, A.W., (1978), "Corrosion of Reinforcing Steel in Concrete and its Relation to Cracking, " The Structural Engineer, 56A, No. 3, March.

BS 8007, (1987), " British Standard Code of Practice for Design of Concrete Structures for Retaining Aqueous Liquids ," British Standards Institution, London.

BS 8110, (1985), " British Standard Structural Use of Concrete, " British Standard Institution, (amended 1989), London.

Canadian Standards Association, (1982), " steel for Prestressed Concrete Tendos, " (G279-M82)

Canadian Standards Association, (1977), " Billet-Steel Bars for Concrete Reinforcement, " (CSA-G30.12-M77).

CEB-FIP MC90 Model Code, (1990), " Model Code for Concrete Structures, " Comitè Euro-International du Béton et Fédération International de la Précontrainte, Lausanne, Switzerland.

Clear, C.A., (1985), " The Effects of Autogemous Healing upon Leakage of Water through Cracks in Concrete, " Cement and Cement Association, Technical Report 559, 5/1985.

Cordes, H. and Bick, D., (1991), " Zum Flüssigkeitstansport an Trennrissen im Stahlbeton, " Beton- und Stahlbetonbau, 86, H.8, pp. 181-186)

Elbadry, M.M., (1988), " Serviceability of Reinforced Concrete Structures , " Ph.D. Thesis, Department of Civil Engineering, The University of Calgary, Calgary, Canada, 294 pp.

Elliott, E. M., (1989), " Design of Circular Concrete Tanks ", MSc Thesis, Department of Civil Engineering, University of Calgary, Calgary, Canada, pp 175.

Gergely, P. and Lutz, L.A., (1968), " Maximum Crack Width in Reinforced Concrete Flexural Members ", ACI Publication SP-20.

Ghali, A., (1990), " Manual and Computer Program PCT, Prestressed Circular Tanks, " Research Report No. CE90-8, (revised 1993), Department of Civil Engineering, The University of Calgary, Calgary, Canada T2N 1N4, 40 pp.

Ghali, A., (1979)," Circular Storage Tanks and Silos, " E. and F.N. Spon Ltd., London, 210 pp.

Ghali, A. and Elbadry, M., (1985), " User's Manual and Computer Program CRACK ," (revised 1991), CE 85-1, Department of Civil Engineering, The University of Calgary, Calgary, Canada T2N 1N4, Revised 1991, 106 pp.

Ghali, A., and Elliott, E., (1992), " Serviceability of Circular Prestressed Concrete Tanks, " ACI Structural Journal, May-June, pp. 345-355.

Ghali, A., and Elliott, E., (1991), " Prestressing of Circular Tanks, " ACI Structural Journal, November-December, pp. 721-729

Ghali, A. and Favre, R., (1986), " Concrete Structures: Stresses and Deformations, " Chapman and Hall, New York and London, 352 pp.

Ghali, A. and Neville, A.M., (1989), " Structural Analysis: A Unified Classical and Matrix Approach, " Chapman and Hall, London and New York, 870 pp.

Ghoneim, G.A.M., (1978), " Nonlinear Finite Element Analysis of Concrete Structures, " Ph.D. Thesis, Department of Civil Engineering, The University of Calgary, Calgary, Canada, T2N 1N4, 249 pp.

Ghoneim, G.A.M. and Ghali, A., (1978), " User Manual for Computer Program FELARC (Finite Element Layered Analysis of Reinforced Concrete), " Department of Civil Engineering, University of Calgary, Calgary, Canada T2N 1N4, 58 pp.

Jofriet, J. C., and Jiang, S., (1991), " Finite Element Prediction of Temperature Gradients in Walls of Cylindrical Concrete Storage Structures, " Canadian Journal of Civil Engineering, 18, pp. 12-19.

König, G. and Fehling, E. , (1988), " Zur Rißbreitenbeschränkung im Stahlbetonbau, " Beton and Stahlbetonbau, 83, H.6 pp. 161-167 and H.7 pp. 199-204.

Kupfer, H., Hilsdorf, H.K., (1969), " Behavior of Concrete Under Biaxial Stresses, " Journal ACI, Proc. V. 66, No. 8, August, pp. 656-666.

Leonhardt, F., (1987), " Cracks and Crack Control at Concrete Structures, " IABSE Proceedings, P-109/87, February, pp. 25-44.

Portland Cement Association, PCA, (1993), " Circular Concrete Tanks Without Prestressing, " Portland Cement Association, Old Orchard Rd., Skokie, Il. 60077, 40 pp.

Priestley, M. J. N., (1985), " Analysis and Design on Circular Prestressed Concrete Storage Tanks, " PCI Journal, July-August, pp. 64-85.

Priestley, M. J. N., (1976), " Ambient Thermal Stresses in Circular Prestressed Concrete Tanks, " ACI Journal, V. 31, No. 10, October, pp. 553-560.

Saenz, L.P., (1964), Disc. of "Equation for the Stress-Strain Curve of Concrete," by Desayi and Krishnan, Journal ACI, Proc. V. 61, No. 9, September, pp. 1229-1235.

Schupack, M., and Poston, R. W., (1989), " Durability of Prestressed Concrete Tanks, " Concrete International Journal, October, pp. 51-58.

Slater, W. M., (1985), " Concrete Water Tanks in Ontario ", Canadian Journal of Civil Engineering, 12, pp. 325-333.

Smith, G.M. and Young, L.E., (1955), " Ultimate Theory in Flexure by Exponential Function, " Journal of the American Concrete Institute, V. 52, No. 3, November, pp. 349-359.

Water storage Working Group, (1990), " State of Art Report: Water Storage Vessels, " FIP Commission on Concrete Storage Vessel Systems, draft document, 34 pp.

Wood, J. H., and Adams, J. R., (1977), " Temperature Gradients in Cylindrical Concrete Reservoirs , " Proceedings of the 6th Australian Conference on the Mechanics of Structures and Materials, Christchurch, No. 2.

APPENDIX A

DERIVATION OF THE NODAL FORCES FOR A PLATE BENDING ELEMENT SUBJECTED TO A TRAPEZOIDAL LOAD DISTRIBUTION

The rectangular plate bending element has 12 degrees of freedom (Fig. A.1), defined as:

$$\{D\} = \begin{Bmatrix} (w,\theta_x,\theta_y)_1 \\ (w,\theta_x,\theta_y)_2 \\ (w,\theta_x,\theta_y)_3 \\ (w,\theta_x,\theta_y)_4 \end{Bmatrix} \qquad (A.1)$$

The matrix of the shape functions [N] is written as (Ghali 19??):

$$[N] = [\ N_1\ \ N_2\ \ N_3\ \ N_4\ \ N_5\ \ N_6\ \ N_7\ \ N_8\ \ N_9\ \ N_{10}\ \ N_{11}\ \ N_{12}\ ] \qquad (A.2)$$

where,

$$N_1 = (1-\xi)\,(1-\eta) - \frac{1}{b}\,(\ N_3 + N_6\ ) + \frac{1}{c}\,(\ N_2 + N_{11}\ )$$

$$N_2 = c\eta\,(\eta-1)^2\,(1-\xi)$$

$$N_3 = -\ b\xi\,(\xi-1)^2\,(1-\eta)$$

$$N_4 = \xi\,(1-\eta) + \frac{1}{b}\,(\ N_3 + N_6\ ) + \frac{1}{c}\,(\ N_5 + N_8\ )$$

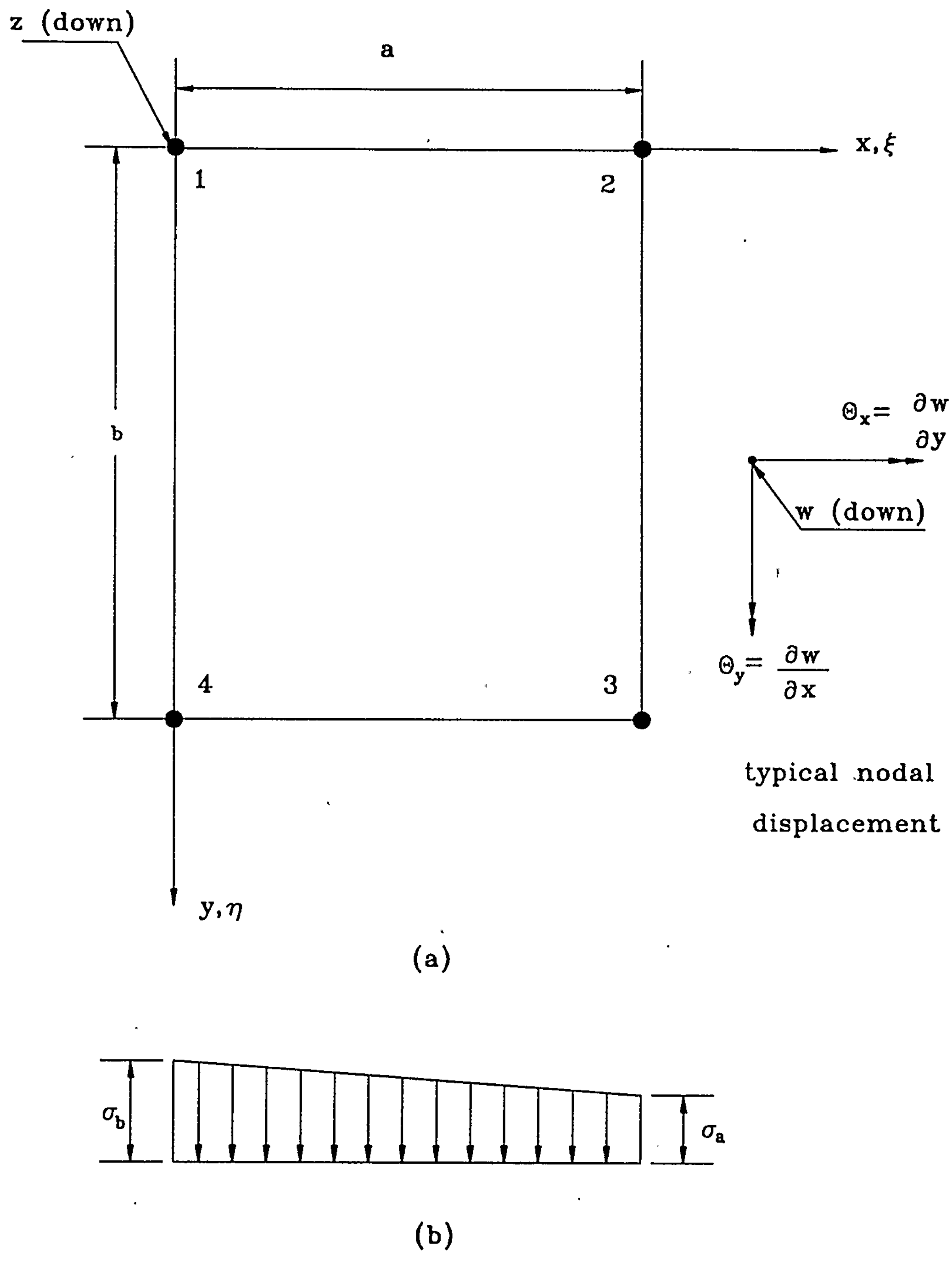

Figure A.1 Rectangular plate bending element

a) Degrees of freedom

b) Trapezoidal loading

$$N_5 = c\eta\,(\eta-1)^2\,\xi$$

$$N_6 = -b\xi^2\,(\xi-1)\,(1-\eta)$$

$$N_7 = \xi\eta + \frac{1}{b}\,(\,N_9 + N_{12}\,) - \frac{1}{c}\,(\,N_5 + N_8\,)$$

$$N_8 = c\eta^2\,(\eta-1)\,\xi$$

$$N_9 = -b\xi^2\,(\xi-1)\,\eta$$

$$N_{10} = (1-\xi)\,\eta - \frac{1}{b}\,(\,N_9 + N_{12}\,) - \frac{1}{c}\,(\,N_2 + N_{11}\,)$$

$$N_{11} = c\eta^2\,(\eta-1)\,(1-\xi)$$

$$N_{12} = -b\xi\,(\xi-1)^2\,\eta$$

The constants a and b are the lengths of the element sides; $\xi = x/a$ and $\eta = y/b$.

The load function q of the trapezoidal load distribution is written as:

$$\begin{aligned} q &= -\,[\,\sigma_a + \frac{(\,\sigma_b - \sigma_a\,)}{a}\,x\,] \\ &= -\,[\,\sigma_a + (\,\sigma_b - \sigma_a\,)\,\xi\,] \end{aligned} \qquad \text{(A.3)}$$

where σ_a and σ_b are the lower and upper load values as shown in Fig. A.2.

The equivalent nodal forces {F} are calculated as follows:

$$\{F\} = \int_0^b\int_0^a [N]\,q\,dx\,dy = a\,b\int_0^1\int_0^1 [N]\,q\,d\xi\,d\eta \qquad \text{(A.4)}$$

The forces at nodes 1 and 2 are given as follows:

$$F_1 = \frac{ab}{4}\,[\sigma_a + \frac{(\sigma_b-\sigma_a)}{3}]$$

$$F_2 = -\frac{a^2b}{8}\left[\frac{\sigma_a}{3} + \frac{2}{15}(\sigma_b-\sigma_a)\right]$$

$$F_3 = -\frac{ab^2}{8}\left[\frac{\sigma_a}{3} + \frac{1}{9}(\sigma_b-\sigma_a)\right]$$

$$F_4 = \frac{ab}{4}\left[\sigma_a + \frac{2(\sigma_b-\sigma_a)}{3}\right]$$

$$F_5 = \frac{a^2b}{8}\left[\frac{\sigma_a}{3} + 0.2(\sigma_b-\sigma_a)\right]$$

$$F_6 = -\frac{ab^2}{8}\left[\frac{\sigma_a}{3} + \frac{2}{9}(\sigma_b-\sigma_a)\right]$$

The forces F_7-F_{12} are the same as F_1-F_6 except F_9 and F_{12} are equal to F_3 and F_6 except with a different sign.

APPENDIX B

CROSS-SECTIONAL AREAS OF STANDARD PRESTRESSED AND NON-PRESTRESSED REINFORCEMENT

Table B.1 Standard Prestressing Strands

Tendon Type	Grade f_{pu} (MPa)	Size Designation	Nominal Dimension	
			Diameter (mm)	Area (mm^2)
Seven Wire Strand	860	13	12.70	99
		15	15.24	140

Table B.2 Standard Deformed Reinforcing Bars

Bar Number	Nominal Diameter (mm)	Noinal Area (mm^2)
10	11.3	100
15	16.0	200
20	19.5	300
25	25.2	500
30	29.9	700
35	35.7	1000